MODELING OF TRANSCRANIAL ELECTRICAL STIMULATION BY FINITE ELEMENT ANALYSIS

by

William Tyler Rath

BS, Linfield College, 2005

Submitted to the Graduate Faculty of

School of Engineering in partial fulfillment

of the requirements for the degree of

Master of Science

University of Pittsburgh

2006

UNIVERSITY OF PITTSBURGH

SCHOOL OF ENGINEERING

This thesis was presented

by

William Tyler Rath

It was defended on

November 20, 2006

and approved by

Mingui Sun, Associate Professor Departments of Electrical and Computer Engineering, Bioengineering, and Neurological Surgery

H. Louis Journee, Professor, Department of Neurological Surgery, University of Groningen, Groningen, the Netherlands

Jeffery Balzer, Associate Professor, Department of Neurological Surgery

Donald Crammond, Assistant Professor, Department of Neurological Surgery

Robert Sclabassi, Professor, Department of Neurological Surgery

Thesis Advisor: Mingui Sun, Associate Professor, Departments of Electrical and Computer Engineering, Bioengineering, and Neurological Surgery

Thesis Co-Advisor: Robert Sclabassi, Professor, Department of Neurological Surgery

Thesis Co-Advisor: H. Louis Journee, Professor Department of Neurological Surgery, University of Groningen, Groningen, the Netherlands

MODELING OF TRANSCRANIAL ELECTRICAL STIMULATION BY FINITE ELEMENT ANALYSIS

William Tyler Rath, MS

University of Pittsburgh, 2006

Transcranial electrical stimulation (TES) appears to be an effective way to monitor the spinal cord while patients are under anesthesia. This method is sensitive to changes in the functioning of the corticospinal tracts. It is a reliable and fast indicator of the status of the spinal cord during surgery. In this research, we develop a model to describe the intracranial voltage, electric field, and activation function distributions associated with transcranial electrical stimulation. Poisson's equation is utilized with boundary conditions modeled after a real human head.

The models, which are a two dimensional (2D) circular volume conductor and a three dimensional (3D) spherical volume conductor, include the inhomogeneous aspects of a human head. These inhomogeneous characteristics impact the flow of current due to volume conductivity differences between the scalp, skull, cerebrospinal fluid, and the brain itself. These results for a theoretical head model show the systematic differences between 2D and 3D models which has not been examined for TES. Knowing the differences between 2D and 3D simulations allows the inference for the results of the 3D case using a 2D model, which saves time and computational resources.

A comparison of the voltages, electric fields, and activation functions is examined to determine the differences between the 2D and 3D models for each quantity. Parameterizations are also performed to show the impact of the different layers of the head. The results from the potentials, electric fields, activation functions and parameterization calculations are used to infer

the systematic differences between 2D and 3D models. This analysis of computational models for TES has not been performed before and is beneficial to diagnosing which areas of the brain are being stimulated during TES and gives an idea of the stimulation threshold needed to achieve muscle responses via TES.

TABLE OF CONTENTS

LIST OF TABLES

LIST OF FIGURES

PREFACE

I would like to express my deepest gratitude and appreciation for the support and guidance from Dr. Louis Journee and Dr. Mingui Sun while I worked on my project. The opportunity to perform my research in Europe was an experience I will never forget. I also want to thank my parents for supporting me every step of the way, emotionally and financially since I became a student. Thank you also to my fellow graduate students in the lab for your patience and insight when I was asking questions about everything.

1.0 INTRODUCTION

Transcranial electrical stimulation is an intraoperative monitoring technique used to ascertain that the corticospinal tract (CST) remains intact during delicate surgeries involving the brain and spinal cord. The electrical signal generated by electrodes placed on the scalp traverses the scalp, skull, CSF, and brain to reach the CST. This signal, sent through the central nervous system (CNS) via alpha motor neurons, achieves a muscle response, which shows neurophysiologists that the CNS is functioning properly.

1.1 MOTIVATION

This research is motivated by clinical application of Transcranial Electrical Stimulation (TES) monitoring being performed currently in Europe and the United States. By modeling TES, we hope to gain a better understanding of the basic concepts of how and why TES works in practice. This knowledge will allow for optimal placement of electrodes for the technique to be more useful in the operating room. Computational models allow for rapid selection and specification of a variety of parameters to be examined such as electrode size or placement, different tissue properties, as well as geometric differences that can be found from clinical data.

To date, a comparison between 2D and 3D models has not been performed for TES. We wish to find the systematic differences between 2D and 3D models for simple geometries to

understand how we can infer the results of a 2D simulation into the 3D real world. By not having to use a 3D model we can save time and computational resources.

We also wish to understand more about how activation functions, which will be explained later in this text, are generated by the stimulating electrode placed on the scalp of the patient. An activation function expresses changes of the electrical field over distance along the axons and indicates where axon membranes will be depolarized or hyperpolarized by the stimulus.[1] The activation function is useful to predict preferential locations along an axon with lowest firing thresholds. By knowing how current/voltage are distributed in a simple model we can infer what stimulation thresholds are necessary to achieve activation functions required for axons to fire action potentials. Knowledge of the thresholds necessary to achieve activation functions would be relevant to neurophysiologists monitoring patients because it would give a baseline for comparison of measurements found during surgical operations.

1.2 BACKGROUND OF TES

Intraoperative monitoring of patients during a variety of surgical procedures has become common practice in the operating room to ensure that patients have minimal post-operative complications. TES has been used for the monitoring of motor tracts during neurosurgical procedures to detect imminent damage to the central nervous system (CNS) in anesthetized patients [1][6]. A variety of factors must be considered when choosing a monitoring technique for neurosurgery, such as the reliability of that technique, how invasive the technique is during

the monitoring procedure, interference with the surgical procedure, rapid updates of the patient status, the capacity to monitor the right and left corticospinal tracts (CST), and whether monitoring of the upper and lower extremities is possible.[2]

TES was first developed in 1980 by Merton and Morton.[3] TES is a commonly used intraoperative monitoring technique in Europe. In anesthetized patients, TES is achieved by placing an anode electrode over the motor cortex region of the brain with the cathode electrode placed approximately five centimeters anteriorly. A single pulse width of approximately 0.1 milliseconds is applied with a voltage of up to 1000 volts. Electromyograms, or EMGs, are observed in both the upper and lower extremities. TES can be used with a lower voltage by using a supra-orbitally placed ground strip and a low impedance anode at the Cz' location.[4] There is a possibility of tissue damage in theory because of the current passing directly through the skin, though no complications have been found using TES due to the short pulse width.[4]

TES is a reliable monitoring technique which allows for the monitoring of motor evoked potentials (MEP) while patients are under anesthesia. TES is also noninvasive, as the electrodes only need to be placed on the scalp of the patient for stimulation. Due to the location of the electrodes in TES it is suitable for a variety of neurological surgeries as well as some orthopedic procedures such as scoliosis corrective surgeries. The feedback, in the form of D and I waves, from TES is very rapid, on the order of tens of milliseconds. This rapid generation is due in part to advancements in stimulators and the ability of neurophysiologists to use modern computers in the operating room which have the capability of handling large amounts of data in a very short time.

One issue with the generation of MEPs during TES is the profound effect that general anesthesia has on these responses. General anesthesia, particularly inhalation agents, decreases

the amplitude of MEPs, making it difficult to record responses from the upper and lower extremities. This depressive effect can be minimized by the utilizing different anesthetic techniques such as total intravenous anesthesia (TIVA) and good communication between the neurophysiologist and anesthesiologist.

One way the electrical signal can be transmitted to the muscles of the upper and lower extremities via TES is through the CST. A MEP may also be observed by electrical depolarization of pyramidal cells in the cortex to axons of the cortical layer, which are tangentially oriented, or parallel to the surface or scalp stimulation electrodes. This tangential orientation is not mentioned previously in literature as it relates to TES. Pyramidal cells give rise to the CST, which in turn transmits a descending electrical signal to the muscle via the lower motor neurons in the spinal cord. Stimulation of the pyramidal cells can elicit the same muscle response as the direct CST stimulation, but the manner in which the signal is generated is different.

Two different waves can be recorded from the spinal cord in response to TES, direct waves and indirect waves, denoted D-waves and I-waves, respectively. D-waves result from the direct stimulation of the CST, but only if the stimulation signal is large enough to surpass the membrane potential. I-waves are produced by the "excitation of axons via synaptic connections ending on the corticospinal tract motor neurons within the motor cortex".[6] All pyramidal cells receive the stimulus generated by TES and transmit the signal to the CST; this signal observed is the D-wave. I-waves are caused by the shorter refractory period of the synaptic connections of the pyramidal cells, leading to the transmission of a smaller signal down the CST to the CNS. I-wave amplitudes are generally smaller than D-wave amplitudes because of how I-waves are generated. D- and I-waves are then transmitted from the CST to the spinal motor neuron which

generates new action potentials when the sum of the inputted D- and I-waves exceeds the membrane threshold potential. These action potentials are then propagated to the muscles resulting in MEPs. The depressive effect of anesthesia significantly affects I-waves, which is why D-waves are generally monitored during TES.[6] An abnormal response from the target muscle group for stimulation would indicate a problem within the CNS and is an immediate indicator to neurophysiologists monitoring the status of the patient.

Several volume conductor models of electrical fields induced by magnetic or electrical stimulation have been developed. These models have been applied to explain where action potentials caused by TES are generated in the CST. These models are useful to explain how TES spreads through the neural structures involved in the generation of MEPs. Models using simple spherical geometric shapes of tissue layers as published by Suihko can help to explain the inverse relation between the latency time of D-waves recorded from epidural measurements and stimulation intensity as reported by Rothwell et al.[8] [9]

2.0 NEUROANATOMY

2.1 MOTOR CORTEX

The brain is the most complex organ of the body and has many different regions, as illustrated in Figure 1.

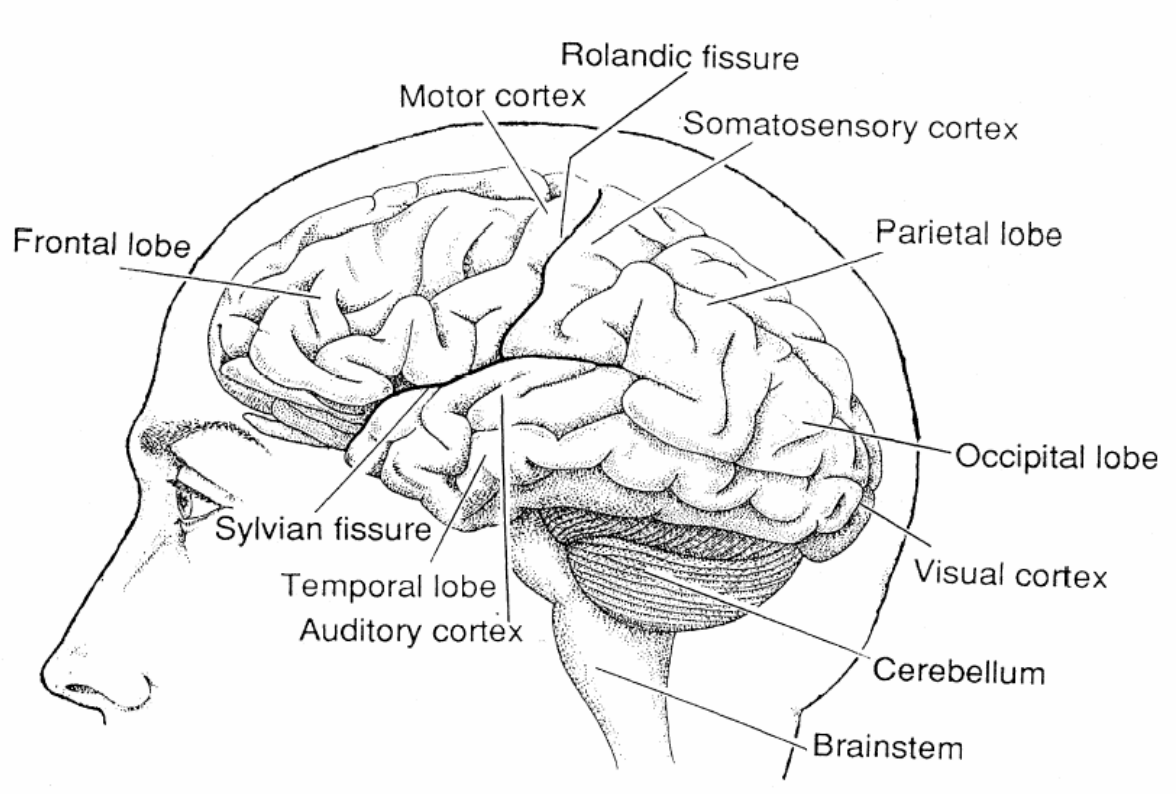

Figure 1: Regions of the brain. [18]

TES is used to stimulate the motor cortex to achieve a muscle response from the patient. This region is accessible for TES due to its location near the skull and this is why TES has been successful in the past.

The motor cortex is responsible for the generation of neural signals that activate muscles.[19] The motor cortex controls opposite sides of the body, in that the left hemisphere of the motor cortex controls movement in the right side of the body, and vice versa. Different parts of the body are controlled by different portions of the motor cortex with more brain cells designated for body parts that need higher precision. Effectors such as the face and hands have grater representation than the trunk or legs, for example. A schematic view of how the motor cortex is organized is shown in Figure 2 below.

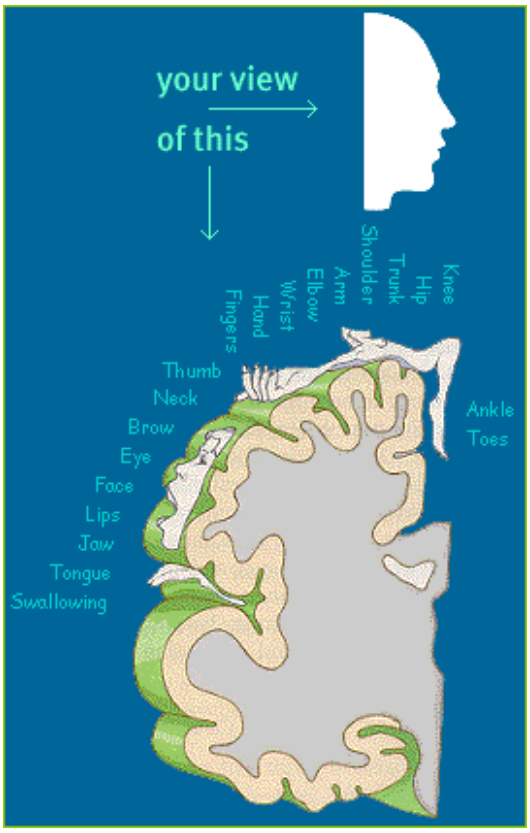

Figure 2: Locations of different body parts in the motor cortex. [18]

Due to the method in which TES is applied, via scalp electrodes, most of the muscle responses are found in the hand or wrist region. These hand responses are due to the relatively short distance the signal transmitted from TES must travel. Some MEPs are observed in the legs, but at higher stimulation amplitudes than those necessary for MEPs to be observed in the hands. The leg responses are predominantly evoked with the anode in the midline between the two hemispheres. The region between the hemispheres of the brain is filled with cerebral spinal fluid (CSF) which is highly conductive, and therefore the stimulation intensity does not decrease much as the signal passes through the CSF. In general the upper extremity MEPs are easier to generate than lower extremity MEPs. Stimulation of the neck and shoulders is generally not desired because it may cause more movement of the patient during surgery which could be harmful to the patient, but can occur do to the spread of current from TES.

2.2 AXONS AND MYELINATION

Nerve cells or neurons are the elementary cells of the CNS. Neurons are composed of a cell body, or soma, axons, and dendrites. A typical neuron is shown in Figure 3.

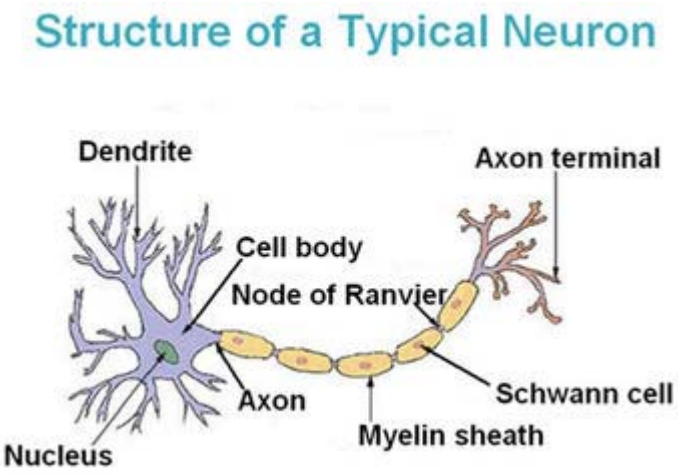

Figure 3: Typical neuron structure.[20]

Axons are long slender projections that arise from the soma and conduct electrical impulses at distal points from the cell body of the neuron [21]. Axons are the primary method of signal transmission throughout the nervous system. Axons are typically approximately one to two micrometers in diameter, but can span nearly half the length of the human body, as in the sciatic nerve.[21] There are two common types of axons, unmyelinated and myelinated axons. In unmyelinated axons, signal propagation will decrease in amplitude the farther it gets from the initiation point. A larger axon diameter will increase the conductance and propagation of action potentials because the internal resistance of the axon is less than a small diameter axon. Unmyelinated axons are common in invertebrates such as squid, where axon diameter is not limited since there are fewer functions necessary for survival of simpler organisms.

In vertebrates the complexity necessary for typical functions of the organism requires many more axons. These axons must be smaller in diameter to fit in the physical confines of the spinal cord, for example. In a myelinated axon, the signal is propagated by saltation between the Nodes of Ranvier, causing a faster conduction, as well as signal amplification to ensure the signal reaches subsequent neuronal populations. Due to the small diameter of axons, they could not conduct action potentials efficiently over long distances. Myelin sheets wrapped around the axons minimize the decreasing amplitude in action potential propagation.

Myelin is a phospholipid insulating layer surrounding the axons of most vertebrates which increases signal conduction along axons. [22] Myelin is formed by glial cells, which include Schwann cells on axons of the peripheral neurons and oligodendrocytes around the axons of the CNS. These glial cells wrap the axon in the phospholipid layer necessary to insulate the axon. The myelin does not cover the entire axon; there are gaps in the myelin to allow ion flow across the axon cell membrane to generate action potentials. These gaps in the myelin are known as Nodes of Ranvier, and the inter-nodal distances are proportional to the diameter of the axon.

The use of Cable theory to describe the function of myelinated axons has been common practice since Lord Kelvin developed it in the mid 1800s. Cable theory involves creating an equivalent circuit model to represent what occurs during depolarization and hyperpolarization of an axon. This circuit includes resistors, capacitors, and batteries to model the elements responsible for current flow in an excited axon.

An example of the electrical model of an axon is shown in Figure 4. The various components are as follows: V_e – external membrane potential, V_i – internal membrane potential, R_a – axial resistance, R – membrane resistance, C – membrane capacitance, V – resting

membrane potential. For the purposes of our research we are looking at a static case, and there is no time dependence. That is, we do not include capacitors in the circuit model shown above in Figure 4.

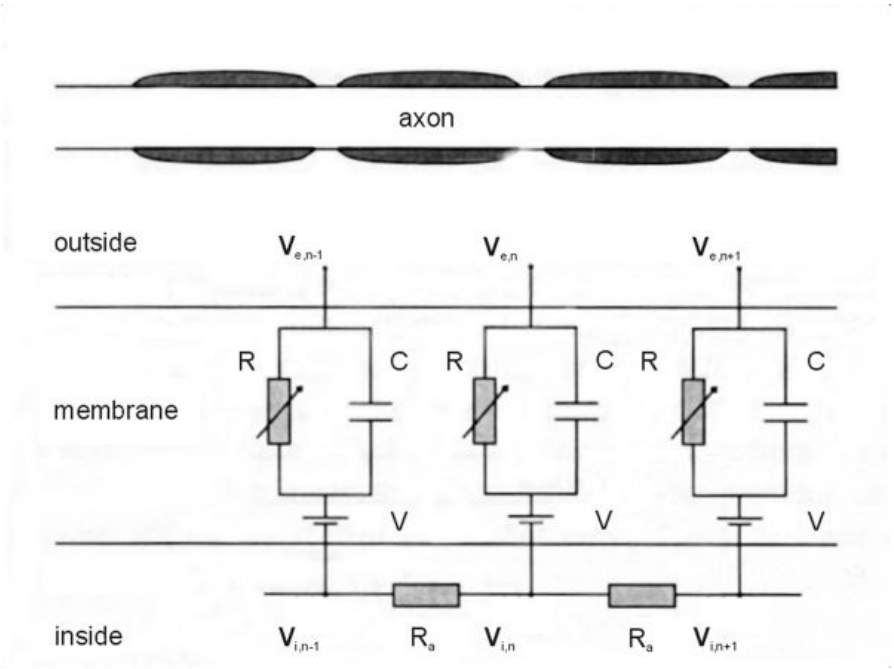

Figure 4: Circuit model for myelinated axon, V_e – external membrane potential, V_i – internal membrane potential, R_a – axial resistance of axon, R – membrane resistance, C – membrane capacitance, V – membrane resting potential.[23]

In order for action potential conduction to occur, there must be some way for the potential difference between the inside and outside of the cell to reach the membrane itself. The access points between the membrane and the outside solution are the Nodes of Ranvier, which are densely packed with sodium channels, which allow the influx of sodium ions to depolarize the membrane allowing action potentials to propagate.

Action potentials can also be triggered by a change in electric field; that is the potential on the outside of the axon is greater than that of the inside, or vice versa. This potential

difference induces a change in the equilibrium of charged ion concentrations to flow across the membrane, causing an action potential to be generated.

2.3 ACTIVATION FUNCTIONS

Activation functions (AF) express the driving force for activating an axon by extracellular electrodes. They indicate the depolarization of myelinated axonal membranes at sub-threshold level for action potential generation. The functions result from a cable model of axons of segmented cylindrical myelin sheets are described and defined by Rattay.[1] A positive value of the activation function implies depolarization of the membrane potential while a negative value indicates hyperpolarization of the membrane potential. Positive AF values correspond with a convex curvature of the potential function whereas negative values denote concave shapes. Maximum values of AFs indicate locations with the lowest stimulation threshold.

According to Basser, the transmembrane potential, V_m, when an electric field is present is[10]:

$$V_m + \tau \frac{\partial V_m}{\partial t} - \lambda^2 \frac{\partial^2 V_m}{\partial^2 x} = -\lambda^2 \frac{\partial E_x}{\partial x} \tag{1}$$

Where τ is the membrane time constant, λ is the length constant of the fiber, and E_x is the component of the electric field parallel to the fiber in question. The right side of the equation above is known as the activation function, and is an important factor in the excitation of axons. This equation only holds for unmyelinated fibers, but can be approximated for myelinated fibers

if the stimulation source is a distance greater than λ from the axon. This is the case for TES, since the length constant of a myelinated axon is usually less than one millimeter and the stimulation is being applied centimeters away from the axon.[10] The differential representation of activation functions is ideal for analytic calculations.

For steady-state stimulation when there are no capacitive effects, such as our model, where the change in potential does not change over distances on the order of the length constant the second and third terms will become negligible, yielding

$$V_m = -\lambda^2 \frac{\partial E_x}{\partial x} \tag{2}$$

This means that the change in electric field along the direction of the axon is the activation function. The activation function component of the stimulation is responsible for action potential generation in the axons.

How the activation function relates to the membrane potential can explained by Figure 4. Each segment is numbered by the index "n". Since myelin sheets are insulators, electrical currents through the neural membrane are confined to the locations at the Nodes of Ranvier. The resistance of the membrane is labeled R, in Figure 4. The trans-membrane current I_m at the n-th node is equal to the quotient of the membrane potential V and impedance across the membrane at the n-th node. This membrane impedance consists of resistor R (resistance of the membrane) and capacitance of the membrane, C_m. V is the difference between the intracellular membrane potential Vi_n and outside potential Ve_n. R_a denotes the intracellular resistor each segment between subsequent nodes. The resistors and capacitor of each segment are considered to have equal values and are hence not assigned an index.

When the differences of external voltages between subsequent nodes like ($Ve_{n+1} - Ve_n$) and ($Ve_n - Ve_{n-1}$) are equal to each other, then the intracellular currents of each segment are also equal to each other. Since the currents through the nodes of the membrane are constant, but in opposite directions, the net trans-membrane current result is zero. According to Ohms law when the current through R is zero, the internal and external voltages Vi_n and Ve_n will be equal to each other. Since there is no change in the net current through the membrane, the membrane potential stays unaltered during stimulation. This situation is present when the direction of the electrical potential is along the same direction of the axon, the so-called potential function, shows a linear increase or decrease.

When subsequent voltage differences over myelin sheets are not equal to each other, then the net trans-membrane current I_m is not equal to zero. When the direction of the current is from outside to inside the axon, hyperpolarization of the membrane occurs due to the relative decrease of the intracellular potential. Similarly, an outward directed current causes depolarization. Gradual increase of subsequent voltage differences along an axon at depolarization implies a concave shape of the potential function.

The AF is computed from second order differences of the potential function, and is similar to the difference of ($Ve_{n+1} - Ve_n$) and ($Ve_n - Ve_{n-1}$) which can be written as:

$$V_m = k * (V_{e_{n+1}} - 2V_{e_n} + V_{e_{n-1}}) \tag{3}$$

The division by the squared segmental length L of the second order difference is included in constant k.

Due to the definition of an activation function, as the 2nd finite difference along the direction of interest, it is logical to investigate radial and tangential activation functions, denoted RAF and TAF respectively. By looking at each component of the activation function we are able to see what components are responsible for stimulation during TES. The decision to examine RAF and TAF is also influenced by physiology. The CST runs radially through the brain; while the cortical axons spread in tangential directions, parallel to the skull. The CST and cortical axons are both responsible for activation function generation. Since our model is a simplified case, we chose to examine RAF and TAF individually to understand how the CST and pyramidal cells may be stimulated individually during TES.

3.0 THEORETICAL AND NUMERICAL MODELS

3.1 POISSON'S EQUATION

We assume that our model is quasi-static. This means there is no time dependence for the build up of current. We also assume all the tissues act resistively only; there is no capacitive property associated with any of the layers of the head. TES frequencies are low enough to allow for these assumptions to be valid. This allows for a much more simplified look at the way voltage and current move through each layer of the head. Under the quasi-static assumption, the electric field, $\overline{E}$, is given by:

$$\overline{E} = -\overline{\nabla}\Phi \tag{4}$$

where Φ is the electric potential.

We have $\overline{J}$, the current density given by:

$$\overline{J} = \sigma\overline{E} + \overline{J_s} \tag{5}$$

where $\overline{E}$ is the electric field created by the stimulating electrode in our model and $\overline{J_s}$ is the impressed current density, which is caused by bioelectric sources in the tissues. This impressed

current density is necessary so current will flow through both the volume conductor and the source of the current, which in this model is the stimulating electrode. [11] Since the source of the current, the TES stimulation, is outside of the volume conductor and the current from the neural activity is much smaller than the stimulation current we have:

$$\overline{J_s} = 0 \tag{6}$$

Maxwell's equations describing electromagnetic systems are given by: [11]

$$\overline{\nabla} \times \overline{E} = -\frac{\partial \overline{B}}{\partial t} \tag{7}$$

$$\overline{\nabla} \times \overline{H} = \overline{J} + \frac{\partial \overline{D}}{\partial t} \tag{8}$$

$$\overline{\nabla} \cdot \overline{B} = 0 \tag{9}$$

$$\overline{\nabla} \cdot \overline{D} = q \tag{10}$$

with $\overline{E}$ as the electric field, $\overline{B}$ as the magnetic flux density, $\overline{H}$ as the magnetic field, $\overline{J}$ the current density mentioned earlier, and $\overline{D}$ is the electric displacement. The second Maxwell's equation, (Eq. (7)) can be modified by taking the divergence of both sides giving:

$$\overline{\nabla} \cdot (\overline{\nabla} \times \overline{H}) = \overline{\nabla} \cdot (\overline{J} + \frac{\partial \overline{D}}{\partial t}) \tag{11}$$

However the displacement current, $\frac{\partial \overline{D}}{\partial t}$, is zero because the system does not depend on time. Furthermore, the divergence of a curl is zero by properties of the dot and cross products, so $\overline{\nabla} \cdot (\overline{\nabla} \times \overline{H}) = 0$.

Thus, we find

$$\overline{\nabla} \cdot \overline{J} = 0 \tag{12}$$

Now, taking the divergence of both sides of Equation (5) and substituting in Equations (6) and (12), the well known Poisson's equation is derived:

$$\overline{\nabla} \cdot (\sigma \overline{\nabla} \Phi) = \overline{\nabla} \cdot \overline{J} \tag{13}$$

In the interior of our model, there is the assumption of no source of current, since there is no significant source of current in the brain caused by neuron activity compared to the stimulation

current. Using Eq. (10), (12), and (13), then Poisson's equation simplifies further to Laplace's equation:

$$\overline{\nabla}^2\Phi = 0 \tag{14}$$

3.2 VOLUME CONDUCTION

Much of electrical engineering deals with circuits containing discrete components such as inductors, capacitors, and resistors.[13] Each of these components is part of the entire circuit, but each is considered a single element that contributes to how the circuit functions. The human body can be viewed as a type of circuit, where the components are distributed throughout the body, that is, there is a conductive medium that is continuous between all the components.[13] This type of circuit is called a volume conductor.

The volume conductor component properties are based on physical properties of the materials involved in the system; in this case the properties of the tissues of the human head were used. An assumption of linearity is imposed to allow for calculations to be made more efficiently. Since linearity is imposed, superposition properties must hold. These properties allow for the scaling potentials used in the models to be scaled and superimposed. In a real human body the tissue properties change with orientation (anisotropy), though this effect is small in the head.[13] Nerve bundles are anisotropic, but their effects on current distribution in the volume conduction are small because the volume of the bundles is small. The anisotropic effects

of the tissue orientation have been documented extensively in muscle fibers, which are not present in our model.

We may view the head as a volume conductor, where the different layers of the head have different conductivities. By definition, conductivity is the inverse of resistivity, given classically by the following equation:

$$\sigma = \frac{1}{\rho} \tag{15}$$

Recall Eq. (5):

$$\overline{J} = \sigma \overline{E} + \overline{J_s} \approx \sigma \overline{E} \tag{5}$$

The current, defined as the current flux through a given area, is given by the following equation: [14]

$$I = \int \overline{J} \cdot d\overline{A} \tag{16}$$

where $d\overline{A} = \overline{n} dA$ with $\overline{n}$ being the vector normal to the area over which the current density is being integrated.

3.3 FINITE ELEMENT METHOD

The Finite Element Method (FEM) is a powerful tool used to solve complex problems that can be explained with partial differential equations (PDEs). FEM was used to solve Poisson's equation, given in Eq. (12), which governs electrostatics for physical systems and was derived above from Maxwell's equations. A PDE involves a function and the partial derivatives of that function.

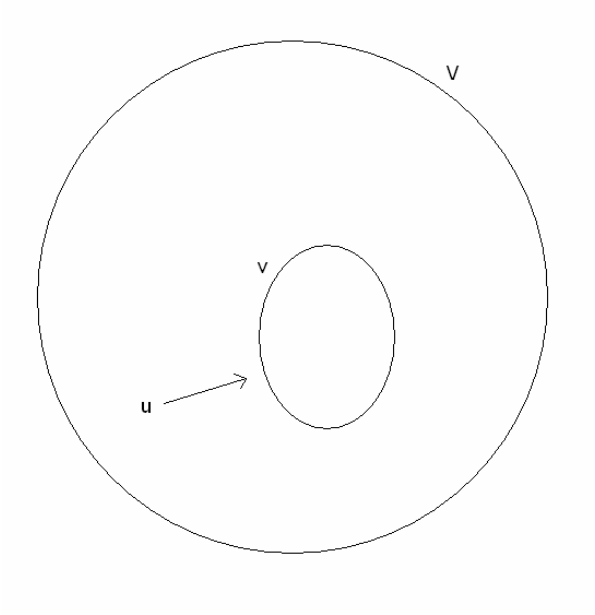

Figure 5: Set theory description.

The following derivative of the FEM is for a three-dimensional function space, Ω , but can be extended or reduced to fit any number of dimensions. The elliptical equation, a more general form of Poisson's and Laplace's equations, is used here to show the derivation:

$$-\nabla\cdot(\sigma\nabla u)+au=f \quad \text{in } \Omega \tag{17}$$

Where u is a scalar field, σ is the conductivity which in general is a matrix or tensor, a is a constant, and f is a source term. It is helpful to point out that when a is set to zero, the above equation becomes the well known Poisson's equation and when $f=0$, we have Laplace's equation.. Generalized Neumann boundary conditions (BCs) are assumed over the whole region.

The first step in the derivation is to project Eq. (17) onto a subspace of *V* where it is contained. This subspace has a dimension of *N*, and lies in *V* as well. To show this mathematically we use Eq. (17). We will use the following notations: d^3x is a volume integral, d^2x is a surface integral, and dx is a line integral.

Assume u is a solution to the elliptical differential equation above, first multiply the equation by a test function v, and integrate over Ω:

$$\int_\Omega \left(-(\nabla\cdot(\sigma\nabla u))\cdot v + a\cdot u\cdot v\right)d^3x = \int_\Omega f\cdot v d^3x \tag{18}$$

Now applying Green's Theorem (Integration by parts) we find:

$$\int_\Omega (v\nabla^2 u+\nabla v\nabla u)d^3x = \oint_{d\Omega} v\frac{\partial u}{\partial n}d^2x \tag{19}$$

Thus, Eq. (18) becomes

$$\int_{\Omega}\left((\sigma\nabla u)\cdot\nabla v + a\cdot u\cdot v\right)d^3x - \oint_{d\Omega}\sigma\cdot v\frac{\partial u}{\partial n}d^2x = \int_{\Omega} f\cdot v d^3x \tag{20}$$

The following boundary condition is applied:

$$\sigma\frac{\partial u}{\partial n} + qu = g \tag{21}$$

which is the generalized Neumann boundary condition. The use of the generalized Neumann boundary condition makes the rest of the derivation consistent. Dirichlet boundary conditions are a special case of the Neumann boundary condition.

When *q* and *g* are equal to zero we find:

$$\frac{\partial u}{\partial n} = 0 \text{ when } r = R, \tag{22}$$

with *r* being the interior region, and *R* being the radius of the boundary. By letting *r* tend to *R*, the solution for *v* will approximate the subspace *V,* which the solution was projected onto in the first step of the derivation.

Since we assumed Neumann boundary conditions on the outer boundary except the electrode locations we see Eq. (20) and (21) become:

$$\int_{\Omega}\left((\sigma\nabla u)\cdot\nabla v + a\cdot u\cdot v\right)d^3x - \oint_{d\Omega}(g - qu)\cdot v d^2x = \int_{\Omega} f\cdot v d^3x \tag{23}$$

The original problem can be restated as the following: Find *u* such that

$$\int_{\Omega}\left((c\nabla u)\cdot\nabla v + a\cdot u\cdot v\right)d^3x - fvdx - \oint_{d\Omega}(g-qu)\cdot v ds = 0 \text{ for all } v \tag{24}$$

Eq. (24) is referred to as the variational or weak form of the elliptical differential equation. The weak form of a differential equation is a form derived through the integration by parts of the equation, which is obtained by substituting the unknown function with a trial function in the governing equation and multiplying by a weighting function.[17] Recall that *u* and *v* are both in the function space *V*. We need to determine a finite-dimensional subspace $v_N \subset V$ where *u* and *v* are contained. This will project the weak form of the differential equation onto the finite-dimensional subspace v_N. Since Eq. (24) is true for all *v*, it is helpful to define *N* basis functions that span *v*, thus $\phi_i \in v_N$. An expansion of *u* can be made in the same basis by:

$$v(x) = u(x) = \sum_{j=1}^{N} U_j \phi_j(x) \tag{25}$$

This is referred to as the Galerkin's method, and substituting *u* and *v* we find

$$\sum_{j=1}^{N}\left(\int_{\Omega}(\sigma\nabla\phi_j)\cdot\nabla\phi_i + a\phi_j\phi_i)d^3x + \oint_{d\Omega} q\phi_j\phi_i d^2x\right)U_j = \int_{\Omega} f\phi_i d^3x + \oint_{d\Omega} g\phi_i d^2x \quad \text{for } i\ldots N \tag{26}$$

Using the following common notations for finite elements we see (26) becomes:

$$K_{i,j} = \int_{\Omega} (\sigma \nabla \phi_j) \cdot \nabla \phi_j d^3x \tag{27}$$

$$M_{i,j} = \int_{\Omega} a \phi_j \phi_i d^3x \tag{28}$$

$$Q_{i,j} = \oint_{d\Omega} q \phi_j \phi_i d^2x \tag{29}$$

$$F_{i,j} = \int_{\Omega} f \phi_i d^3x \tag{30}$$

$$G_i = \oint_{d\Omega} g \phi_i d^2x \tag{31}$$

Thus, Eq. (26) can be written in matrix form, which is much more compact, as:

$$(\vec{\vec{K}} + \vec{\vec{M}} + \vec{\vec{Q}})\vec{\vec{U}} = \vec{\vec{F}} + \vec{\vec{G}} \tag{32}$$

where $\vec{\vec{U}}$, is the solution matrix. It is not necessary to distinguish between $\vec{\vec{K}}$, $\vec{\vec{M}}$, and $\vec{\vec{Q}}$ or $\vec{\vec{F}}$ and $\vec{\vec{G}}$. This allows for Eq. (32) to be written in a much simpler form,

$$\vec{\vec{K}}\vec{\vec{U}} = \vec{\vec{F}} \tag{33}$$

FEM discretizes the subspace of interest by meshing it with a finite number of elements and nodes where the PDE is evaluated, as stated mathematically in Eq. (25). The elements of the mesh have a necessary condition that they must be continuous between the elements, ensuring that the entire subspace is covered. This makes the FEM approximation very close to the

analytical solution, especially when the mesh is refined. A refined mesh has more nodes, and as the number of nodes approaches infinity, the solution approaches the analytic solution. Typical elements utilized by the software are triangular or rectangular elements in 2D and pyramid or brick elements in 3D.

FEM can be summarized as the following: *A projection of the weak form of a differential equation onto a finite-dimensional function space.* [15][16]

4.0 METHODS – 2D VERSUS 3D

4.1 MODEL SPECIFICS

Due to the complexity of the model, FEM was chosen to perform the simulations instead of analytic methods. Closed form solutions for complex geometries are not easily calculated, whereas a numerical approximation can be made that is very close to the actual analytic solution. These numerical approximations can be calculated quickly and efficiently using the computer.

The proportions of the model were taken from an average human head with an assumed diameter of 16 cm. The different layers of the head, the scalp, skull, CSF, and brain were each given conductivities and thicknesses found in literature.[24][25][26][27] Table 1 shows the conductivities and thicknesses used in the standard TES model. Each of these layers was modeled as homogeneous to minimize computation time and allow for an understanding of the basic concepts involved in TES to be observed. The different layers can be seen in Figure 6.

Table 1: Conductivity values and layer thicknesses that were used in the 4-layer TES model.

Region	Conductivity (S/m)	Thickness (mm)
Scalp	0.4	5
Skull	0.015	7
CSF	1.4	4
Brain	0.15	64
Electrode	10000	5

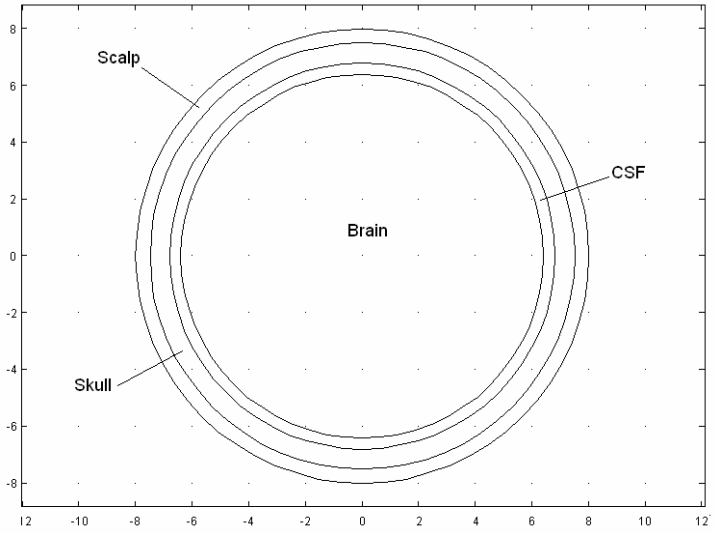

Figure 6: Layers of the head model.

A stimulating voltage of 100V was used in the simulations. This value was arbitrary as the system is linear and is scalable to achieve any voltage desired. The use of DC voltages in the simulations provides for generality of Poisson's equation over all frequencies since we assume the tissue conductivities have no dielectric components, i.e., no capacitive effects. The head is also assumed to contain no net free charge, which would indicate an unnatural voltage/current source in the body. This is a logical assumption due to the low-frequency of the pulses used in TES, and the fact that the stimulation current will be multiple orders of magnitude larger than any biologically generated current sources that may be present in the cell membranes.

One of the foremost questions that needed to be addressed concerned the outer boundary of the model. A physical representation was desired to model what would occur in a real person. The current must remain inside the head the whole time it is being applied to simulate current behavior in a real human head. Having current leap out of the scalp at arbitrary points is not physically possible, so boundary conditions (BCs) were chosen to take this effect into account. For the electrodes, where the voltage was to be applied, Dirichlet BCs were chosen. This form

of boundary condition allows the value of a function to be imposed on the boundary of the region.[27] Since the input is a constant voltage, Dirichlet BC's were chosen to stimulate the scalp regions covered by the electrodes, this allowed for modeling of the current to be applied directly to the scalp via the electrodes. The electrodes were set to Dirichlet BCs without loss of generality because the volume conduction system is linear. This boundary setting allowed for current flow into the model via the stimulating electrode, and out through the return electrode. The outside of the model was given Neumann BCs, $\nabla\phi = 0$, where ϕ is the electric potential; to ensure all the current of the system was contained inside the model. Neumann BCs allow the normal derivative of the function to be imposed on the boundary of the region being examined.[28] The Neumann BCs forced the current to remain inside the head region when a voltage was applied to the electrodes. These choices of BCs approximate the real physical attributes of a human head most closely for the simulations performed.

4.2 VALIDATION OF SIMULATIONS

Three-dimensional (3D) models will approach reality of TES better when compared to two-dimensional (2D) models and should be considered as first choice. However, 2D simulations are less complex to design and take a very small amount of time to calculate when compared to 3D simulations. A comparison between 2D and 3D models is necessary to elucidate differences in the computed results. By understanding the systematic errors incurred, we are able to perform 2D simulations and infer the results of a 3D simulation. This saves time and computational resources. To our knowledge, no such data about the systematic differences between 2D and 3D simulations is published for TES-models of the human head. This thesis provides an overview of

the systematic errors between potentials, electric fields, and activation functions referring to stimulus thresholds that one may encounter using a 2-D model instead of 3D.

A 2D circular model and 3D spherical model were created to show the systematic errors between simulations of 2D and 3D models. These models were created using simple geometries to gain a better understanding of these systematic differences between the simulations. To ensure a good comparison between the 2D and 3D models, the central slice of the 3D model was compared to the 2D model. The central slice had the same dimensions as the 2D model, so the effects of the 3rd dimension would be easy to compare with the 2D case. The geometry does not change significantly for small perturbations from the central slice; as shown in Figure 7.

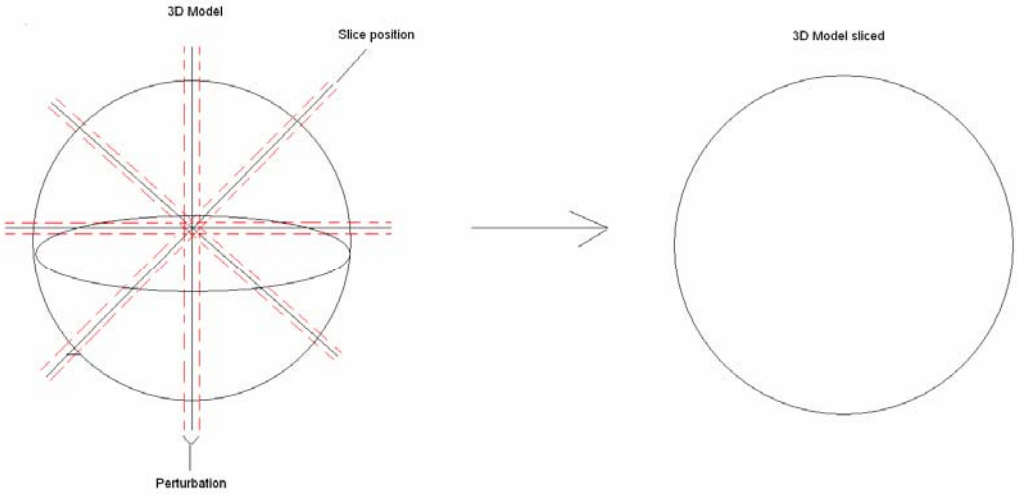

Figure 7: Slices of a simple model to verify the comparison between 2D and 3D. The solid lines are slices to be examined; the dashed lines are perturbations around the main slices.

Using slices that are a large distance from the center slice in the spherical model will yield very different results and there will be a significant increase in the error between the 2D and 3D

cases. This error will be caused by the geometric changes between the 2D and 3D cases. If we look at the central slice of a 3D spherical model and compare it to the 2D circular model we created, the geometry is exactly the same. But if we examine a slice that is a large distance to one side or the other in the 3D spherical model, the geometry will be different between the 3D case and its 2D representation as shown in Figure 8.

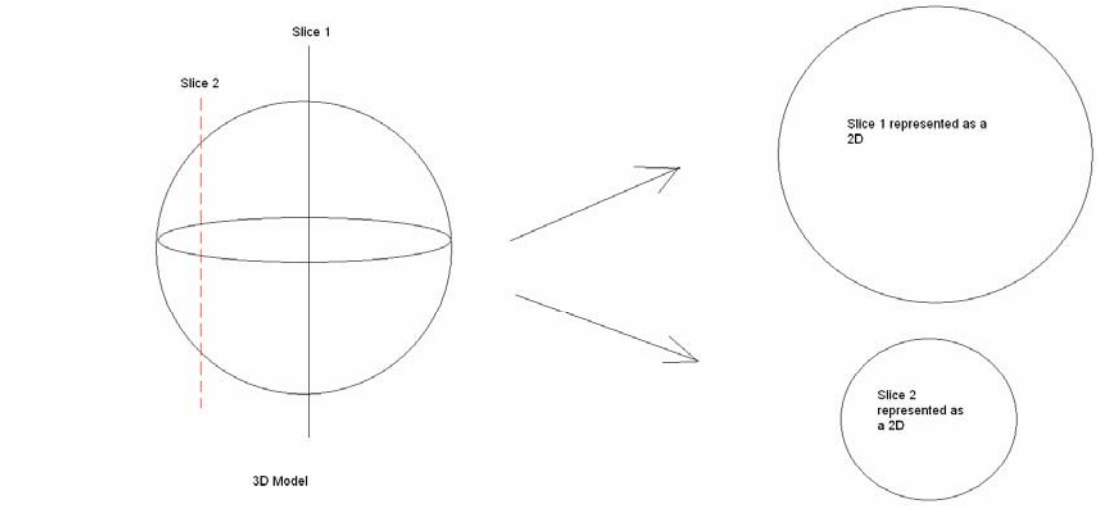

Figure 8: Large perturbations in slice positions yield very different results when a 3D model is to be represented as a 2D case.

An important reason to use 2D simulations is because there is no way to examine the potential distributions, electric fields, or activation functions of a 3D model without "slicing" it, which is essentially looking at a 2D slice of the 3D model. In most cases a central slice is of

interest and by knowing the differences between the 2D and 3D simulations we can focus primarily on 2D models with much less computational complexity.

Due to the constraints of 2D, potential values can only be calculated in one plane, such as the xy-plane. Thus, it is assumed that the values measured in 2D models will be higher than those in 3D models. This is because in a 3D model the potential can spread out in the third direction, such as the z-direction thus dissipating more rapidly than in a 2D model. To show the systematic differences between 2D and 3D models, a simple case was designed with only two stimulating electrodes and a single layered conducting disk between them, see Figure 9. The conductivity of the disk must be different than the conductivity of the electrodes to see a difference in the distribution of the potential values. The disk was arbitrarily set to the same conductivity of brain.

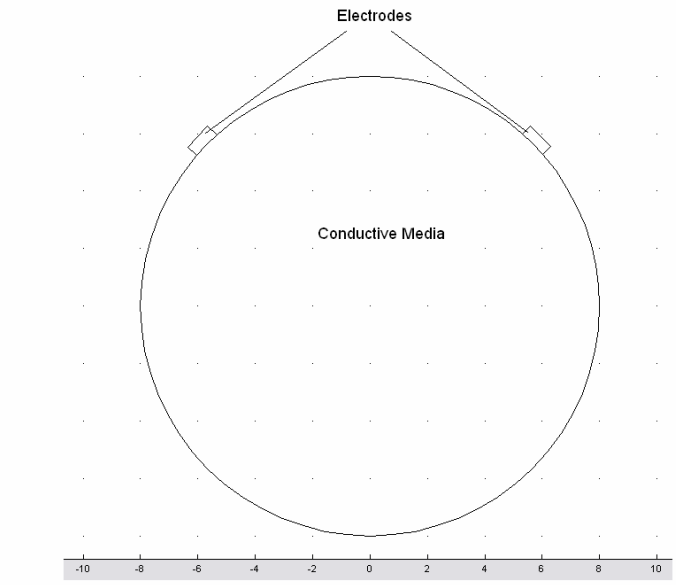

Figure 9: Simple case of TES model.

TES is modeled more closely using a more realistic four layer model that included the scalp, skull, CSF layer, and brain, see Figure 10. The ventricles shown in the model are representations of the CSF filled ventricles found in a real human head. The ventricles modeled are not to scale because scale sized ventricles caused the FEM model to become unstable.

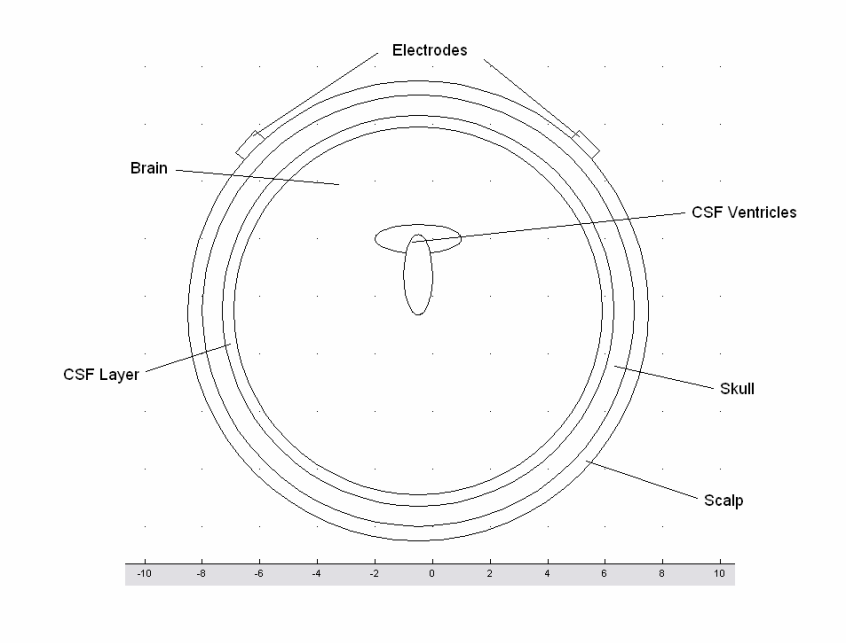

Figure 10: Schematic of the model.

In order to measure the potential at various points in the model a grid was constructed to plot measuring points throughout the model. A variety of measuring grids were tried by changing the number of points where the potential was evaluated along a line extending radially from the center of the sphere to the outer layer. The number of points was spaced ranging from a

tenth of a millimeter to one centimeter. This spacing can be thought of as the resolution of the model. A resolution of one millimeter was chosen because this grid allowed for smoother curves to be calculated while the computation time was reasonable. A higher number of points, or resolution, increased the computational time dramatically, doubling the resolution resulted in up to four times longer computation time. Having the one millimeter resolution yielded a matrix with 81 rows by 361 columns; with the starting point counted as the end point again to make sure all points were included. The measuring points were defined by plotting a point every millimeter along a line extending radially from the center of the model to the surface. A line extending radially from the center of the model to the surface at every degree from zero to 360 was plotted, so all the points in the model are covered and have at least one millimeter resolution desired for the simulations. The grid of a typical model is shown in Figure 11.

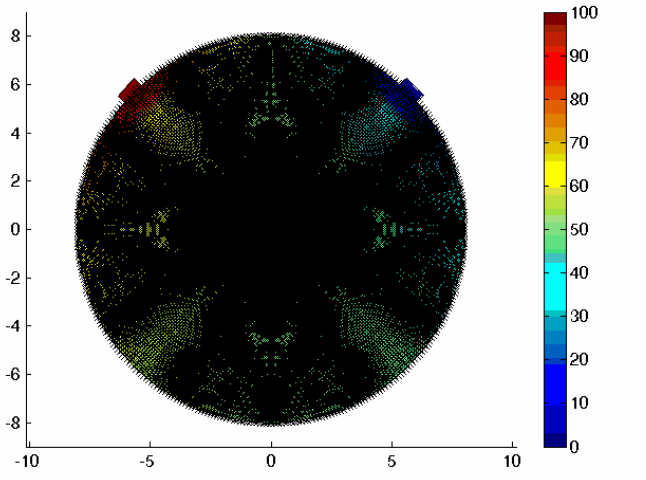

Figure 11: Grid of measuring points in the models.

The electric potential was calculated using Femlab 3.1, the electric field and radial and tangential activation functions were calculated from these values. This data was then plotted to determine what was happening in the models. An algorithm that computes radial and tangential electrical fields and radial and tangential activation functions by first and second order differences was designed. The radial electric field was calculated by taking the difference between the potential values and dividing by the length of the separation between the two points being evaluated along a line extending radially from the center of the model to the exterior. The tangential electric field was calculated taking the difference between potential values at a specified radius and dividing by the distance separating the points being evaluated. The radial and tangential activation functions were calculated in a similar manner as the radial and tangential electric fields respectively, but the difference was taken between the electric field values instead of the potential.

In the radial direction the difference grid is 1mm. For the tangential orientation, corrections are made for the tangential intervals which are linearly related with the radius to the middle point of the sphere (3D) or disk (2D). For suppression of large variances in the results from the FEM models, the algorithm performs a triangular low pass finite impulse response (FIR) filter with Full Width Half Maximum (FWHM to be explained later) equal to 7mm for the tangential direction. This value is empirically chosen as a compromise between spatial resolution and noise suppression. The width of the peaks of the activation functions and electrical field functions undergo negligible widening within 5%, which is below the variations introduced by the computational noise. Appendix A contains the code for the models.

Radial activation functions are calculated using points measured from the center of the model to the outside of the scalp layer. The 2^{nd} finite difference of these points is the RAF. By

examining each trajectory from the middle to the exterior we get a picture of how the distribution of the RAF spreads through the model. The RAF is plotted as a function of angle in Figure 12. Recall that the negative electrode is at the 135 degree location and the stimulating electrode is at the 225 degree location.

(a) (b)

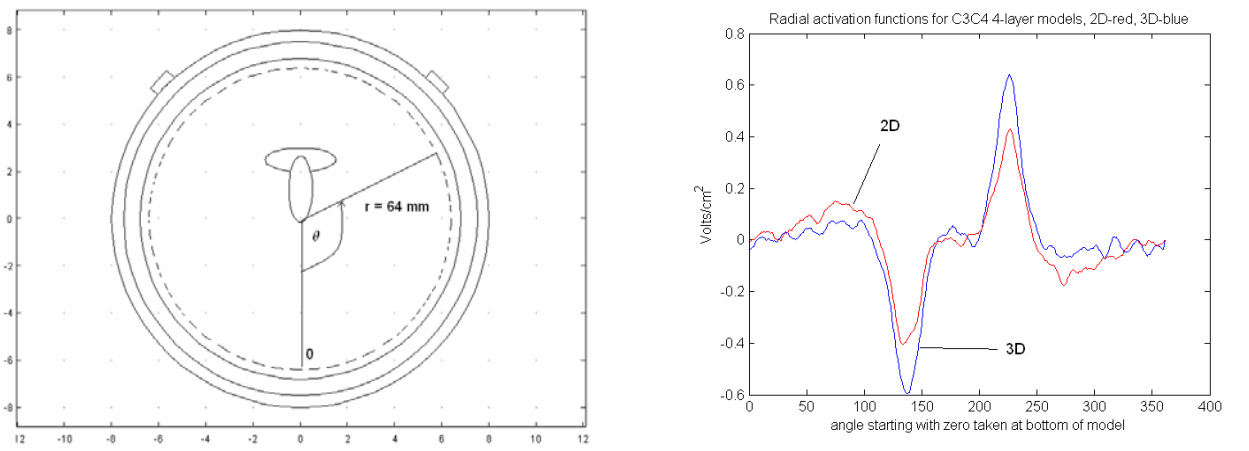

Figure 12: (a) The location where the RAF was calculated. (b) Plotting of the RAF at cortical level.

Tangential activation functions are calculated at a set radius, using points next to each other on that radius to find the 2nd finite difference between those points. This is the definition of the TAF. An examination at cortical level is the most pertinent since that is where the stimulation is going to occur. The TAF is plotted as a function of angle around the circle or sphere as shown in Figure 13.

(a) (b)

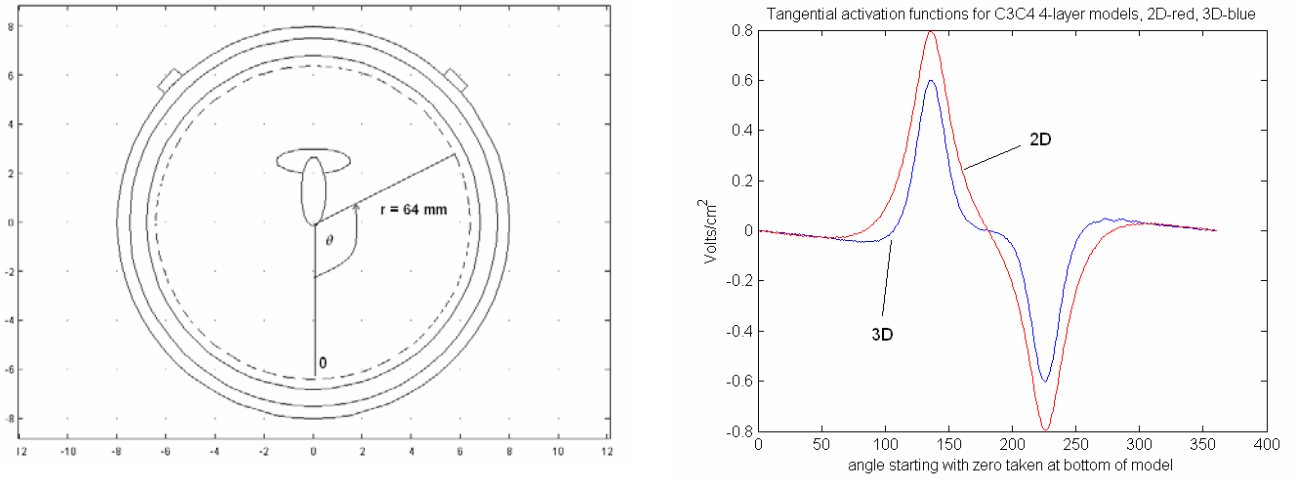

Figure 13: (a) The location where the TAF was calculated. (b) Plotting of the TAF at cortical level

4.3 ELECTRODE ORIENTATIONS

A variety of electrode orientations were simulated in the models. These different orientations were similar to montages used in clinically, i.e., the locations chosen to model are classified according to the 10-20 system of electrode placement. In the 10-20 system, each lobe in the brain has a letter to identify it, and a number is assigned to each hemisphere, (even for the right,

odd for the left) to identify the location of the electrode at that point.[30] If an electrode is placed directly between the hemispheres of the brain it is given the letter ‘z’ to signify it is not on either hemisphere. These 10-20 electrode locations give a general mapping of the outside of the human head with respect to the inside, which allows for consistent electrode placement for recording or stimulation via electrodes on the scalp.

The electrode orientations simulated were C3-C4, C3-CZ, CZ with an electrode directly opposite on the sphere (diametric), C3 with epidural stimulation, and finally C3 with cortical stimulation. The diametric simulations were performed to help understand the systematic differences between 2D and 3D using a symmetric model. Epidural and surface cortical stimulation are used in the treatment of pain and cortical mapping.[31]

When plotting the results of the electric potential and fields, 2D models with and without ventricles are presented, as well as plots of the center slice of 3D models, along with the 3D surface plots. Contour lines are plotted in the 2D models to show equipotential lines throughout the model. These equipotential lines are not shown in 3D models because the software was not able to plot contour lines efficiently for electric potential in 3D models. This problem was deemed unimportant because if a slice plot of the 3D model is taken, the contour lines shown would be similar to those seen in the 2D models.

Plots are shown for the C3-C4 electrode orientation, all of the orientations can be found in Appendix B: Electrode Orientations.

C3-C4 Orientation:

The potential values for the 2D model with the C3-C4 electrode locations are shown in Figure 14. The equipotential lines in the model show the effects of the different layers in the model. The high resistive properties of the skull are evident by the close proximity of the equipotential lines inside the electrodes. The CSF layer has a higher conductivity which is evident by the large spaces between the contour lines in the CSF layer. The ventricles in the middle of Figure 14 are set to the same conductivity as the brain, but were changed in a parameterization to see what the effects are of the CSF ventricles in the middle of the brain between the hemispheres of the brain.

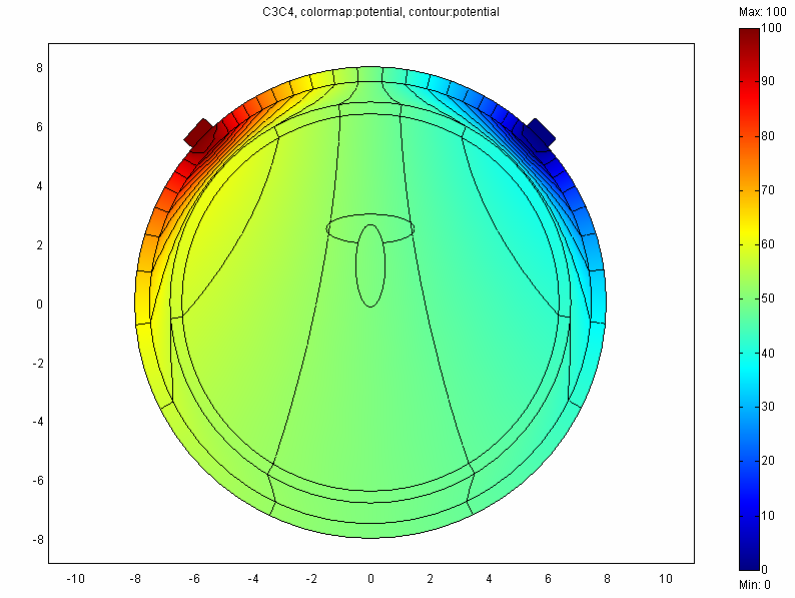

Figure 14: 2D potential model with C3-C4 electrode placement and no ventricles.

Figure 15 shows the electric field in the C3-C4 electrode montage with the average scalp, skull, and CSF thickness. The higher fields are shown at the top of the color scale, and occur in the skull since that is where the highest potential difference occurs.

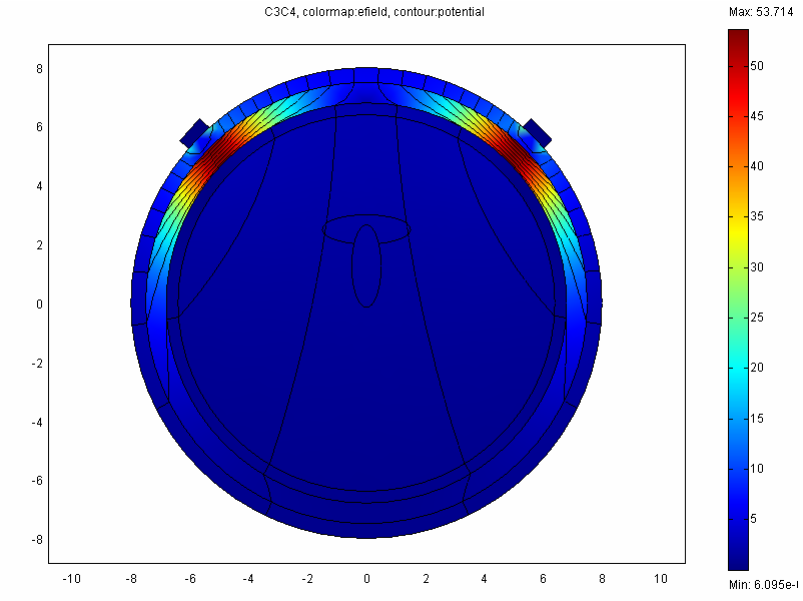

Figure 15: 2D electric field model with C3-C4 electrode locations, no ventricles.

The 3D model potential is shown in Figure 16 looks very similar to that of the 2D potential shown above in Figure 14. Although the contour lines are not shown in the 3D model they looked similar to those shown in the 2D models.

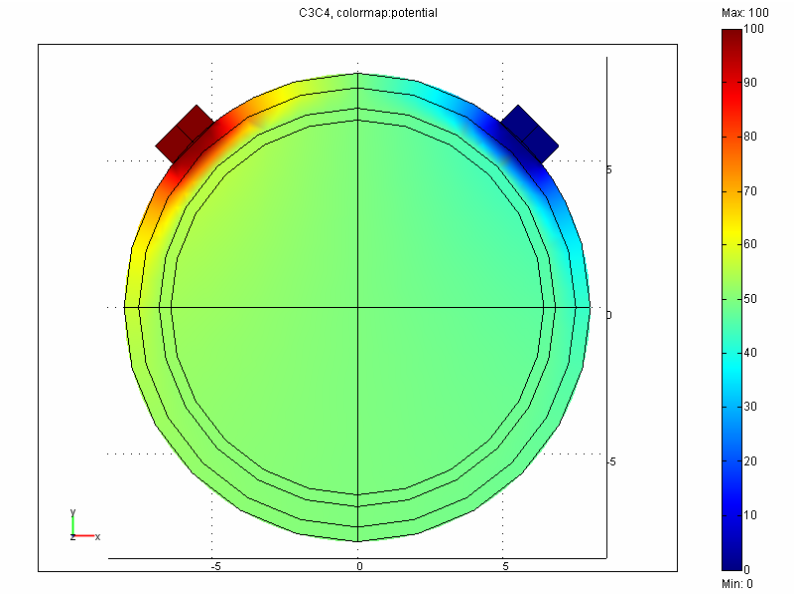

Figure 16: 3D potential model with C3-C4 electrode placement and no ventricles, center slice shown.

The electric field for a 3D model with the C3-C4 electrode locations is shown in Figure 17. Just as in the 2D case the highest electric field values are in the skull, though the values are not as large as the 2D because the electric field spread out in the 3rd dimension.

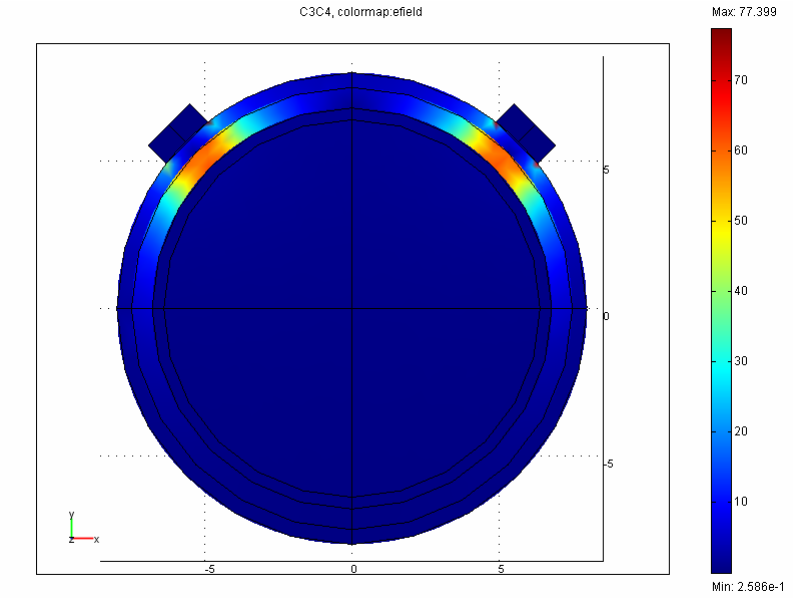

Figure 17: 3D electric field model with C3-C4 electrode locations, no ventricles.

A view of the potential on the surface of the 3D model is shown in Figure 18. The spread of potential is very uniform across the surface of the model because of the conductivity value set in the boundary conditions.

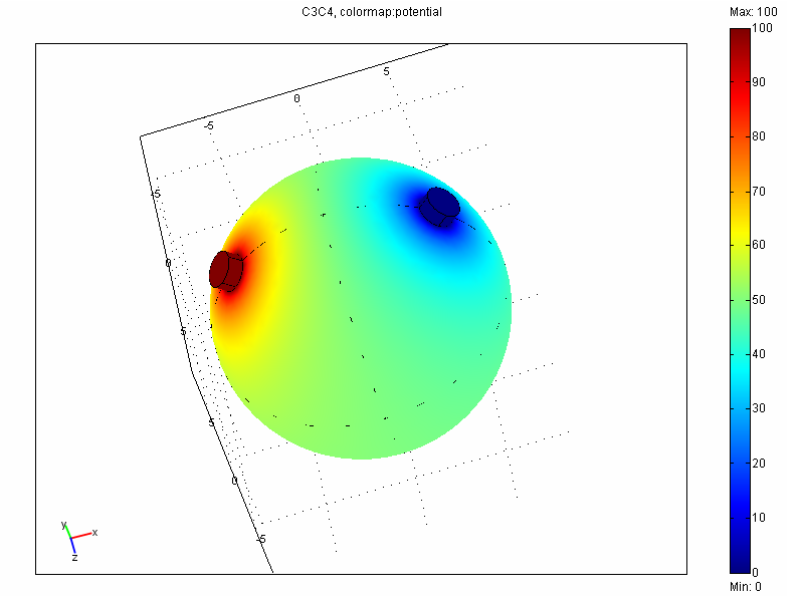

Figure 18: 3D surface potential for C3-C4 model.

Figure 19 shows the surface electric field for the 3D model. The high electric field observed where the electrode attaches to the scalp is due to the drop in potential across the scalp from the highly conductive electrode.

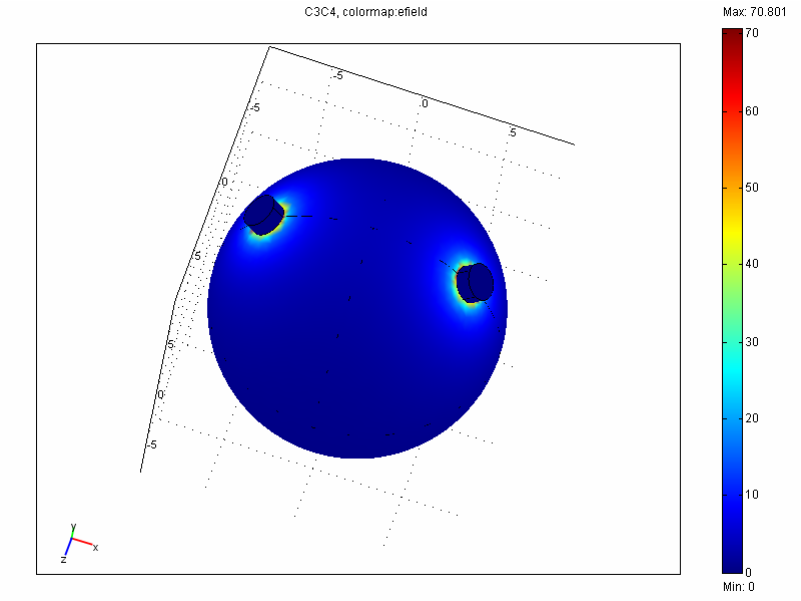

Figure 19: 3D surface plot of electric field for C3-C4 electrode locations.

4.4 MODEL PARAMETERIZATIONS

The C3-C4 locations are the most commonly used for TES in clinical applications, and multiple parameterizations have been performed with this orientation. A variety of parameterizations such as scalp, skull, and CSF thicknesses are tried, as well as adding CSF filled ventricles to better approximate some of the inhomogeneities within the skull. In models without the CSF ventricles, the conductivities of the ventricles were set to match the conductivity of brain. This

allows for a direct comparison of how equipotential lines are affected by the higher conductivity of CSF.

The parameterizations performed in the simulations were a homogeneous model, adding CSF filled ventricles in the middle of the brain, scalp, skull, and CSF parameterizations. The homogeneous model was created using a single conductor between the electrodes on the scalp. The conductivity of the homogenous model was set to the same conductivity of brain in the layered simulations with a value of 0.15 S/m. The CSF ventricles were set to the same conductivity as brain in the rest of the parameterizations to ensure the effects seen would only be from the differing thicknesses in the layers. The scalp parameterizations were performed by reducing the thickness of the scalp layer by half and not changing the thickness of the skull and CSF layers. The skull and CSF parameterizations were performed in the same manner. This allowed for the observation of the effects from each layer individually to see the impact from the layers on the model. The layer thicknesses for the parameterizations are shown in Table 2.

Table 2: Model parameterizations

Layer in the model	Scalp Parameterization	Skull Parameterization	CSF Parameterization
	Thickness (cm)	Thickness (cm)	Thickness (cm)
Scalp	0.5 to 0.25	0.5	0.5
Skull	0.7	0.7 to 0.35	0.7
CSF	0.4	0.4	0.4 to 0.2

The homogeneous parameterization model is shown in Figure 20. The potential drop is not nearly as large at the cortical level corresponding to inside the electrodes as it is in the layered models.

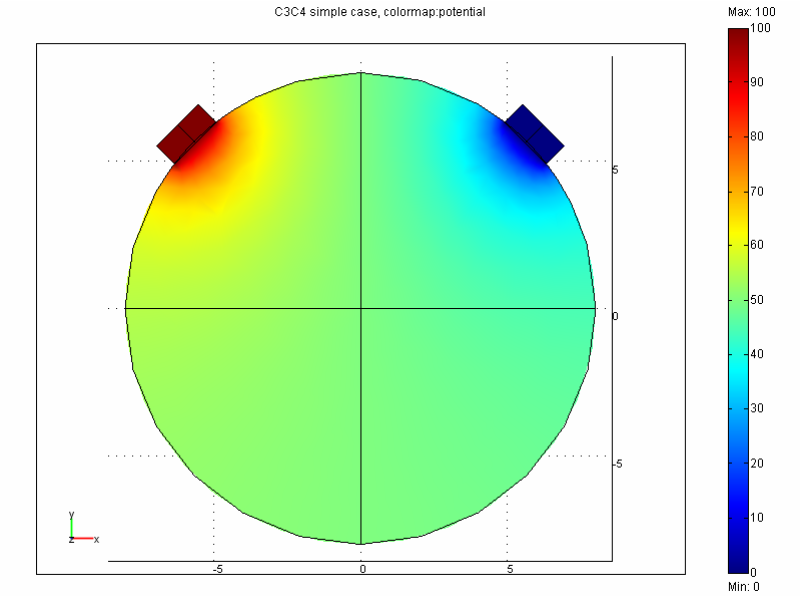

Figure 20: Electric potential for the homogeneous model.

Figure 21 shows the electric field for the homogeneous case. The largest electric fields occur at the points where the electrode joins the homogenous region. The corner points show the highest electric field, the large magnitude of the value may be caused by the significant difference between the radius of the electrode and the diameter of the model. The small radius of the electrode will have a larger potential drop than that of the sphere, resulting in larger values at the points where the electrode meets the model.

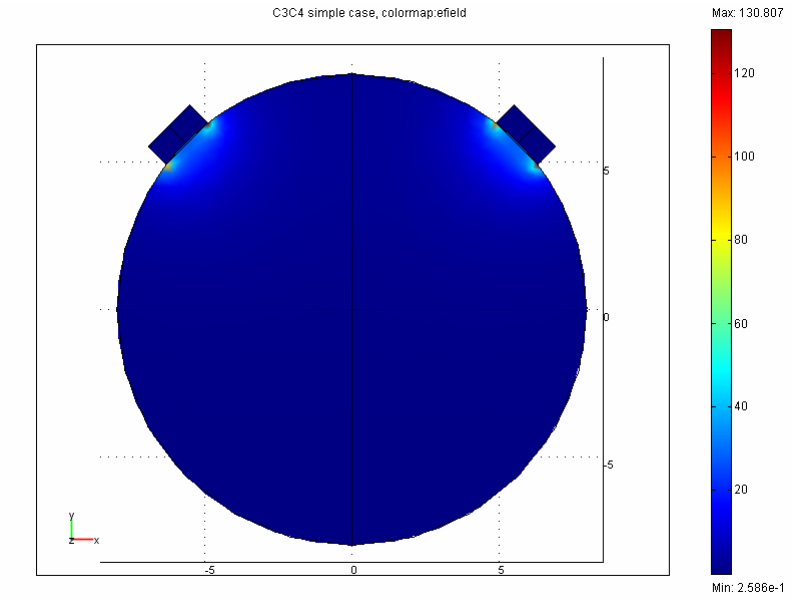

Figure 21: Electric field for the homogeneous model.

Examining Figure 22 we see how the ventricles filled with CSF affect the path of the equipotential lines. The higher conductivity causes the equipotential contour lines to bow around the ventricles.

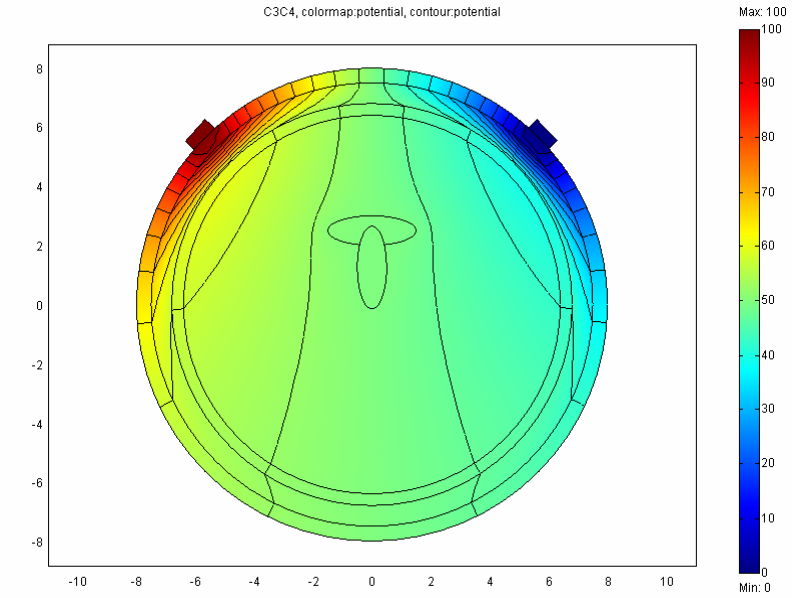

Figure 22: 2D potential model with C3-C4 electrode placement with ventricles.

The electric field in the CSF layer and CSF filled ventricles is very low because of the high conductivity. This is shown in Figure 23; notice the slightly higher electric field values that surround the ventricles. This is due to the change in conductivity between the brain and CSF ventricles.

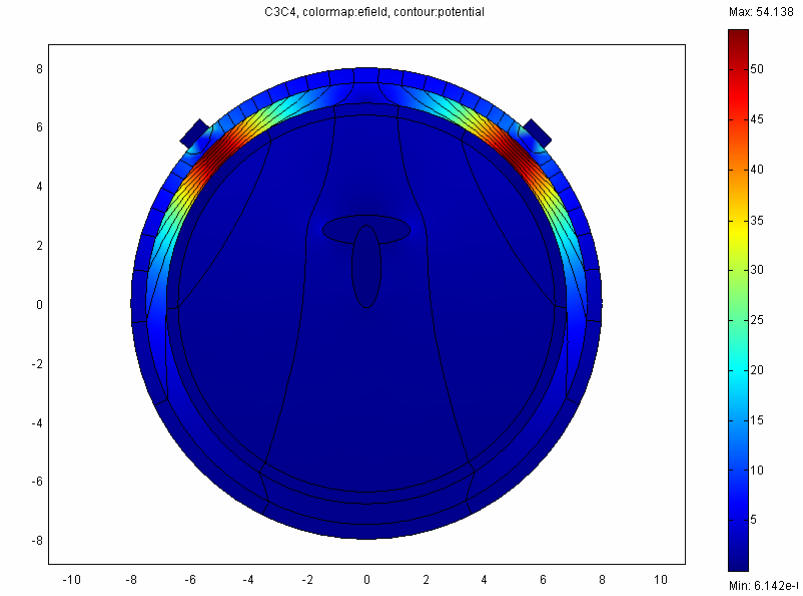

Figure 23: 2D electric field model with C3-C4 electrode locations with ventricles.

Figure 24 shows the scalp parameterization. The general dispersion of electric potential is very similar to the model using average values for the thickness of the scalp, skull, and CSF layers, in Figure 14.

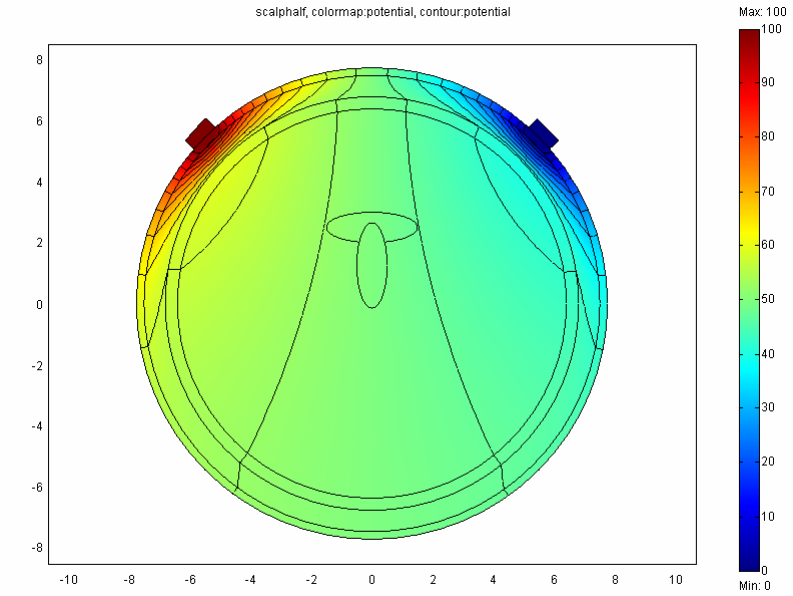

Figure 24: Electric potential for scalp parameterization.

The electric field for the scalp parameterization is shown in Figure 25. Again the highest gradient occurs in the skull layer, just as in the standard C3-C4 model.

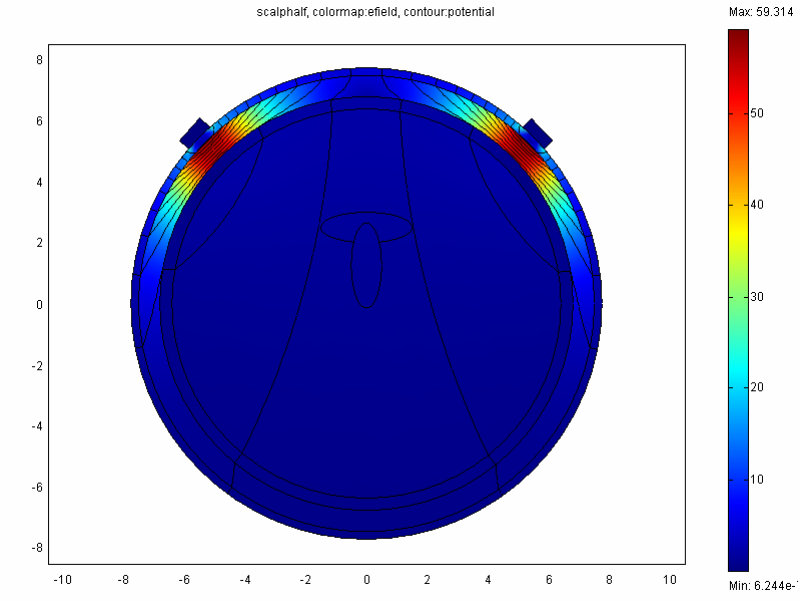

Figure 25: Electric field for scalp parameterization.

The skull parameterization is shown in Figure 26. The thinner skull layer allows more potential to traverse the skull, causing higher values in the brain.

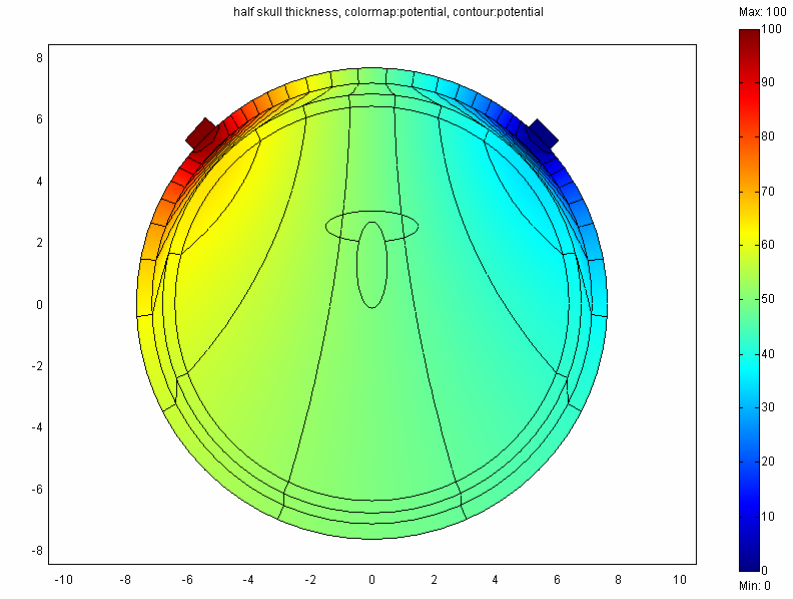

Figure 26: Electric potential for skull parameterization.

Figure 27 shows the electric field in the skull parameterization model, and again the highest field values are in the skull layer.

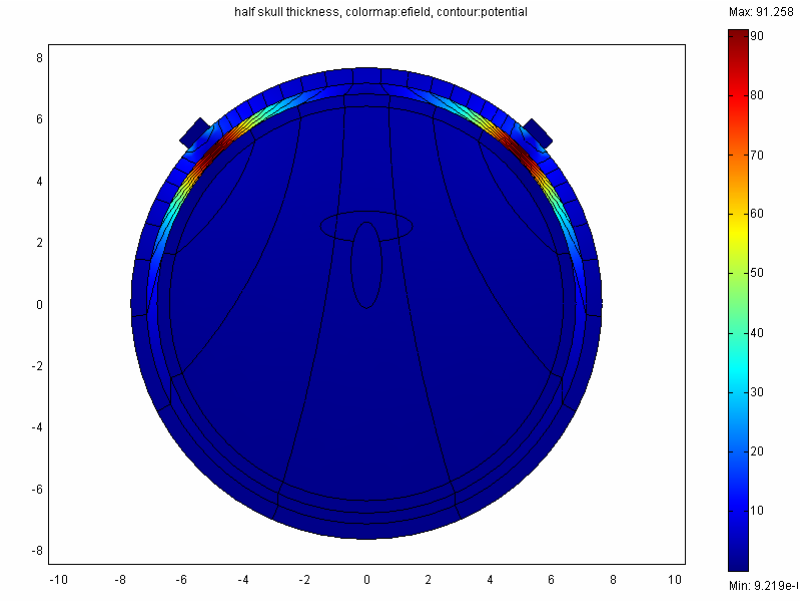

Figure 27: Electric field for skull parameterization.

Reducing the thickness of the CSF layer by half is shown in Figure 28. The thin CSF layer impact is not very noticeable due to the high resistive properties of the skull which is much thicker than the CSF layer in this particular model parameterization.

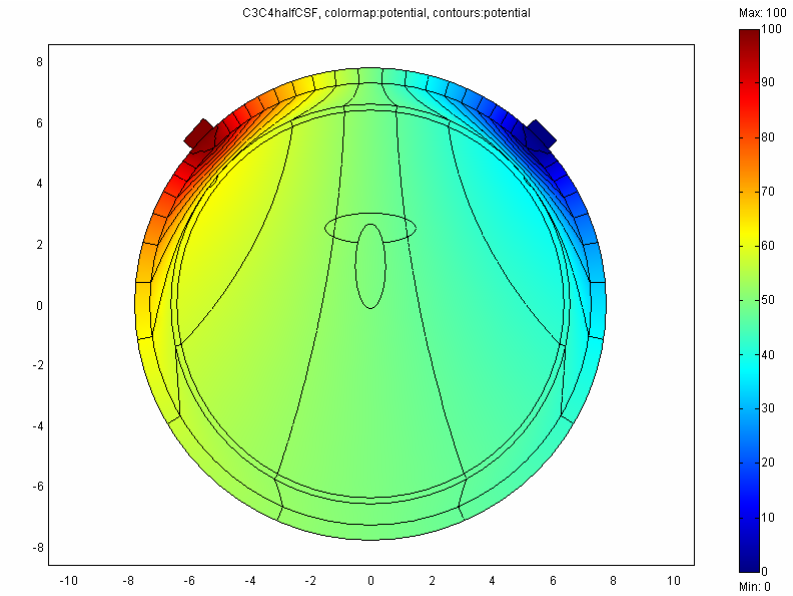

Figure 28: Electric potential for CSF parameterization.

Figure 29 displays the electric field for the CSF layer parameterization model. The highest field still occurs in the skull, and is lowest in the CSF layer.

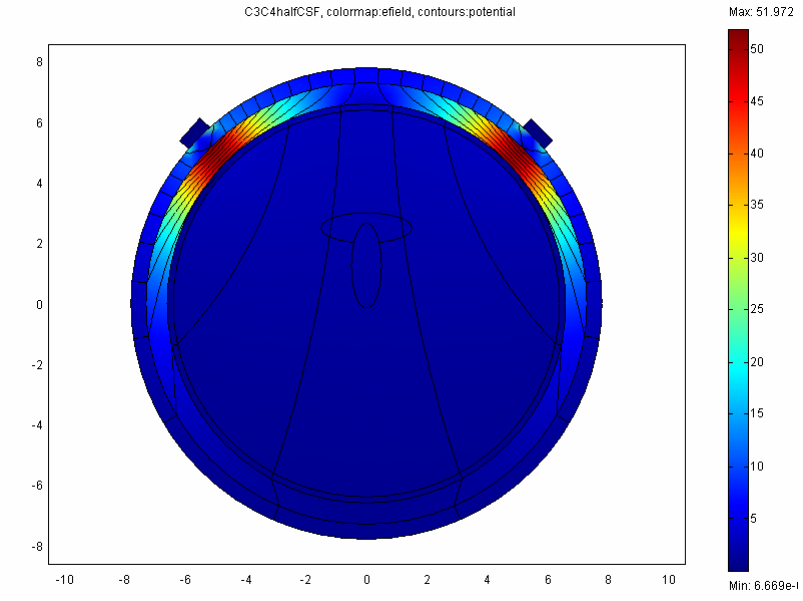

Figure 29: Electric field for CSF parameterization.

5.0 QUANTITATIVE RESULTS

5.1 POTENTIAL

In order to understand the systematic differences between the calculations in 2D and 3D models we first examined a simple case. The potential values calculated in the homogeneous model with C3-C4 electrode locations, denoted C3-C4hom, is shown in Table 3.

Table 3: Potential values for 2D & 3D homogeneous models at cortical level.

Electrode montages	Inside stimulating electrode for C3-C4			At max value		
	Amp 2D (V)	Amp 3D (V)	Error in %	Amp 2D (V)	Amp 3D (V)	Error %
C3-C4hom	72.75	65.857	10.5	73.069	65.986	10.7

A comparison of the potential values in the model is examined first because electric fields and activation functions are both calculated from the potential values. From Table 3 it is easy to see that the potential values between the 2D and 3D models varied by a little more than 10%. This error was computed by taking the potential of the 2D model and subtracting the 3D model potential value, then dividing the whole quantity by the 3D potential value. The decision to use the 3D model values for the division was because we assumed the 3D model better approximates a real head. The 10% error is not a significant variation and would indicate that a 2D model

would be satisfactory for estimating the potential in a 3D model. The potentials measured in the 3D model are lower than those in the 2D model, which is logical due to the extra dimension for the potential to disperse into. The potential in a 2D model is forced to follow the same boundary conditions as in 3D, but the values are restricted to a plane so they must change more rapidly to satisfy the boundary conditions, see Figure 30.

(a) (b)

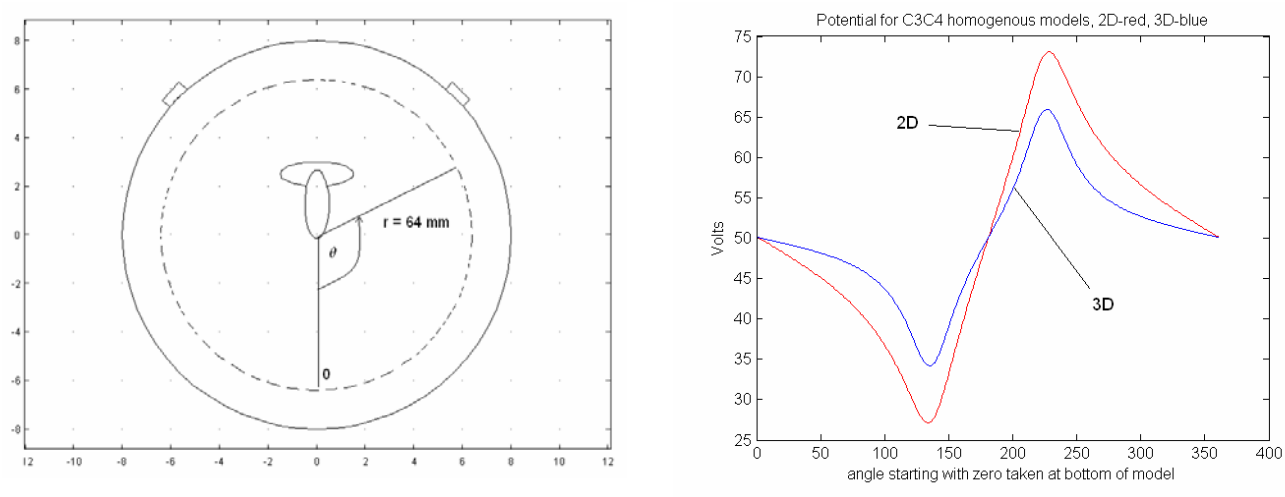

Figure 30: (a) The location where the potential was calculated. (b) The potential values in homogeneous models.

When we compare the homogeneous models with the more complex four layer models we see noticeable effects of the different layers, namely the skull layer acting as an insulator in the layered models, reducing the magnitude of the potential measured in the cortex. Inspection of Figure 30 and Figure 31 shows the effects of the layer on the values of the potential in the simulations. The potential values have much smaller magnitudes in the layered models, and thus change more gradually than the homogeneous models

(a) (b)

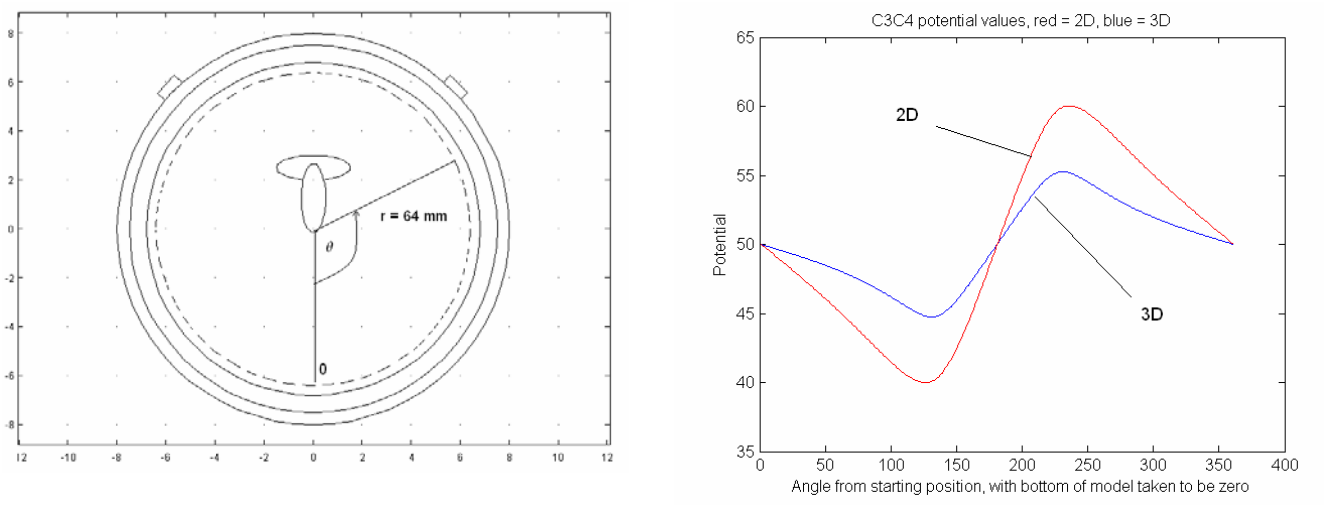

Figure 31: (a) The location where the potential was calculated. (b) The potential values for the 2D & 3D 4-layered TES models at cortical level.

Table 4 shows the potential values for the layered TES models inside the stimulating electrode, as well as the maximum value in the model, which was usually shifted by one degree to the left or right of the center of the electrode.

Table 4: Potential values for all TES models inside stimulating electrode and at maximum values at cortical level.

Electrode montages	Measured inside stimulating electrodes for each model			At max value		
	Amp 2D (V)	Amp 3D (V)	Error in %	Amp 2D (V)	Amp 3D (V)	Error %
C3-C4	59.521	55.138	7.95	60.026	55.255	8.63
C3-Cz	55.722	53.043	5.05	57.152	53.467	6.89
Diametric	62.086	56.3	15.8	62.09	56.302	10.3

Examining the maximum potentials in the homogeneous C3-C4 model and the C3-C4 model with the four different layers of the head we find that in the 2D case the difference in potential is approximately 13 volts, where as in the 3D case, the difference is 10.7 volts between the homogeneous and layered models. The error between the potential values of the 2D and 3D cases in the simple model was about 10.7 percent, while the difference in the layered model was 8.63 percent. This data was taken from Table 3 and Table 4.

The effects of the skull layer are seen in Figure 32, where the 2D and 3D homogeneous models, denoted 2D hom and 3D hom respectively, are compared with the 2D and 3D layered models.

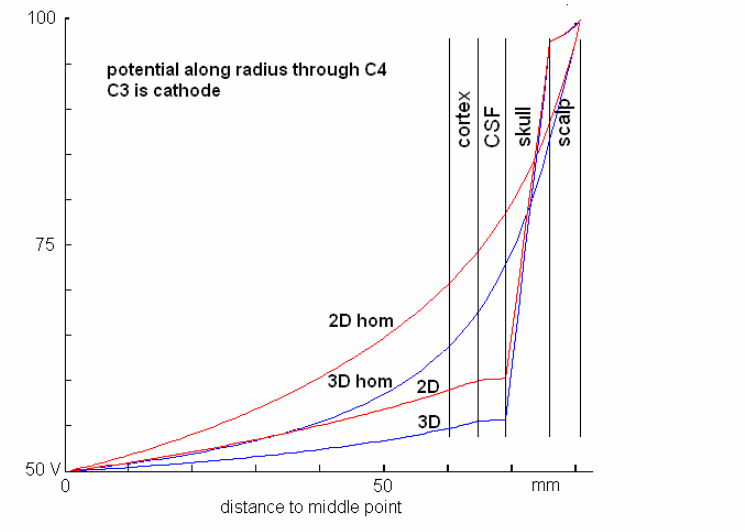

Figure 32: Potential values of 2D & 3D homogeneous and layered models.

5.2 ELECTRIC FIELD

Electric fields are important in safety studies; the energy dissipation showing the locations of "hot spots", where tissue damage could occur during TES, can easily be calculated from the electric field values. The first case to be examined is the homogeneous case, and then the 4-layer model showing the radial and tangential electric field distribution will be looked at.

In the homogeneous case, shown in Figure 33, we see how the radial electric field (REF) magnitude changes as we go around the model. This shows points of high and low electric field at the negative and positive electrode locations. These points have the highest gradient of potential change, so they have the highest electric field magnitudes. The direction of the REF corresponds to the positive and negative electrodes; at the negative electrode the REF has a negative value, whereas at the positive electrode the REF is positive. The electrodes were defined in the boundary conditions as positive 100V and 0V respectively. These boundary conditions make the current flow from the positive electrode toward the negative electrode, yielding the different signs of the REF in Figure 33.

(a) (b)

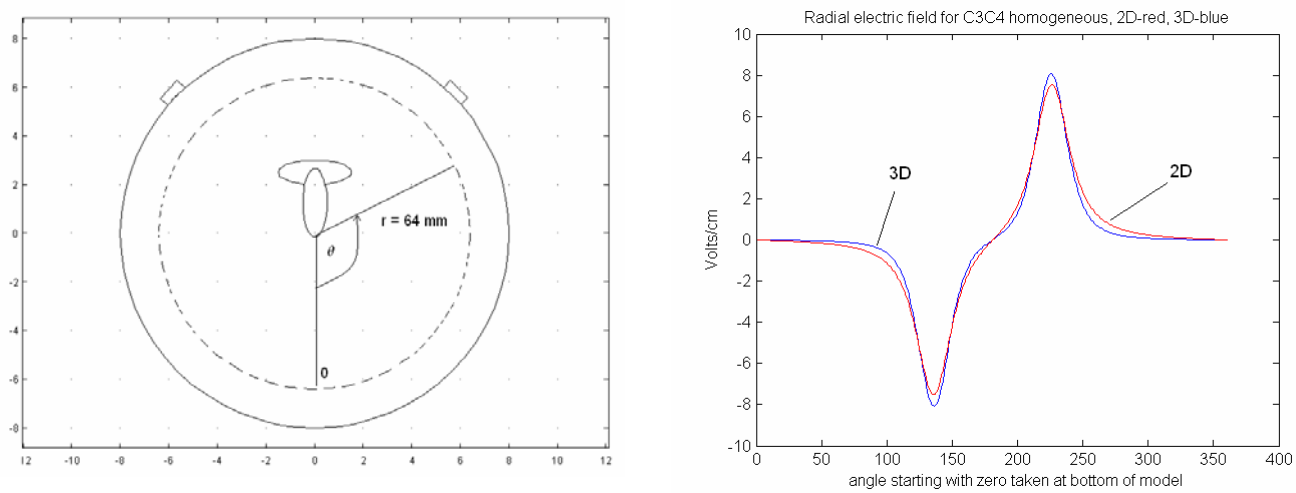

Figure 33: (a) The location where the REF was calculated. (b) Plotting the REF for C3-C4 homogeneous models, at cortical layer.

The error between the 2D and 3D REF for the homogeneous case is shown in Figure 34. The error ranges up to about 25 percent except for a couple of singularity points such as the endpoints of the calculations and the middle point of the model. The end points are singularities

of the model, meaning a division by zero, because of how the error is calculated. The values at those points are do not yield any useful information and have unrealistic values and can be neglected. The middle point has a larger error because there is a relatively large difference between the magnitudes of the 2D and 3D REF. The 2D and 3D REF also cross paths which causes a switching of the sign in the data, which explains the concave portions around the middle point.

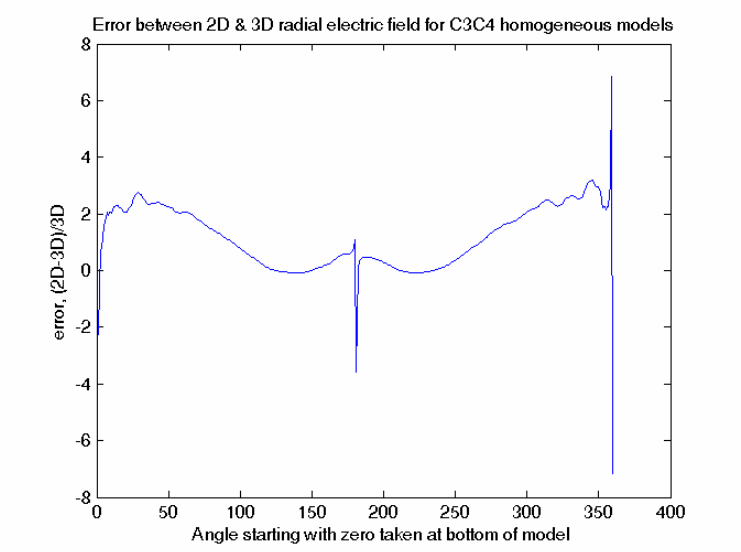

Figure 34: Error between 2D & 3D radial electric field for the homogeneous case, at cortical layer.

The tangential electric field (TEF) for the homogeneous case acts a bit differently than the REF, as shown in Figure 35. This is because the TEF is calculated using neighboring points at a particular radius, instead of points going down to the center of the circle or sphere. These points change greatly at the electrodes because of the interface between the electrode and the conductive media, causing the steep increase or decrease in the slope, around 135^{o} and 225^{o} respectively.

(a) (b)

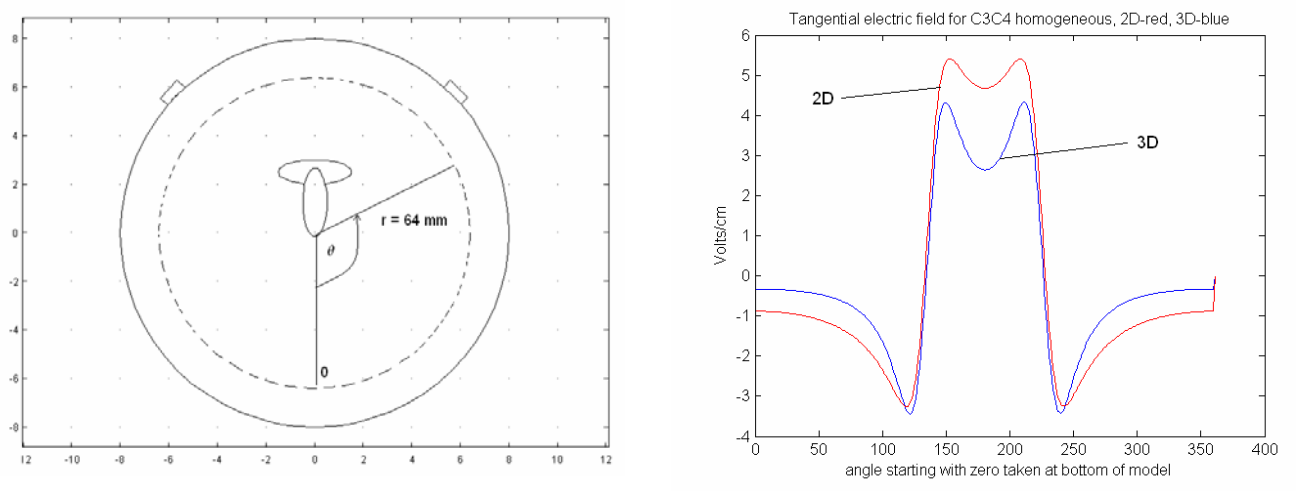

Figure 35: (a) The location where the TEF was calculated. (b) Plotting the TEF for C3-C4 homogeneous models at cortical layer.

Figure 36 shows the error between the 2D and 3D TEF for the homogeneous models. The highest error between the TEF models is at the positive and negative electrodes, which are singularities of the model. We see that the TEF in the 2D case has a higher magnitude than the 3D case, also an indication of the dispersion of the electric field into the 3rd dimension. There is a larger error in the TEF than the REF calculations, which indicates the effect of the 3rd dimension because each model must fit the same initial boundary conditions.

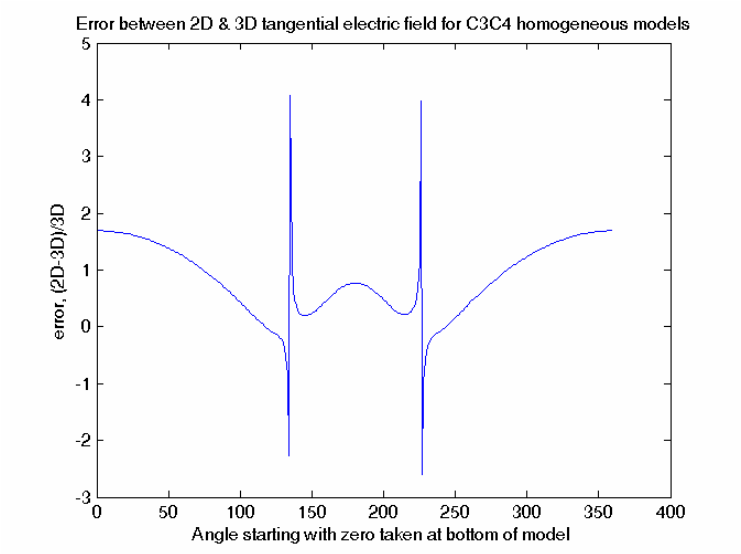

Figure 36: Error between 2D & 3D tangential electric field for the homogeneous case, taken at cortical layer.

Since the layered models are more realistic than the simple homogeneous case, the results from those simulations will be examined next. As with the potential calculations in the previous models, the REF for the layered model has a lower magnitude for both the 2D and 3D cases. This decrease mainly is caused by the skull layer, the same reason the potential values were lower in the layered models than the homogeneous case. The low and high peaks in Figure 37

are indicators of the negative and positive electrodes respectively, just as in the homogeneous case shown in Figure 33.

(a) (b)

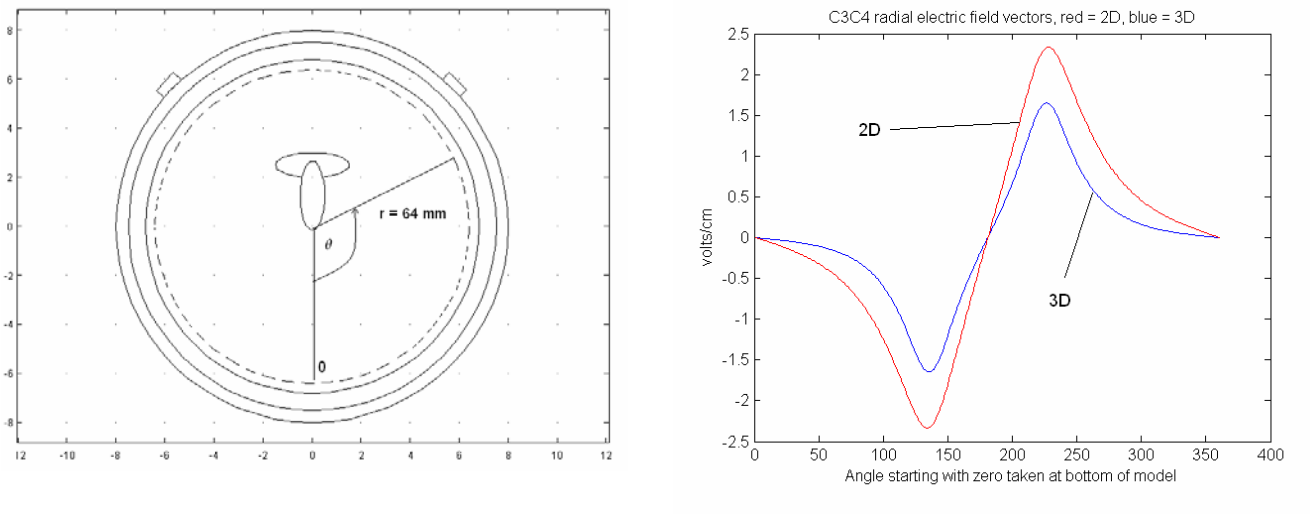

Figure 37: (a) The location where the REF was calculated. (b) Plotting the REF for C3-C4 layered model, at cortical layer.

The error between the magnitudes of the 2D and 3D cases for the REF of the layered model, shown in Figure 38, has an almost identical error distribution as the homogenous case. The scale is a bit different, which is due to the skull layer inhibiting the dispersion of the electric field in general for both the 2D and 3D cases.

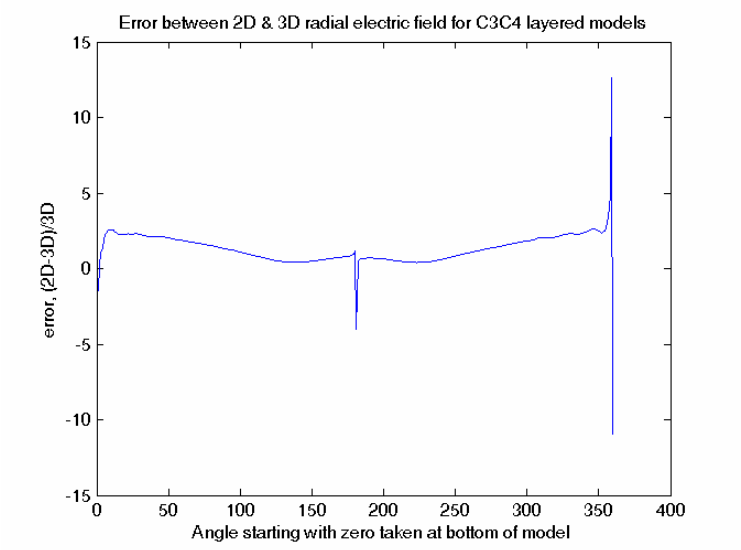

Figure 38: Error between 2D & 3D radial electric field in the 4-layered model taken at cortical layer.

The TEF for the layered models also have a lower magnitude than the homogeneous cases, but the interesting parts are the electrodes. The region between the electrodes is concave in the homogeneous case, but convex in the layered models. This occurs because the scalp and skull layers distribute the field more evenly throughout the thickness of each layer. So instead of acting like a single point of stimulation, as is the case in the homogeneous case, the effective

stimulation area becomes larger, but has a smaller magnitude. This causes the TEF to become convex at the middle point of the model, see Figure 39.

(a) (b)

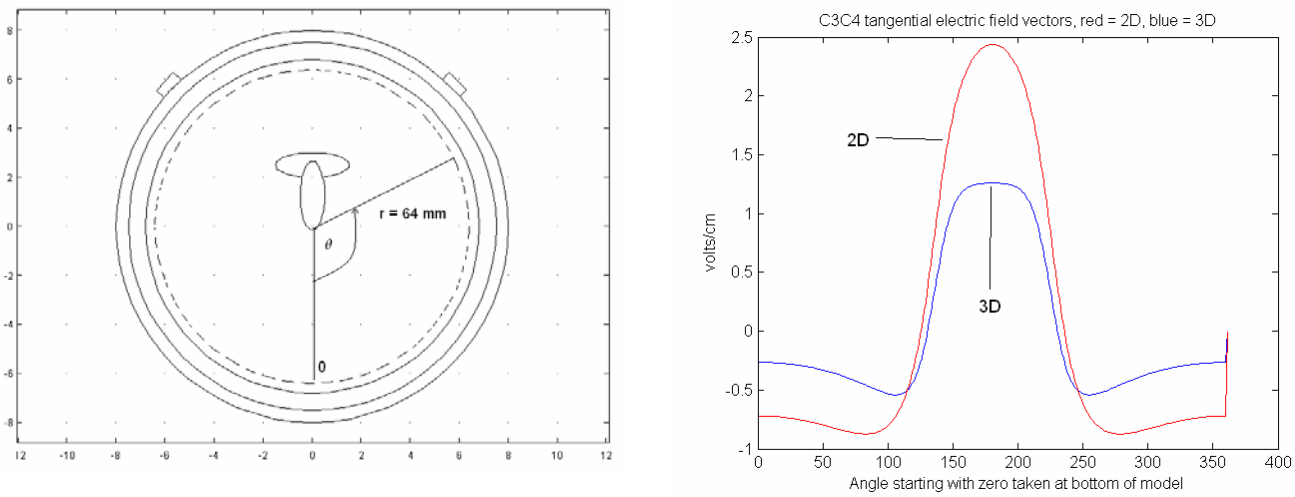

Figure 39: (a) The location where the TEF was calculated. (b) Plotting the TEF for C3-C4 layered model, at cortical layer.

The error for the TEF in the layered model, Figure 40, is similar in shape to the homogeneous case; there is no more error between the 2D and 3D cases for the TEF in the layered model than that of the homogeneous case. The two spikes occur at 135^{o} and 225^{o} respectively, corresponding to the electrode locations. These points are singularities in the model just as they were in the homogeneous case. The magnitude of the singularities is larger for the layered case than the homogeneous case, but we can neglect these points because we know they carry no useful information.

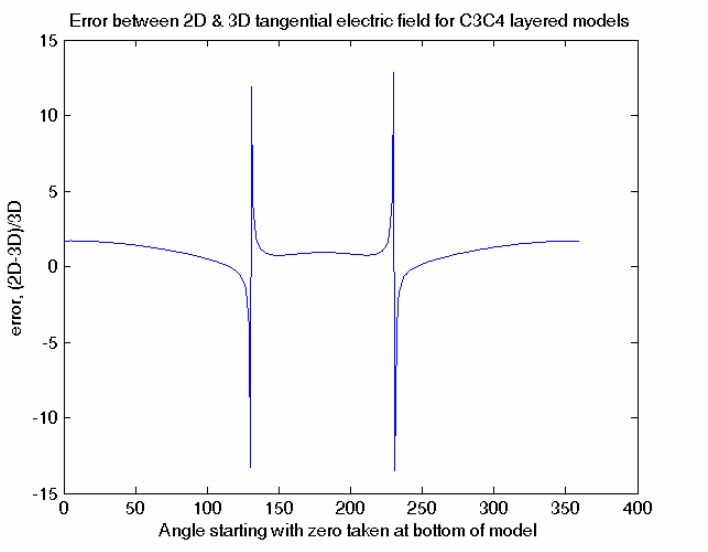

Figure 40: Error between 2D & 3D tangential electric field in the layered model, taken at cortical layer.

5.3 ACTIVATION FUNCTIONS

An examination of the activation functions in the models led to interesting discoveries in the behavior of the different components of the activation functions. First we will look at the RAF

differences between 2D and 3D for the C3-C4 homogeneous case, see Figure 41, which shows the magnitude of the RAF at the cortical level for all angles. From Table 5 we can see a significant difference in the magnitudes of the RAFs between 2D and 3D, indicating that the effect of the 3rd dimension is quite noticeable when the RAF is calculated. The error is negative because the magnitude of the RAF in the 2D model is considerably smaller than the 3D model.

The maximum values for the RAF and TAF in the homogeneous cases are shown in Table 5. The Full Width Half Maximum (FWHM) values are used to describe the activation function's resolution, as shown in Figure 41. The FWHM is defined by the angle of spread in the activation function in question, the units are degrees defining the width of the half maximal value, as the name describes.

One observation made was the magnitude of the 3D RAF was larger than the 2D RAF values. This was caused by the larger change in the potential values as they were calculated in the models. The larger change in the potential values of the 3D model accounts for greater changes in the RAF, since it is the second order difference. The larger 3D magnitude also switches the sign of the error between the 2D and 3D RAF models. The magnitude of the error is the main concern in the models, not the direction, so the sign can be neglected for comparison purposes.

(a) (b)

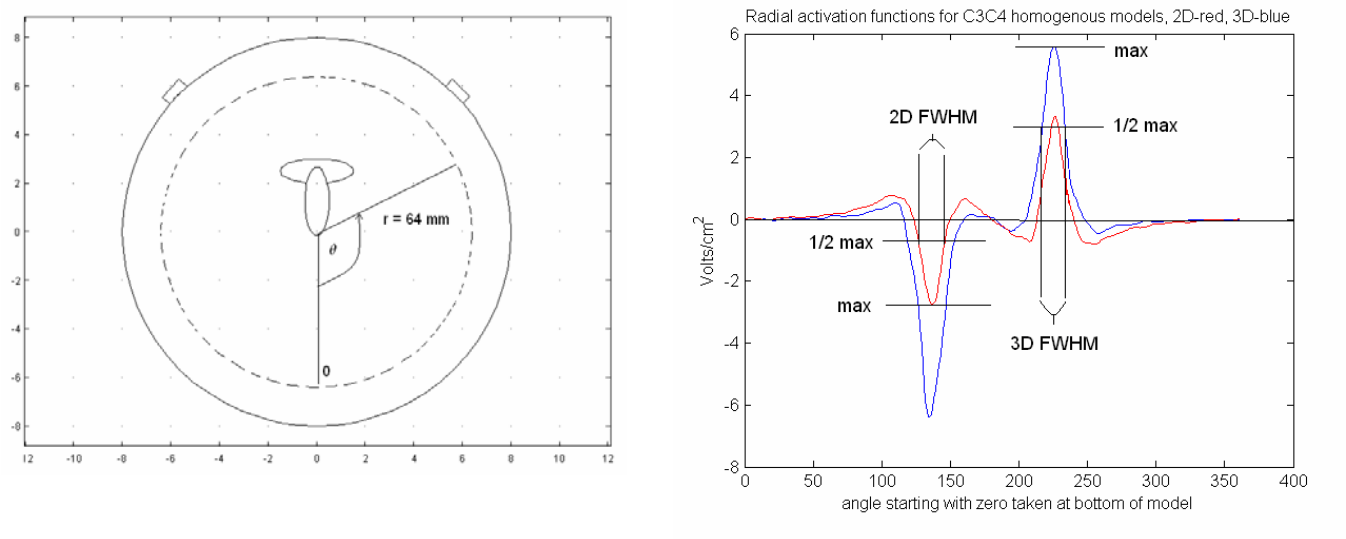

Figure 41: (a) The location where the RAF was calculated. (b) Plotting the RAF in 2D & 3D homogeneous models.

Table 5: Activation functions for 2D & 3D homogeneous models at cortical level.

Electrode montages	Radial @ Max Value for C3-C4			Tangential @ Max Value for C3-C4					
	2D (V/cm^2)	3D (V/cm^2)	Error %	2D (V/cm^2)	3D (V/cm^2)	Error %	FWHM 2D	FWHM 3D	FWHM %
C3-C4hom	3.3409	5.5893	-40.2	-4.4996	-4.4703	0.655	14R 17T	17R 16T	17.6 6.25

Next, examining the TAF in the simple models we find very little variation between the 2D and 3D models. Examining Figure 42 we see very little change between the 2D and 3D models graphically. It is less than 1 %, which presumably is insignificant. This is due to the homogeneity of the conductor between the electrodes.

(a) (b)

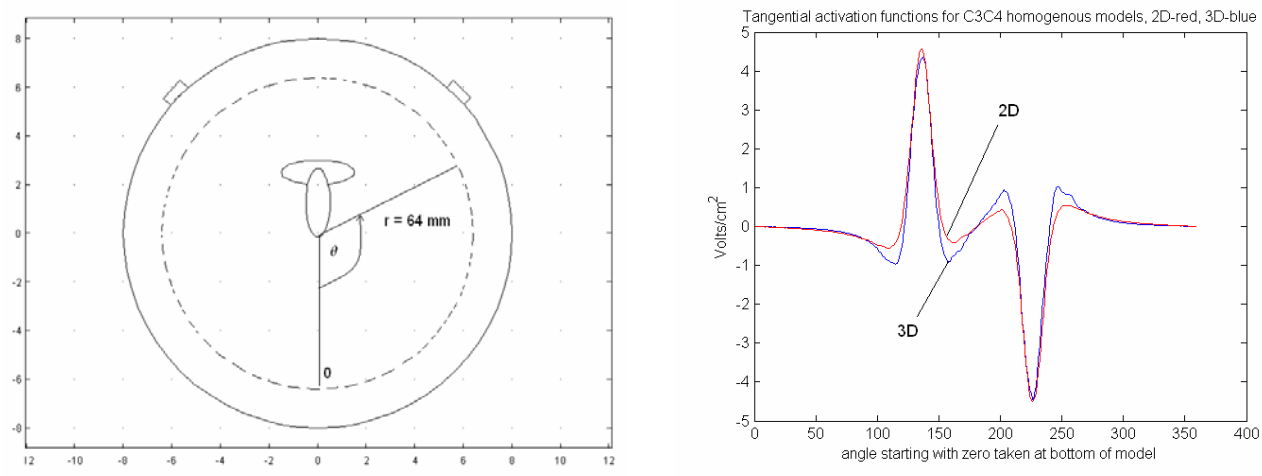

Figure 42: (a) The location where the TAF was calculated. (b) Plotting the TAF for 2D &3D homogeneous models.

The C3-C4 model with different layers differed quite a bit from the homogeneous case, which again indicates the importance of the layers in the model. The RAF in the layered model was similar in the size of the error, around 33 percent, which is still quite large, see Table 6. See Figure 43 for how the 2D and 3D RAF magnitudes are related graphically.

Table 6: Activation functions for all TES models inside stimulating electrode and at maximum value, at cortical level.

Electrode montages	Radial@ Max Value for C3-C4 @ Max Value for C3-CZ and diametric			Tangential @ Max Value for C3-C4 @ Max Value for C3-CZ and diametric					
	2D (V/cm^2)	3D (V/cm^2)	Error %	2D (V/cm^2)	3D (V/cm^2)	Error %	FWHM 2D	FWHM 3D	FWHM %
C3-C4	0.4318	0.6409	-32.6	-0.7949	-0.6027	31.9	34T 23R	25T 22R	36 4.5
C3-CZ	0.6626	0.7645	-13.3	-0.9526	-0.7024	35.6	31T 24R	26T 27R	19.2 11.1
Diametric	0.3326	0.5329	-37.6	-0.7056	-0.5519	27.8	33T 22R	25T 26R	32 15.4

(a) (b)

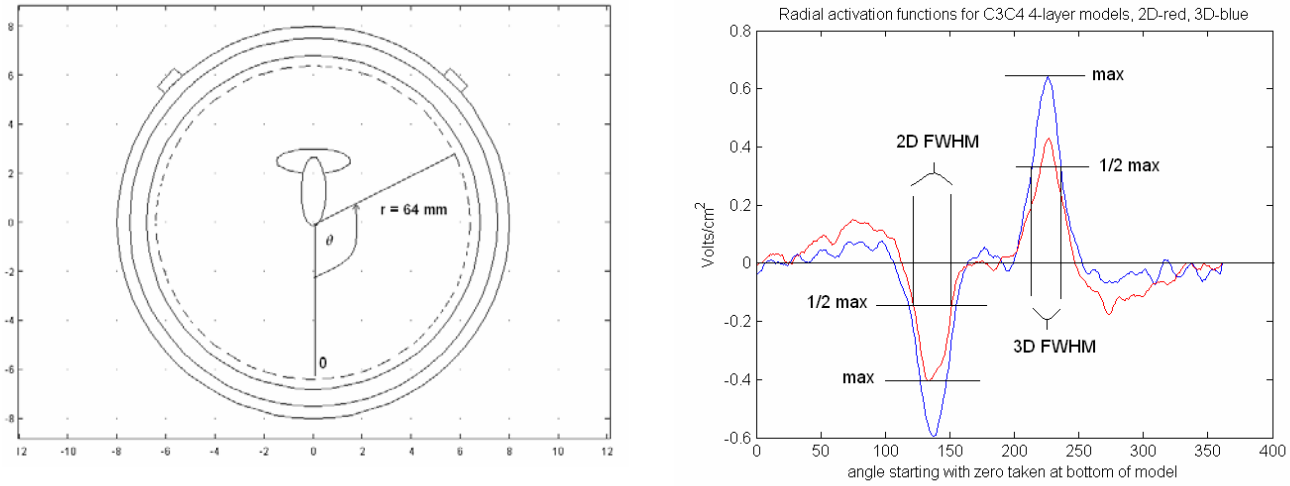

Figure 43: (a) The location where the RAF was calculated. (b) Plotting the RAF for C3-C4 layered model.

The layered models make the FWHM wider than the homogenous case since the stimulation is dispersed through the scalp and skull layers, making the effective stimulation location larger, but with a smaller magnitude due to the insulating properties of the skull. Figure 44 shows a comparison between the layered and homogeneous models with the FWHM measurements.

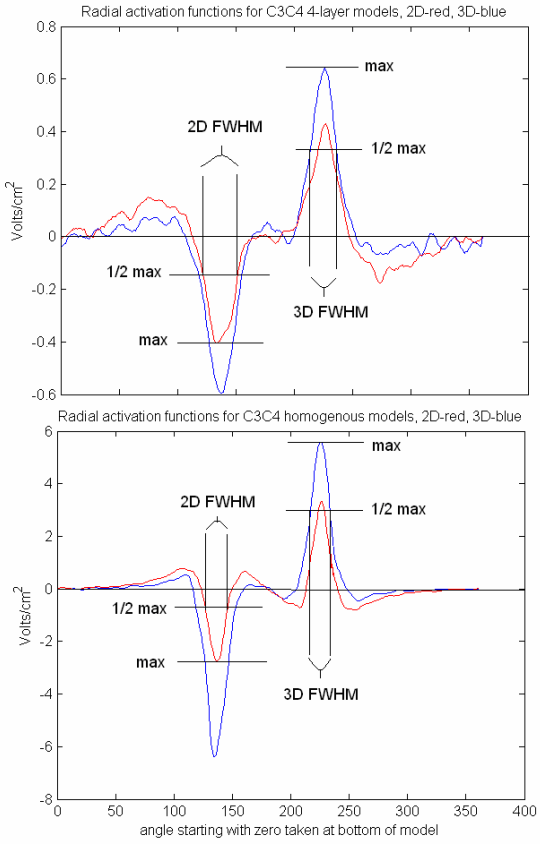

Figure 44: A comparison of the FWHM for the layered and homgeneous cases. The layered model is on top.

The major difference between the simple case and the layered case occurred in the TAF values, as shown in Figure 45. The TAF values in the 2D and 3D cases varied by approximately 32% which is two orders of magnitude greater than the values calculated in the C3-C4 simple case where the error was around 0.65%. Knowing this relationship between 2D and 3D will allow us to do the simulations and infer the results for more complex models.

(a) (b)

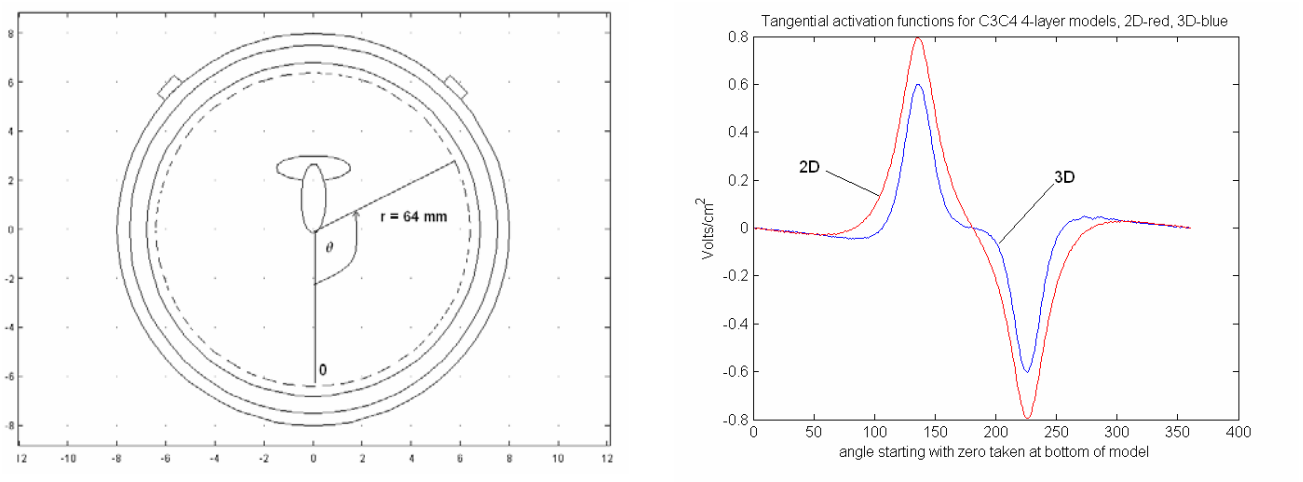

Figure 45: (a) The location where the TAF was calculated. (b) Plotting the TAF for C3-C4 layered models.

One observation was the switching of the direction of the activation function when looking at radial or tangential stimulation. In radial activation functions the negative electrode had a negative activation function, and the positive electrode had a positive activation function. But in the tangential activation function, the negative electrode induced a positive activation function, and the positive electrode caused a negative activation function. The switch in direction is caused by the radial or tangential electric fields which are compared in Figure 46. The switch in direction or the radial and tangential activation functions are shown in Figure 47. The observation of this switching in direction has clinical significance since the orientation of the CST and the cortical axons that synapt on the upper motor neurons are radial and tangential,

respectively.[33][33] By knowing how the different components of the AF stimulate different regions of the brain will help figure out which areas of the brain are being stimulated during TES.

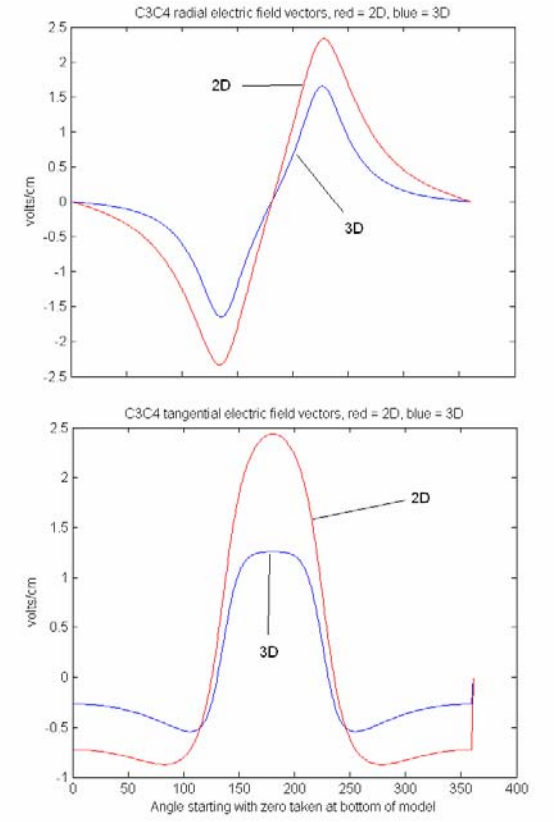

Figure 46: Comparison of radial and tangential electric fields.

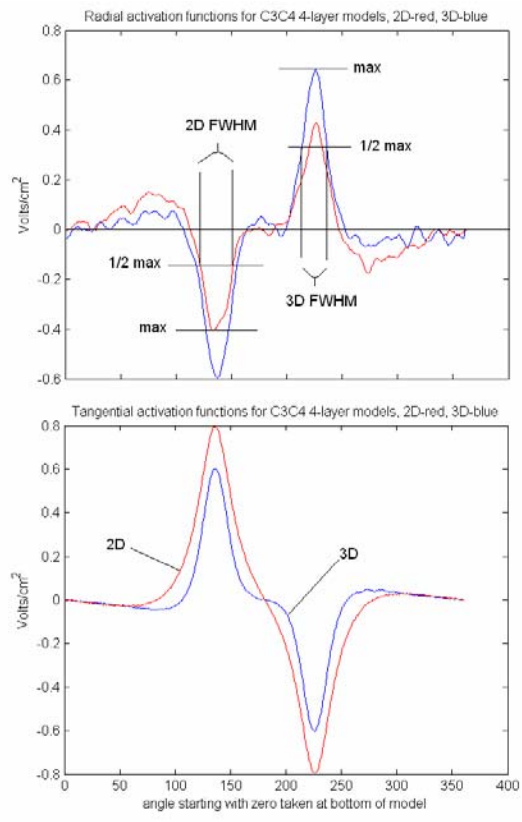

Figure 47: Comparison of radial and tangential activation functions.

The REF has the maximum magnitude at the middle of the electrode locations, similarly the RAF, which was calculated from the 2nd order difference, follows the same general curve. The RAF is less smooth is partly due to the elliptical symmetry of the spatial filter used to separate the useful data from the noise in the AF calculations. The filter is effectively one radial raster point in the radial direction and seven segmental raster points in the tangential direction, which was found empirically to preserve the desired resolution. The TEF has its maximum

change in magnitude at the electrode locations, and at the negative electrode location the TEF is positive, which is why the TAF has a positive value at the negative electrode. Similarly since the TEF is negative at the positive electrode the TAF has a negative value.

5.4 PARAMETERIZATIONS

Parameterizations of the scalp, skull, and CSF layer were performed to show the influence each layer has on the model. The thickness of each layer was decreased by half, with the other layers remaining the same thickness as in the original simulations.

The maximum values for the potentials, RAF, and TAF values in 2D and 3D are shown in the Table 7 and Table 8, respectively.

Table 7: Potential values for parameterizations of C3-C4 electrode orientation at the cortical level.

Electrode montages	Potential values inside the stimulating electrode			At max value		
	Amp 2D (V)	Amp 3D (V)	Error in %	Amp 2D(V)	Amp 3D (V)	Error %
C3-C4_half skull	63.805	57.555	10.9	64.294	57.669	11.5
C3-C4_half CSF	61.411	56.827	8.06	61.889	56.957	8.66
C3-C4_half scalp	58.764	54.781	7.27	59.08	54.856	7.7

Table 8: Activation function values for parameterizations of C3-C4 electrode orientation at cortical level, where T designates tangential activation functions and R signifies radial activation functions for the Full Width-Half Maximum (FWHM).

Electrode montages	Radial @ max value			Tangential @ max value					
	2D (V/cm^2)	3D (V/cm^2)	Err %	2D (V/cm^2)	3D (V/cm^2)	Err %	FWHM 2D	FWHM 3D	FWHM %
C3-C4_half skull	0.795	1.1337	-25.3	-1.3748	-1.0914	25.9	28T 22R	25T 25R	12 T 12 R
C3-C4_half CSF	0.5753	0.8656	-33.5	-1.0529	-0.875	20.3	30T 24R	24T 25R	25 T 4 R
C3-C4_half scalp	0.4761	0.7286	-34.7	-0.8636	-0.6519	32.5	28T 24R	24T 24R	16.7 T 0 R

6.0 DISCUSSION

6.1 POTENTIAL

The decision to examine the central slice in the xy-plane of the 3D model was made to ensure a good comparison between the same points in each model. By defining all the measuring points to be in the xy-plane, we were sure to compare voltages that would take into account the maximum effect of the added z-dimension. Due to the geometry of the model, polar coordinates were chosen to map out points to measure electric potential which have a 1mm resolution throughout the model.

A comparison between the homogeneous models and layered models showed the impact of the skull layer on the potential magnitude measured at the cortical level. The potential followed an almost identical path through the skull for the 2D and 3D case, the only difference being the magnitude of the potential measured at cortical level, which was not significant compared to the stimulating voltage, recall Figure 32. The difference between 2D and 3D in the layered models was also smaller than the difference between 2D and 3D in the homogenous case, where the errors between the 2D and 3D were 8.63% and 10.7%, respectively. This small difference was also caused by the skull layer restricting the flow of potential into the 3rd dimension in the 3D model because the high resistance of the skull did not allow current to flow easily into the 3rd dimension. This caused the 3D model to approximate the 2D model more

closely. In the homogeneous case, there is nothing to restrict the potential from distributing in the z-direction, so the difference between the 2D and 3D is larger.

Due to the 10% difference between the potential of the 2D and 3D models we can conclude that for centrally located slices in the 3D case, we find 2D to be a good approximation for the 3D case. The potential model provides all the data necessary to calculate the electric fields and activation functions.

6.2 ELECTRIC FIELD

The REF distribution follows the same general shape as the potential distribution, with a negative value of the REF found inside the cortex below the negative electrode and a positive value in the region stimulated by the positive electrode. This is logical because the REF is calculated from points extending radially from the center of the model to the outer layer, and the values used to calculate the REF come directly from the electric potential calculated in the first model.

The homogeneous and layered models magnitude of the REF differed significantly which was caused by the insulating properties of the skull. The difference between the error of the 2D and 3D homogeneous models and the difference in the error between the 2D and 3D layered models were both less than 25%, see Figure 34 and Figure 38, respectively. The reason for this small difference between the 2D and 3D layered models was because the skull impacted the magnitude of the potential measured inside the model in a similar manner for each model. The layer thickness and conductivity was consistent for the 2D and 3D models, so it had to impact each model in a similar fashion.

The TEF behaves differently than the REF, see Figure 46. The largest change in TEF occurs at the electrodes because the TEF is calculated using neighboring points at the cortical level. There is a steep increase or decrease in the field inside the model corresponding to the electrode locations. This differs from the REF where the values found inside the electrode locations achieved local maximum and minimum values, that is, the slope was zero. Inside the negative electrode the TEF has a positive slope, caused by the potential values on the outside of the electrode being larger than the potential of the electrode. The effect is switched for the positive electrode, in that the region around the electrode has smaller potential values than the electrode, so the slope is negative inside the positive electrode.

The difference in behavior of the REF and TEF shows how the components of the electric field may affect the axons of the brain depending on how those axons are oriented. The CST is oriented radially or perpendicular to the cortex, while the cortical axons are oriented tangentially, or parallel to the surface of the cortex. In order to propagate a signal down an axon, a change in the electric field in the direction of the axon is necessary. The change in electric field along the direction of the axon is the activation function, which is explained in section 6.3.

6.3 ACTIVATION FUNCTIONS

Another important effect to examine is the activation function (AF), which is responsible for action potential propagation along axons. Recall an activation function can be defined as the 2nd difference of potential along a specified path.[10] A large change in the electric field will cause a larger magnitude in the activation function. Knowing how AFs behave will lead to an understanding of which specific locations in the motor cortex are being stimulated during TES.

An examination of radial activation functions (RAF), as well as tangential activation functions (TAF) was performed for the different electrode montages, as well as for the simple case for comparison purposes. Previous work has been done on RAFs and TAFs have been examined in computer models by Manola.[31][35] The motivation for TAFs is due to the orientation of axons in the brain. Many axons run parallel to the surface of the cortex, and these axons are more likely to be stimulated by the activation function spreading out tangentially away from the stimulating electrode. Cortical axons which run parallel to the cortical layer are believed to be stimulated by the tangential component of the activation function.

Activation functions are calculated directly from the electric field values. For the RAF, the distribution of the magnitude mimics the distribution of the REF magnitudes fairly closely; recall Figure 37 and Figure 43. The small perturbations seen in the RAF are caused by numerical variations since the 2^{nd} order difference is calculated using actual data from the simulations, which was filtered to extract the desired information.

The TAF is calculated by taking the difference in the TEF values. If we examine the region of the cortex inside the negative electrode, we see the TAF is positive; this is because the TEF has a positive slope inside the negative electrode. The opposite effect is seen for the positive electrode, with the TAF having a negative slope, see Figure 45. The transition point occurs in the middle of the model because of the symmetry built into the model and the homogenous conductivities of each layer which was set in the boundary conditions.

During TES monitoring, the RAF is responsible for the activation of the CST, while the TAF is responsible for stimulating the cortical axons, as previously mentioned. This is because the CST runs radially through the brain, while the cortical axons spread out tangentially in the cortex, parallel to the scalp. The combination of the radial and tangential components of the AF

is responsible for the effectiveness of TES in neuromonitoring since both components act simultaneously to stimulate the CST and cortical axons in the brain. Knowing how the activation function components, RAF and TAF, affect specific parts of the brain during TES is valuable information to help with our basic understanding of how the human brain functions in the first place.

6.4 PARAMETERIZATIONS

It is important to note the relationship between the parameterized models and the standard C3-C4 model constructed. The potential in the models with varying scalp, skull, and CSF layers are along the same order as the potential values measured in the standard model. Changing the skull thickness resulted in the most significant change in the potential values between the models, with a difference of approximately 4 volts in the 2D cases, and 2 volts in the 3D models. The differences between the 2D and 3D models for the other parameterizations were less significant than the skull parameterization which shows the layer thickness has very little to do with the calculations. The important factor is that the different layers are present, not the actual thickness of the layers.

Since the different layers in the parameterization were each decreased in thickness by half, the activation functions, and potentials, had slightly larger values than those in the standard C3-C4 model. The percent differences between each of the activation functions were comparable in all the parameterization and standard models; this was a further indication of the independence of the geometry and solutions in the models.

7.0 SUMMARY OF CONTRIBUTIONS

A comparison between 2D and 3D models of TES to determine the potential systematic differences has not been performed before. This research gives insight into those differences which allows for simulations to be computed in 2D and infer the results of a 3D case. A graphical view of how potential, electric fields, and activation functions are dispersed through the simple models created gives insight into how the different layers influence each of the parameters examined. It is important to recognize that the difference between the parameterizations of the scalp, skull, and CSF layer had very little effect on the general flow of current through the model. But the absence of the layers caused the model to act quite differently, as was shown in the homogeneous model.

The numerical results found yield the relationships between the 2D and 3D simulations necessary to make the inferences between the two models. The ratios summarized in the tables can be used as a general rule, but are not absolute since the geometries here are simplified to gain a more complete understanding of how TES affects the human head.

The examination of the different components of the activation functions gives insight to the basic principles of TES. Understanding how the different components are responsible for stimulating the CST or cortical axons is very helpful to understanding how TES works because the head is essentially a black box to which stimulation is applied and the patient response is monitored by neurophysiologists. Knowing which regions of the brain are being stimulated

during TES will lead to the technique being improved. These improvements may include changing the stimulation magnitudes, changing the size of the electrodes used during TES, or modifying the locations where the electrodes are placed on the scalp.

8.0 CONCLUSION

The models created yield a basic understanding of the physics involved in TES. The behavior of the potential, electric fields, and activation functions shown in these simple models allows for conjectures to be made on more geometrically complex simulations. By understanding the physical principles of TES in a simple model we are able to understand and predict if the results found in more complex models are correct. The comparison between 2D and 3D models yields guidelines for the systematic differences between the models, allowing for the use of 2D models to infer the results of the 3D case which saves time and computational resources.

The different components of the AF have been examined to see the effect of the radial and tangential components during TES. Different regions of the brain are stimulated by each component and the combination of both the RAF and TAF are responsible for the effectiveness of TES in the operating room.

9.0 FUTURE WORK

Simple models yield a basic understanding of the principles of TES, but more realistic models are needed to understand how the anisotropic components of the human body influence the distribution of current. The next stage of research will involve realistic geometries to better approximate what is happening during TES. The non-linear and time dependent dynamics of the biological tissues should be modeled to better approximate a real human head. Realistic image data obtained by MRI and DTI should be utilized as well. By understanding how specific parts of the anatomy influence potential, electric field, and activation functions, a much clearer picture of how TES is actually working in the human head can be obtained. Improvements can be made to TES to enhance its success in the operating room based on the realistic models, ensuring the best possible monitoring for the patient during surgical procedures.

APPENDIX A - MODEL CODE

Model Geometries Code

Homogeneous Models
2D Models

```
% Electrodes at C3 and C4 locations

brain_size = 6.4; % measurements in cm
CSF_size = 0.4;
skull_size = 0.7;
scalp_size = 0.5;
%electrode_length = 1; electrode_height = 0.75;
kx1 = 0;
kx2 = 1;
ky1 = 0;
ky2 = 0.5;
theta = -pi/4 - 0.01;%rotation of electrodes, angle used to position right electrode
rad = brain_size+CSF_size+skull_size+scalp_size;
phi = pi/4 - 0.12;%angle used to position left electrode
x_r = (rad-0.1)*cos(theta - 0.05);
y_r = (rad-0.1)*sin(theta - 0.05);
x_l = (rad-0.1)*cos(phi + 0.05);
y_l = (rad-0.1)*sin(phi + 0.05);

a = circ2(0, 0, brain_size);
b = circ2(0, 0, brain_size+CSF_size);
c = circ2(0, 0, brain_size+CSF_size+skull_size);
d = circ2(0, 0, brain_size+CSF_size+skull_size+scalp_size);
e = rect2(kx1, kx2, ky1, ky2);%right electrode
e = rotate(e, theta);
e = move(e, x_r, -y_r);
e = e - e*d;
f = rect2(kx1, kx2, ky1, ky2);%left electrode
f = rotate(f, -theta +0.05);
f = move(f, -x_l, y_l);
f = f - f*d;
```

```
geom = geomcoerce('solid', {d e f});


% Electrode at C3 and CZ

brain_size = 6.4; % measurements in cm
CSF_size = 0.4;
skull_size = 0.7;
scalp_size = 0.5;
%electrode_length = 1; electrode_height = 0.75;
kx1 = 0;
kx2 = 1;
ky1 = 0;
ky2 = 0.5;
theta = -pi/4 - 0.01;%rotation of electrodes, angle used to position right electrode
rad = brain_size+CSF_size+skull_size+scalp_size;
phi = pi/2;%angle used to position top electrode
x_r = (rad-0.1)*cos(theta - 0.05);
y_r = (rad-0.1)*sin(theta - 0.05);
x_l = (rad-0.1)*cos(phi - 0.055);
y_l = (rad-0.1)*sin(phi);
csf_loop1x = 1.5; % x axis length of csf ellipse
csf_loop1y = .5; % y axis length of csf ellipse
csf_loop2x = .5;
csf_loop2y = 1.4;
s_x = 0; % x value for center of horizontal csf ellipse in brain
s_y = 2.5; % y value for center of horizontal csf ellipse in brain
t_x = 0; % x value for center of vertical csf ellipse in brain
t_y = 1.25; %y value for center of vertical csf ellipse in brain

a = circ2(0, 0, brain_size);
b = circ2(0, 0, brain_size+CSF_size);
c = circ2(0, 0, brain_size+CSF_size+skull_size);
d = circ2(0, 0, brain_size+CSF_size+skull_size+scalp_size);
e = rect2(kx1, kx2, ky1, ky2);%right electrode
e = rotate(e, theta);
e = move(e, x_r, -y_r);
e = e - e*d;
f = rect2(kx1, kx2, ky1, ky2);%top electrode
f = rotate(f, 0);
f = move(f, -x_l, y_l);
f = f - f*d;
s = ellip2(s_x, s_y, csf_loop1x, csf_loop1y);
t = ellip2(t_x, t_y, csf_loop2x, csf_loop2y);
u = s -(t*s);
```

```
geom = geomcoerce('solid', {d e f});


% Electrodes on opposite ends of model

brain_size = 6.4; % measurements in cm
CSF_size = 0.4;
skull_size = 0.7;
scalp_size = 0.5;
%electrode_length = 1; electrode_height = 0.75;
kx1 = 0;
kx2 = 1;
ky1 = 0;
ky2 = 0.5;
theta = 0;%rotation of electrodes, angle used to position right electrode
rad = brain_size+CSF_size+skull_size+scalp_size;
phi = 0;%angle used to position top electrode
x_r = (rad-0.1)*cos(theta);
y_r = (rad-0.1)*sin(theta);
x_l = (rad-0.1)*cos(phi);
y_l = (rad-0.1)*sin(phi);
csf_loop1x = 1.5; % x axis length of csf ellipse
csf_loop1y = .5; % y axis length of csf ellipse
csf_loop2x = .5;
csf_loop2y = 1.4;
s_x = 0; % x value for center of horizontal csf ellipse in brain
s_y = 2.5; % y value for center of horizontal csf ellipse in brain
t_x = 0; % x value for center of vertical csf ellipse in brain
t_y = 1.25; %y value for center of vertical csf ellipse in brain

a = circ2(0, 0, brain_size);
b = circ2(0, 0, brain_size+CSF_size);
c = circ2(0, 0, brain_size+CSF_size+skull_size);
d = circ2(0, 0, brain_size+CSF_size+skull_size+scalp_size);
e = rect2(kx1, kx2, ky1, ky2);%right electrode
e = rotate(e, theta);
e = move(e, y_r-0.5, -x_r-0.5);
e = e - e*d;
f = rect2(kx1, kx2, ky1, ky2);%top electrode
f = rotate(f, phi);
f = move(f, y_l-0.5, x_l);
f = f - f*d;
s = ellip2(s_x, s_y, csf_loop1x, csf_loop1y);
t = ellip2(t_x, t_y, csf_loop2x, csf_loop2y);
u = s -(t*s);
```

```
geom = geomcoerce('solid', {d e f});
```

3D Models

```
% Geometry for C3C4 electrode locations
brain_size = 6.4; % measurements in cm
CSF_size = 0.4;
skull_size = 0.7;
scalp_size = 0.5;
electrode_diameter = 1;
electrode_height = 1;
angle = pi/4;
r = 7.8;
x=r*cos(angle);
y=r*sin(angle);


a = sphere3(brain_size, 'pos', [0 0 0], 'axis', [0 0 0], 'rot', 0);
b = sphere3(brain_size+CSF_size, 'pos', [0 0 0], 'axis', [0 0 0], 'rot', 0);
c = sphere3(brain_size+CSF_size+skull_size, 'pos', [0 0 0], 'axis', [0 0 0], 'rot', 0);
d = sphere3(brain_size+CSF_size+skull_size+scalp_size, 'pos', [0 0 0], 'axis', [0 0 0], 'rot', 0);
e = cylinder3(electrode_diameter, electrode_height, 'pos', [x y 0], 'axis', [1 1 0], 'rot', 0);
e = e - e*d;
f = cylinder3(electrode_diameter, electrode_height, 'pos', [-x y 0], 'axis', [-1 1 0], 'rot', 0);
f = f - f*d;

geom = geomcoerce('solid', {d e f});


%3-D TES model, CZC3

brain_size = 6.4; % measurements in cm
CSF_size = 0.4;
skull_size = 0.7;
scalp_size = 0.5;
electrode_diameter = 1;
electrode_height = 1;
angle = pi/4;
r = 7.8;
x=r*cos(angle);
y=r*sin(angle);


a = sphere3(brain_size, 'pos', [0 0 0], 'axis', [0 0 0], 'rot', 0);
b = sphere3(brain_size+CSF_size, 'pos', [0 0 0], 'axis', [0 0 0], 'rot', 0);
c = sphere3(brain_size+CSF_size+skull_size, 'pos', [0 0 0], 'axis', [0 0 0], 'rot', 0);
```

```
d = sphere3(brain_size+CSF_size+skull_size+scalp_size, 'pos', [0 0 0], 'axis', [0 0 0], 'rot', 0);
e = cylinder3(electrode_diameter, electrode_height, 'pos', [x y 0], 'axis', [1 1 0], 'rot', 0);
e = e - e*d;
f = cylinder3(electrode_diameter, electrode_height, 'pos', [0 r 0], 'axis', [0 1 0], 'rot', 0);
f = f - f*d;

geom = geomcoerce('solid', {d e f});


%3-D TES model, CZopp

brain_size = 6.4; % measurements in cm
CSF_size = 0.4;
skull_size = 0.7;
scalp_size = 0.5;
electrode_diameter = 1;
electrode_height = 1;
angle = pi/4;
r = 7.8;
x=r*cos(angle);
y=r*sin(angle);


a = sphere3(brain_size, 'pos', [0 0 0], 'axis', [0 0 0], 'rot', 0);
b = sphere3(brain_size+CSF_size, 'pos', [0 0 0], 'axis', [0 0 0], 'rot', 0);
c = sphere3(brain_size+CSF_size+skull_size, 'pos', [0 0 0], 'axis', [0 0 0], 'rot', 0);
d = sphere3(brain_size+CSF_size+skull_size+scalp_size, 'pos', [0 0 0], 'axis', [0 0 0], 'rot', 0);
e = cylinder3(electrode_diameter, electrode_height, 'pos', [0 -r-1 0], 'axis', [0 1 0], 'rot', 0);
e = e - e*d;
f = cylinder3(electrode_diameter, electrode_height, 'pos', [0 r 0], 'axis', [0 1 0], 'rot', 0);
f = f - f*d;

geom = geomcoerce('solid', {d e f});
```

Initial Conditions

Homogeneous 2D Models

```
Made for C3C4, C3CZ, CZOpp
% all values for electrodes must be unique
% also no overlapping values allowed
% tes.elec_dist = 3;

tes.elec_pos_loc = [1 2 3];
```

```
tes.elec_neg_loc = [4 5 6];
tes.elec_pos_value = 100;
tes.elec_neg_value = 0;
```

Homogeneous 3D Models

```
%Initial Conditions for TES_3D_C3C4simple

tes.elec_pos_loc = [5 6 7 10 11];
tes.elec_neg_loc = [16 17 20 21 22];
tes.elec_pos_value = 100;
tes.elec_neg_value = 0;


%Initial Conditions for TES_3D_C3CZsimple

tes.elec_pos_loc = [5 6 9 15 17];
tes.elec_neg_loc = [18 19 22 23 24];
tes.elec_pos_value = 100;
tes.elec_neg_value = 0;


%Initial Conditions for TES_3D_CZoppsimple

tes.elec_pos_loc = [10 11 14 24 26];
tes.elec_neg_loc = [5 6 7 15 16];
tes.elec_pos_value = 100;
tes.elec_neg_value = 0;
```

Geometry of Layered Models

2D Cases

```
% Electrodes at C3 and C4 locations

brain_size = 6.4; % measurements in cm
CSF_size = 0.4;
skull_size = 0.7;
scalp_size = 0.5;
%electrode_length = 1; electrode_height = 0.75;
kx1 = 0;
kx2 = 1;
ky1 = 0;
```

```
ky2 = 0.5;
theta = -pi/4 - 0.01;%rotation of electrodes, angle used to position right electrode
rad = brain_size+CSF_size+skull_size+scalp_size;
phi = pi/4 - 0.12;%angle used to position left electrode
x_r = (rad-0.1)*cos(theta - 0.05);
y_r = (rad-0.1)*sin(theta - 0.05);
x_l = (rad-0.1)*cos(phi + 0.05);
y_l = (rad-0.1)*sin(phi + 0.05);
csf_loop1x = 1.5; % x axis length of csf ellipse
csf_loop1y = .5; % y axis length of csf ellipse
csf_loop2x = .5;
csf_loop2y = 1.4;
s_x = 0; % x value for center of horizontal csf ellipse in brain
s_y = 2.5; % y value for center of horizontal csf ellipse in brain
t_x = 0; % x value for center of vertical csf ellipse in brain
t_y = 1.25; %y value for center of vertical csf ellipse in brain

a = circ2(0, 0, brain_size);
b = circ2(0, 0, brain_size+CSF_size);
c = circ2(0, 0, brain_size+CSF_size+skull_size);
d = circ2(0, 0, brain_size+CSF_size+skull_size+scalp_size);
e = rect2(kx1, kx2, ky1, ky2);%right electrode
e = rotate(e, theta);
e = move(e, x_r, -y_r);
e = e - e*d;
f = rect2(kx1, kx2, ky1, ky2);%left electrode
f = rotate(f, -theta +0.05);
f = move(f, -x_l, y_l);
f = f - f*d;
s = ellip2(s_x, s_y, csf_loop1x, csf_loop1y);
t = ellip2(t_x, t_y, csf_loop2x, csf_loop2y);
u = s -(t*s);

geom = geomcoerce('solid', {a b c d e f t u});


% Electrode at C3 and top CZ

brain_size = 6.4; % measurements in cm
CSF_size = 0.4;
skull_size = 0.7;
scalp_size = 0.5;
%electrode_length = 1; electrode_height = 0.75;
kx1 = 0;
kx2 = 1;
ky1 = 0;
```

```
ky2 = 0.5;
theta = -pi/4 - 0.01;%rotation of electrodes, angle used to position right electrode
rad = brain_size+CSF_size+skull_size+scalp_size;
phi = pi/2;%angle used to position top electrode
x_r = (rad-0.1)*cos(theta - 0.05);
y_r = (rad-0.1)*sin(theta - 0.05);
x_l = (rad-0.1)*cos(phi - 0.055);
y_l = (rad-0.1)*sin(phi);
csf_loop1x = 1.5; % x axis length of csf ellipse
csf_loop1y = .5; % y axis length of csf ellipse
csf_loop2x = .5;
csf_loop2y = 1.4;
s_x = 0; % x value for center of horizontal csf ellipse in brain
s_y = 2.5; % y value for center of horizontal csf ellipse in brain
t_x = 0; % x value for center of vertical csf ellipse in brain
t_y = 1.25; %y value for center of vertical csf ellipse in brain

a = circ2(0, 0, brain_size);
b = circ2(0, 0, brain_size+CSF_size);
c = circ2(0, 0, brain_size+CSF_size+skull_size);
d = circ2(0, 0, brain_size+CSF_size+skull_size+scalp_size);
e = rect2(kx1, kx2, ky1, ky2);%right electrode
e = rotate(e, theta);
e = move(e, x_r, -y_r);
e = e - e*d;
f = rect2(kx1, kx2, ky1, ky2);%top electrode
f = rotate(f, 0);
f = move(f, -x_l, y_l);
f = f - f*d;
s = ellip2(s_x, s_y, csf_loop1x, csf_loop1y);
t = ellip2(t_x, t_y, csf_loop2x, csf_loop2y);
u = s -(t*s);

geom = geomcoerce('solid', {a b c d e f t u});

% Electrodes on opposite ends of model

brain_size = 6.4; % measurements in cm
CSF_size = 0.4;
skull_size = 0.7;
scalp_size = 0.5;
%electrode_length = 1; electrode_height = 0.75;
kx1 = 0;
kx2 = 1;
ky1 = 0;
ky2 = 0.5;
```

```
theta = 0;%rotation of electrodes, angle used to position right electrode
rad = brain_size+CSF_size+skull_size+scalp_size;
phi = 0;%angle used to position top electrode
x_r = (rad-0.1)*cos(theta);
y_r = (rad-0.1)*sin(theta);
x_l = (rad-0.1)*cos(phi);
y_l = (rad-0.1)*sin(phi);
csf_loop1x = 1.5; % x axis length of csf ellipse
csf_loop1y = .5; % y axis length of csf ellipse
csf_loop2x = .5;
csf_loop2y = 1.4;
s_x = 0; % x value for center of horizontal csf ellipse in brain
s_y = 2.5; % y value for center of horizontal csf ellipse in brain
t_x = 0; % x value for center of vertical csf ellipse in brain
t_y = 1.25; %y value for center of vertical csf ellipse in brain

a = circ2(0, 0, brain_size);
b = circ2(0, 0, brain_size+CSF_size);
c = circ2(0, 0, brain_size+CSF_size+skull_size);
d = circ2(0, 0, brain_size+CSF_size+skull_size+scalp_size);
e = rect2(kx1, kx2, ky1, ky2);%right electrode
e = rotate(e, theta);
e = move(e, y_r-0.5, -x_r-0.5);
e = e - e*d;
f = rect2(kx1, kx2, ky1, ky2);%top electrode
f = rotate(f, phi);
f = move(f, y_l-0.5, x_l);
f = f - f*d;
s = ellip2(s_x, s_y, csf_loop1x, csf_loop1y);
t = ellip2(t_x, t_y, csf_loop2x, csf_loop2y);
u = s -(t*s);

geom = geomcoerce('solid', {a b c d e f t u});

% Electrodes at C3 and on the epidural layer

brain_size = 6.4; % measurements in cm
CSF_size = 0.4;
skull_size = 0.7;
scalp_size = 0.5;
%electrode_length = 1; electrode_height = 0.5;
kx1 = 0;
kx2 = 1;
ky1 = 0;
ky2 = 0.5;
theta = -pi/4 - 0.01;%rotation of electrodes, angle used to position right electrode
```

```
rad = brain_size+CSF_size+skull_size+scalp_size;
rad2 = brain_size+CSF_size;
%electrode on cortex measurements
hx1 = 0;
hx2 = 1;
hy1 = 0;
hy2 = 2;
phi = pi/4 - 0.15;%angle used to position left electrode
x_r = (rad-0.1)*cos(theta - 0.05);
y_r = (rad-0.1)*sin(theta - 0.05);
x_l = (rad2-0.05)*cos(phi + 0.05);
y_l = (rad2-0.05)*sin(phi + 0.05);
csf_loop1x = 1.5; % x axis length of csf ellipse
csf_loop1y = .5; % y axis length of csf ellipse
csf_loop2x = .5;
csf_loop2y = 1.4;
s_x = 0; % x value for center of horizontal csf ellipse in brain
s_y = 2.5; % y value for center of horizontal csf ellipse in brain
t_x = 0; % x value for center of vertical csf ellipse in brain
t_y = 1.25; %y value for center of vertical csf ellipse in brain

a = circ2(0, 0, brain_size);
b = circ2(0, 0, brain_size+CSF_size);
c = circ2(0, 0, brain_size+CSF_size+skull_size);
d = circ2(0, 0, brain_size+CSF_size+skull_size+scalp_size);
e = rect2(kx1, kx2, ky1, ky2);%right electrode
e = rotate(e, theta);
e = move(e, x_r, -y_r);
e = e - e*d;
f = rect2(hx1, hx2, hy1, hy2);%left electrode
f = rotate(f, -theta +0.05);
f = move(f, -x_l, y_l);
g = a+b+c+d;
h = g - f*g;
s = ellip2(s_x, s_y, csf_loop1x, csf_loop1y);
t = ellip2(t_x, t_y, csf_loop2x, csf_loop2y);
u = s -(t*s);

geom = geomcoerce('solid', {e h t u});


% Electrodes at C3 and on the cortex

brain_size = 6.4; % measurements in cm
CSF_size = 0.4;
skull_size = 0.7;
```

```
scalp_size = 0.5;
%electrode_length = 1; electrode_height = 0.5;
kx1 = 0;
kx2 = 1;
ky1 = 0;
ky2 = 0.5;
theta = -pi/4 - 0.01;%rotation of electrodes, angle used to position right electrode
rad = brain_size+CSF_size+skull_size+scalp_size;
rad2 = brain_size;
%electrode on cortex measurements
hx1 = 0;
hx2 = 1;
hy1 = 0;
hy2 = 2;
phi = pi/4 - 0.15;%angle used to position left electrode
x_r = (rad-0.1)*cos(theta - 0.05);
y_r = (rad-0.1)*sin(theta - 0.05);
x_l = (rad2-0.05)*cos(phi + 0.05);
y_l = (rad2-0.05)*sin(phi + 0.05);
csf_loop1x = 1.5; % x axis length of csf ellipse
csf_loop1y = .5; % y axis length of csf ellipse
csf_loop2x = .5;
csf_loop2y = 1.4;
s_x = 0; % x value for center of horizontal csf ellipse in brain
s_y = 2.5; % y value for center of horizontal csf ellipse in brain
t_x = 0; % x value for center of vertical csf ellipse in brain
t_y = 1.25; %y value for center of vertical csf ellipse in brain

a = circ2(0, 0, brain_size);
b = circ2(0, 0, brain_size+CSF_size);
c = circ2(0, 0, brain_size+CSF_size+skull_size);
d = circ2(0, 0, brain_size+CSF_size+skull_size+scalp_size);
e = rect2(kx1, kx2, ky1, ky2);%right electrode
e = rotate(e, theta);
e = move(e, x_r, -y_r);
e = e - e*d;
f = rect2(hx1, hx2, hy1, hy2);%left electrode
f = rotate(f, -theta +0.05);
f = move(f, -x_l, y_l);
g = a+b+c+d;
h = g - f*g;
s = ellip2(s_x, s_y, csf_loop1x, csf_loop1y);
t = ellip2(t_x, t_y, csf_loop2x, csf_loop2y);
u = s -(t*s);

geom = geomcoerce('solid', {e h t u});
```

Layered 3D Models Geometry

```
% Geometry for C3C4 electrode locations
brain_size = 6.4; % measurements in cm
CSF_size = 0.4;
skull_size = 0.7;
scalp_size = 0.5;
electrode_diameter = 1;
electrode_height = 1;
angle = pi/4;
r = 7.8;
x=r*cos(angle);
y=r*sin(angle);


a = sphere3(brain_size, 'pos', [0 0 0], 'axis', [0 0 0], 'rot', 0);
b = sphere3(brain_size+CSF_size, 'pos', [0 0 0], 'axis', [0 0 0], 'rot', 0);
c = sphere3(brain_size+CSF_size+skull_size, 'pos', [0 0 0], 'axis', [0 0 0], 'rot', 0);
d = sphere3(brain_size+CSF_size+skull_size+scalp_size, 'pos', [0 0 0], 'axis', [0 0 0], 'rot', 0);
e = cylinder3(electrode_diameter, electrode_height, 'pos', [x y 0], 'axis', [1 1 0], 'rot', 0);
e = e - e*d;
f = cylinder3(electrode_diameter, electrode_height, 'pos', [-x y 0], 'axis', [-1 1 0], 'rot', 0);
f = f - f*d;

geom = geomcoerce('solid', {a b c d e f});




%3-D TES model, CZC3
brain_size = 6.4; % measurements in cm
CSF_size = 0.4;
skull_size = 0.7;
scalp_size = 0.5;
electrode_diameter = 1;
electrode_height = 1;
angle = pi/4;
r = 7.8;
x=r*cos(angle);
y=r*sin(angle);


a = sphere3(brain_size, 'pos', [0 0 0], 'axis', [0 0 0], 'rot', 0);
b = sphere3(brain_size+CSF_size, 'pos', [0 0 0], 'axis', [0 0 0], 'rot', 0);
c = sphere3(brain_size+CSF_size+skull_size, 'pos', [0 0 0], 'axis', [0 0 0], 'rot', 0);
```

```
d = sphere3(brain_size+CSF_size+skull_size+scalp_size, 'pos', [0 0 0], 'axis', [0 0 0], 'rot', 0);
e = cylinder3(electrode_diameter, electrode_height, 'pos', [x y 0], 'axis', [1 1 0], 'rot', 0);
e = e - e*d;
f = cylinder3(electrode_diameter, electrode_height, 'pos', [0 r 0], 'axis', [0 1 0], 'rot', 0);
f = f - f*d;

geom = geomcoerce('solid', {a b c d e f});


%3-D TES model, CZopp
brain_size = 6.4; % measurements in cm
CSF_size = 0.4;
skull_size = 0.7;
scalp_size = 0.5;
electrode_diameter = 1;
electrode_height = 1;
angle = pi/4;
r = 7.8;
x=r*cos(angle);
y=r*sin(angle);


a = sphere3(brain_size, 'pos', [0 0 0], 'axis', [0 0 0], 'rot', 0);
b = sphere3(brain_size+CSF_size, 'pos', [0 0 0], 'axis', [0 0 0], 'rot', 0);
c = sphere3(brain_size+CSF_size+skull_size, 'pos', [0 0 0], 'axis', [0 0 0], 'rot', 0);
d = sphere3(brain_size+CSF_size+skull_size+scalp_size, 'pos', [0 0 0], 'axis', [0 0 0], 'rot', 0);
e = cylinder3(electrode_diameter, electrode_height, 'pos', [0 -r-1 0], 'axis', [0 1 0], 'rot', 0);
e = e - e*d;
f = cylinder3(electrode_diameter, electrode_height, 'pos', [0 r 0], 'axis', [0 1 0], 'rot', 0);
f = f - f*d;

geom = geomcoerce('solid', {a b c d e f});


%3-D TES model, epidural stimulation geometry
brain_size = 6.4; % measurements in cm
CSF_size = 0.4;
skull_size = 0.7;
scalp_size = 0.5;
electrode_diameter = 1;
electrode_height = 1;
electrode_probe_height = 2;
angle = pi/4;
r = 7.8;
r1 = brain_size+CSF_size - 0.2;
x=r*cos(angle);
```

```
y=r*sin(angle);
x1=r1*cos(angle);
y1=r1*sin(angle);

a = sphere3(brain_size, 'pos', [0 0 0], 'axis', [0 0 0], 'rot', 0);
b = sphere3(brain_size+CSF_size, 'pos', [0 0 0], 'axis', [0 0 0], 'rot', 0);
c = sphere3(brain_size+CSF_size+skull_size, 'pos', [0 0 0], 'axis', [0 0 0], 'rot', 0);
d = sphere3(brain_size+CSF_size+skull_size+scalp_size, 'pos', [0 0 0], 'axis', [0 0 0], 'rot', 0);
e = cylinder3(electrode_diameter, electrode_height, 'pos', [x y 0], 'axis', [1 1 0], 'rot', 0);
e = e - e*d;
f = cylinder3(electrode_diameter, electrode_probe_height, 'pos', [-x1 y1 0], 'axis', [-1 1 0], 'rot',
0);
%f = f - f*d;
g = a + b + c + d;
h = g - f*g;
% j = d - f*d;
% k = c - f*c;
% m = b - f*b;

geom = geomcoerce('solid', {e h});


%3-D TES model, cortical stimulation geometry
brain_size = 6.4; % measurements in cm
CSF_size = 0.4;
skull_size = 0.7;
scalp_size = 0.5;
electrode_diameter = 1;
electrode_height = 1;
electrode_probe_height = 2.5;
angle = pi/4;
r = 7.8;
r1 = brain_size - 0.2;
x=r*cos(angle);
y=r*sin(angle);
x1=r1*cos(angle);
y1=r1*sin(angle);

a = sphere3(brain_size, 'pos', [0 0 0], 'axis', [0 0 0], 'rot', 0);
b = sphere3(brain_size+CSF_size, 'pos', [0 0 0], 'axis', [0 0 0], 'rot', 0);
c = sphere3(brain_size+CSF_size+skull_size, 'pos', [0 0 0], 'axis', [0 0 0], 'rot', 0);
d = sphere3(brain_size+CSF_size+skull_size+scalp_size, 'pos', [0 0 0], 'axis', [0 0 0], 'rot', 0);
e = cylinder3(electrode_diameter, electrode_height, 'pos', [x y 0], 'axis', [1 1 0], 'rot', 0);
e = e - e*d;
f = cylinder3(electrode_diameter, electrode_probe_height, 'pos', [-x1 y1 0], 'axis', [-1 1 0], 'rot',
0);
```

```
%f = f - f*d;
g = a + b + c + d;
h = g - f*g;


geom = geomcoerce('solid', {e h});
```

Layered Model Initial Conditions

2D Models

```
Made for C3C4, C3CZ
% all values for electrodes must be unique
% also no overlapping values allowed
% tes.elec_dist = 3;

tes.elec_pos_loc = [1 2 3];
tes.elec_neg_loc = [4 5 6];
tes.elec_pos_value = 100;
tes.elec_neg_value = 0;

CZOpp
% all values for electrodes must be unique
% also no overlapping values allowed
% tes.elec_dist = 3;

tes.elec_pos_loc = [3 4 6];
tes.elec_neg_loc = [1 2 5];
tes.elec_pos_value = 100;
tes.elec_neg_value = 0;

C3Epi
% all values for electrodes must be unique
% also no overlapping values allowed
% tes.elec_dist = 3;

tes.elec_pos_loc = [5];
tes.elec_neg_loc = [8 9 10];
tes.elec_pos_value = 10;
tes.elec_neg_value = 0;

C3Cort
```

```
% all values for electrodes must be unique
% also no overlapping values allowed
% tes.elec_dist = 3;

tes.elec_pos_loc = [7];
tes.elec_neg_loc = [10 11 12];
tes.elec_pos_value = 10;
tes.elec_neg_value = 0;
```

3D Models

```
%Initial Conditions for TES_3D_C3C4

tes.elec_pos_loc = [9 10 11 22 23];
tes.elec_neg_loc = [40 41 44 45 46];
tes.elec_pos_value = 100;
tes.elec_neg_value = 0;


%Initial Conditions for TES_3D_C3CZ

tes.elec_pos_loc = [17 18 21 39 41];
tes.elec_neg_loc = [42 43 46 47 48];
tes.elec_pos_value = 100;
tes.elec_neg_value = 0;

%Initial Conditions for TES_3D_CZopp

tes.elec_pos_loc = [22 23 26 48 50];
tes.elec_neg_loc = [17 18 19 27 28];
tes.elec_pos_value = 100;
tes.elec_neg_value = 0;


%Initial Conditions for TES_3D_epidural

tes.elec_pos_loc = [25];
tes.elec_neg_loc = [46 47 50 51 52];
tes.elec_pos_value = 10;
tes.elec_neg_value = 0;


%Initial Conditions for TES_3D_cortical

tes.elec_pos_loc = [29];
```

```
tes.elec_neg_loc = [50 51 54 55 56];
tes.elec_pos_value = 10;
tes.elec_neg_value = 0;
```

Potential Models

2D Cases

```
Made for C3C4, C3CZ, CZOpp
global tes

TES_2D_geom_C3C4;
TES_2D_init;

fem.geom = geomcoerce('solid', {a b c d e f t u});
%plotstuff = fem.geom;


fem.version.name = 'FEMLAB 3.1';
fem.var = {'epsilon0_es' '8.854187817e-12'};
fem.shape = {'shlag(2,"V")'};
fem.border = 1;
fem.appl.mode = 'Electrostatics';
fem.appl.assignsuffix = '_es';
fem.draw.s.objs = {}; fem.draw.s.name = {};
fem.draw.p.objs = {}; fem.draw.p.name = {};
fem.draw.c.objs = {}; fem.draw.c.name = {};

fem.appl.bnd.V0 = {[0] [0] tes.elec_pos_value tes.elec_neg_value};
fem.appl.bnd.type = {'cont' 'nD0' 'V' 'V'};

% Make vector with columns describing BC for each boundary segment
% By default, make all borders with 'cont' condition
fem.appl.bnd.ind = ones(1, geominfo(fem.geom, 'Od', [1], 'Out', 'no'));

% Compute which subdomains border each segment
bd_border = geominfo(fem.geom, 'Od', [1], 'Out', 'ud');

% Boundary segment i is an outside border if
% bd_border(1,i)*bd_border(2,i) = 0, so
bd_border = bd_border(1,:).*bd_border(2,:);
```

```
% Set outside borders to 'nD0' condition
fem.appl.bnd.ind(find(bd_border==0)) = 2;

% Set electrode voltage
fem.appl.bnd.ind(tes.elec_pos_loc) = 3;
fem.appl.bnd.ind(tes.elec_neg_loc) = 4;

% Set subdomain conductivites
% electrodes, scalp, skull, CSF layer, brain, CSF vessicles
fem.appl.equ.epsilonr = {10000 10000 0.4 0.015 1.4 0.15 0.15 0.15};

% Create equ, bnd, pnt structures
fem = multiphysics(fem)

% Create mesh
fem.mesh = meshinit(fem);
fem.xmesh = meshextend(fem);
fem.rmesh = meshrefine(fem);

% Solve equation
fem.sol=femlin(fem);

%fem.sol.u(find(fem.sol.u > 200)) = 200;
close all;
%geomplot(fem,'edgelabels','on','edgearrows','on');
postplot(fem, 'tridata', 'V');
hold on;

%postplot(fem, 'tridata', 'V', 'contdata', 'V', 'contlevels', 100, 'contbar', 'off', 'contstyle', 'bginv')
% elec_midpointbox;


%% Radial lines drawn when plot used for each variable
theta = [-pi/2:pi/180:3*pi/2];
rad = [0:0.5:8];
for i = 1:length(rad)
   x_mid(i,:) = rad(i)*cos(theta);
   y_mid(i,:) = rad(i)*sin(theta);
   plot(x_mid(i,:), y_mid(i,:),'xk')
   hold on;
end

plot(x_mid, y_mid);

 xy=[x_mid(:), y_mid(:)]';
%  xy1=[x_mid_1(:), y_mid_1(:)]';
```

```
 %xy2=[x_mid_2(:), y_mid_2(:)]';
 v_C3C4=postinterp(fem, 'V', xy);
%  hold on;
 %v1=postinterp(fem, 'V', xy1);
 %hold on;
%  v2=postinterp(fem, 'V', xy2);
 %hold on;
xyv_rad_C3C4 = [x_mid(:), y_mid(:), v_C3C4(:)]';
%xy1v = [x_mid_1(:), y_mid_1(:), v(:)]';
% xy2v = [x_mid_2(:), y_mid_2(:), v(:)]'
%v = postinterp(fem, 'V', [x_mid(:); y_mid(:)]);

%Element number in matrix corresponding to radii in model
element = [rad*2 + 1]';
rad = [(element - 1)/2];

% getting potentials for specific radii, radii plotted from r=0 to r=8, in
% half cm steps
 for i = 1:length(rad);
    for j = 1:length(theta);
    v_tang_2D(i,j) = v_C3C4(i + (j-1)*17);
    end
 end

 %Plotting potential at one radius in the model.
  for i = 17;
    for j = 1:length(theta);
    v_tang_2D_17(j) = v_C3C4(i + (j-1)*17);
    end
 end

% measuringpoints_test;

% rad = [5:1:6];
% theta = [pi/8:pi/48:7*pi/8];
% rad_1 = [0:1:8];
% theta_1 = [7*pi/8:pi/8:17*pi/8];
% rad_2 = [0:0.5:8];
% theta_2 = [pi/4:pi/8:3*pi/4];
% % %radial_points;
% x_mid = rad*cos(theta);
% y_mid = rad*sin(theta);
% x_mid_1 = rad_1*cos(theta_1);
% y_mid_1 = rad_1*sin(theta_1);
% x_mid_2 = rad_2*cos(theta_2);
% y_mid_2 = rad_2*sin(theta_2);
```

```
% %Circles of varying diameter
% theta = [0:pi/48:2*pi];
% rad = [2:1:6];
% for i = 1: length(rad)
%     x_mid = rad(i)*cos(theta);
%     y_mid = rad(i)*sin(theta);
%     plot(x_mid, y_mid, 'xk');
%     hold on;
% end
% %Plotting points radially "outside" where electrodes are on scalp
% theta_1 = [7*pi/8:pi/8:17*pi/8];
% rad_1 = [0:1:8];
% for i = 1: length(rad_1);
%     x_mid_1 = rad_1(i)*cos(theta_1);
%     y_mid_1 = rad_1(i)*sin(theta_1);
%     plot(x_mid_1, y_mid_1, 'xk')
%     hold on;
% end
% %Plotting points radially "inside" where electrodes are on scalp
% theta_2 = [pi/4:pi/8:3*pi/4];
% rad_2 = [0:0.5:8];
% for i = 1: length(rad_2)
%     x_mid_2 = rad_2(i)*cos(theta_2);
%     y_mid_2 = rad_2(i)*sin(theta_2);
%     plot(x_mid_2, y_mid_2, 'xk')
%     %hold on;
% end

%General form for postinterp
%y = postinterp(fem, 'V', xx); % for potential
%y = postinterp(fem, 'normE_es', xx);  % for electric field

% Example code from website in favorites list.
% x=linspace(-10,10,10);
% y=linspace(-10,10,10);
% [x,y]=meshgrid(x,y);
% xx=[x(:),y(:)]';
% result=postinterp(fem,'u',xx,'ext',1);

% for i = length(theta);
%     v = postinterp(fem, 'V', [x_mid; y_mid]);
%     hold on;
% end
```

```
Epidural stimulation model
global tes

TES_2D_geom_epidural;
TES_2D_epidural_init;

fem.geom = geomcoerce('solid', {e h t u});
%plotstuff = fem.geom;


fem.version.name = 'FEMLAB 3.1';
fem.var = {'epsilon0_es' '8.854187817e-12'};
fem.shape = {'shlag(2,"V")'};
fem.border = 1;
fem.appl.mode = 'Electrostatics';
fem.appl.assignsuffix = '_es';
fem.draw.s.objs = {}; fem.draw.s.name = {};
fem.draw.p.objs = {}; fem.draw.p.name = {};
fem.draw.c.objs = {}; fem.draw.c.name = {};

fem.appl.bnd.V0 = {[0] [0] tes.elec_pos_value tes.elec_neg_value};
fem.appl.bnd.type = {'cont' 'nD0' 'V' 'V'};

% Make vector with columns describing BC for each boundary segment
% By default, make all borders with 'cont' condition
fem.appl.bnd.ind = ones(1, geominfo(fem.geom, 'Od', [1], 'Out', 'no'));

% Compute which subdomains border each segment
bd_border = geominfo(fem.geom, 'Od', [1], 'Out', 'ud');

% Boundary segment i is an outside border if
% bd_border(1,i)*bd_border(2,i) = 0, so
bd_border = bd_border(1,:).*bd_border(2,:);

% Set outside borders to 'nD0' condition
fem.appl.bnd.ind(find(bd_border==0)) = 2;

% Set electrode voltage
fem.appl.bnd.ind(tes.elec_pos_loc) = 3;
fem.appl.bnd.ind(tes.elec_neg_loc) = 4;

% Set subdomain conductivites
% scalp, skull, CSF layer, electrode, brain, CSF vessicles
fem.appl.equ.epsilonr = {0.4 0.015 1.4 10000 0.15 1.4 1.4};

% Create equ, bnd, pnt structures
```

```
fem = multiphysics(fem)

% Create mesh
fem.mesh = meshinit(fem);
fem.xmesh = meshextend(fem);
fem.rmesh = meshrefine(fem);

% Solve equation
fem.sol=femlin(fem);

%fem.sol.u(find(fem.sol.u > 200)) = 200;
close all;
%geomplot(fem,'edgelabels','on','edgearrows','on');
postplot(fem, 'tridata', 'V');
hold on;

%postplot(fem, 'tridata', 'V', 'contdata', 'V', 'contlevels', 100, 'contbar', 'off', 'contstyle', 'bginv')
% elec_midpointbox;

% measuringpoints_test;

% rad = [5:1:6];
% theta = [pi/8:pi/48:7*pi/8];
% rad_1 = [0:1:8];
% theta_1 = [7*pi/8:pi/8:17*pi/8];
% rad_2 = [0:0.5:8];
% theta_2 = [pi/4:pi/8:3*pi/4];
% % %radial_points;
% x_mid = rad*cos(theta);
% y_mid = rad*sin(theta);
% x_mid_1 = rad_1*cos(theta_1);
% y_mid_1 = rad_1*sin(theta_1);
% x_mid_2 = rad_2*cos(theta_2);
% y_mid_2 = rad_2*sin(theta_2);

% %Circles of varying diameter
% theta = [0:pi/48:2*pi];
% rad = [2:1:6];
% for i = 1: length(rad)
%     x_mid = rad(i)*cos(theta);
%     y_mid = rad(i)*sin(theta);
%     plot(x_mid, y_mid, 'xk');
%     hold on;
% end
% %Plotting points radially "outside" where electrodes are on scalp
% theta_1 = [7*pi/8:pi/8:17*pi/8];
```

```
% rad_1 = [0:1:8];
% for i = 1: length(rad_1);
%     x_mid_1 = rad_1(i)*cos(theta_1);
%     y_mid_1 = rad_1(i)*sin(theta_1);
%     plot(x_mid_1, y_mid_1, 'xk')
%     hold on;
% end
% %Plotting points radially "inside" where electrodes are on scalp
% theta_2 = [pi/4:pi/8:3*pi/4];
% rad_2 = [0:0.5:8];
% for i = 1: length(rad_2)
%     x_mid_2 = rad_2(i)*cos(theta_2);
%     y_mid_2 = rad_2(i)*sin(theta_2);
%     plot(x_mid_2, y_mid_2, 'xk')
%     %hold on;
% end

%% Radial lines drawn when plot used for each variable
theta = [-pi/2:pi/180:3*pi/2];
rad = [0:0.5:8];
for i = 1:length(rad)
   x_mid(i,:) = rad(i)*cos(theta);
   y_mid(i,:) = rad(i)*sin(theta);
   plot(x_mid(i,:), y_mid(i,:),'xk')
   hold on;
end

plot(x_mid, y_mid);
 xy=[x_mid(:), y_mid(:)]';
 v_C3Epi=postinterp(fem, 'V', xy);
 xyv_rad_C3Epi = [x_mid(:), y_mid(:), v_C3Epi(:)]';

 % getting potentials for specific radii, radii plotted from r=0 to r=8, in
% half cm steps
 for i = 1:length(rad);
   for j = 1:length(theta);
   v_tang_2D(i,j) = v_C3Epi(i + (j-1)*81);
   end
 end

 %Plotting potential at one radius in the model.
%   for i = 14;
%     for j = 1:length(theta);
%     v_tang_2D_14(j) = v_C3Epi(i + (j-1)*81);
%     end
%   end
```

```
%Writing data to csv file
csvwrite('C3Epivents_2D', v_tang_2D');

%Plotting points radially "outside" where electrodes are on scalp
% theta_1 = [0:pi/8:2*pi];
% rad_1 = [0:0.5:8];
% for i = 1: length(rad_1);
%     x_mid_1(i,:) = rad_1(i)*cos(theta_1);
%     y_mid_1(i,:) = rad_1(i)*sin(theta_1);
%     plot(x_mid_1(i,:), y_mid_1(i,:), 'xk')
%     hold on;
% end
%Plotting points radially "inside" where electrodes are on scalp
% theta_2 = [pi/4:pi/8:3*pi/4];
% rad_2 = [0:0.5:8];
% for i = 1: length(rad_2)
%     x_mid_2(i,:) = rad_2(i)*cos(theta_2);
%     y_mid_2(i,:) = rad_2(i)*sin(theta_2);
%     plot(x_mid_2(i,:), y_mid_2(i,:), 'xk')
%     hold on;
% end

%% Plots lines radially
%plot(x_mid, y_mid, x_mid_1, y_mid_1, x_mid_2, y_mid_2);

% plot(x_mid, y_mid);
%  xy=[x_mid(:), y_mid(:)]';
%  v_C3Epi=postinterp(fem, 'V', xy);
%  xyv_rad_C3Epi = [x_mid(:), y_mid(:), v_C3Epi(:)]';
% Plotting values for electric potential at each point
%simplepointsbox;
%[v Ex Ey] = postinterp(fem, 'V', 'Ex_es', 'Ey_es', [x0; y0]);
%[v Ex Ey] = postinterp(fem, 'V', 'Ex_es', 'Ey_es', [rad; theta]);

% x_mid=linspace(rad*cos(0), rad*cos(2*pi), pi/48);
% y_mid=linspace(rad*sin(0), rad*sin(2*pi), pi/48);
% [x_mid,y_mid]=meshgrid(x_mid,y_mid);

%  xy=[x_mid(:), y_mid(:)]';
%  v_C3Epi=postinterp(fem, 'V', xy);
%  xyv_rad_C3Epi = [x_mid(:), y_mid(:), v_C3Epi(:)]';
% %  xy1=[x_mid_1(:), y_mid_1(:)]';
%  %xy2=[x_mid_2(:), y_mid_2(:)]';
%  v_C3Epi=postinterp(fem, 'V', xy);
```

```
%  xyv_rad_C3Epi = [x_mid(:), y_mid(:), v_C3Epi(:)]';
% %  hold on;
%  %v1=postinterp(fem, 'V', xy1);
%  %hold on;
% %  v2=postinterp(fem, 'V', xy2);
%  %hold on;
% xyv_rad_C3Epi = [x_mid(:), y_mid(:), v_C3Epi(:)]';
% %xy1v = [x_mid_1(:), y_mid_1(:), v(:)]';
% % xy2v = [x_mid_2(:), y_mid_2(:), v(:)]'
% %v = postinterp(fem, 'V', [x_mid(:); y_mid(:)]);
%
% %General form for postinterp
% %y = postinterp(fem, 'V', xx); % for potential
% %y = postinterp(fem, 'normE_es', xx);  % for electric field
%
% % Example code from website in favorites list.
% % x=linspace(-10,10,10);
% % y=linspace(-10,10,10);
% % [x,y]=meshgrid(x,y);
% % xx=[x(:),y(:)]';
% % result=postinterp(fem,'u',xx,'ext',1);
%
% % for i = length(theta);
% %     v = postinterp(fem, 'V', [x_mid; y_mid]);
% %     hold on;
% % end
```

Cortical Stimulation

```
global tes

TES_2D_geom_cortex;
TES_2D_cortex_init;

fem.geom = geomcoerce('solid', {e h t u});
%plotstuff = fem.geom;


fem.version.name = 'FEMLAB 3.1';
fem.var = {'epsilon0_es' '8.854187817e-12'};
fem.shape = {'shlag(2,"V")'};
fem.border = 1;
```

```
fem.appl.mode = 'Electrostatics';
fem.appl.assignsuffix = '_es';
fem.draw.s.objs = {}; fem.draw.s.name = {};
fem.draw.p.objs = {}; fem.draw.p.name = {};
fem.draw.c.objs = {}; fem.draw.c.name = {};

fem.appl.bnd.V0 = {[0] [0] tes.elec_pos_value tes.elec_neg_value};
fem.appl.bnd.type = {'cont' 'nD0' 'V' 'V'};

% Make vector with columns describing BC for each boundary segment
% By default, make all borders with 'cont' condition
fem.appl.bnd.ind = ones(1, geominfo(fem.geom, 'Od', [1], 'Out', 'no'));

% Compute which subdomains border each segment
bd_border = geominfo(fem.geom, 'Od', [1], 'Out', 'ud');

% Boundary segment i is an outside border if
% bd_border(1,i)*bd_border(2,i) = 0, so
bd_border = bd_border(1,:).*bd_border(2,:);

% Set outside borders to 'nD0' condition
fem.appl.bnd.ind(find(bd_border==0)) = 2;

% Set electrode voltage
fem.appl.bnd.ind(tes.elec_pos_loc) = 3;
fem.appl.bnd.ind(tes.elec_neg_loc) = 4;

% Set subdomain conductivites
% scalp, skull, CSF layer, brain, electrode, CSF vessicles
fem.appl.equ.epsilonr = {0.4 0.015 1.4 0.15 10000 1.4 1.4};

% Create equ, bnd, pnt structures
fem = multiphysics(fem)

% Create mesh
fem.mesh = meshinit(fem);
fem.xmesh = meshextend(fem);
fem.rmesh = meshrefine(fem);

% Solve equation
fem.sol=femlin(fem);

%fem.sol.u(find(fem.sol.u > 200)) = 200;
close all;
%geomplot(fem,'edgelabels','on','edgearrows','on');
postplot(fem, 'tridata', 'V');
```

```
hold on;

%postplot(fem, 'tridata', 'V', 'contdata', 'V', 'contlevels', 100, 'contbar', 'off', 'contstyle', 'bginv')
% elec_midpointbox;

% measuringpoints_test;

% rad = [5:1:6];
% theta = [pi/8:pi/48:7*pi/8];
% rad_1 = [0:1:8];
% theta_1 = [7*pi/8:pi/8:17*pi/8];
% rad_2 = [0:0.5:8];
% theta_2 = [pi/4:pi/8:3*pi/4];
% % %radial_points;
% x_mid = rad*cos(theta);
% y_mid = rad*sin(theta);
% x_mid_1 = rad_1*cos(theta_1);
% y_mid_1 = rad_1*sin(theta_1);
% x_mid_2 = rad_2*cos(theta_2);
% y_mid_2 = rad_2*sin(theta_2);

% %Circles of varying diameter
% theta = [0:pi/48:2*pi];
% rad = [2:1:6];
% for i = 1: length(rad)
%     x_mid = rad(i)*cos(theta);
%     y_mid = rad(i)*sin(theta);
%     plot(x_mid, y_mid, 'xk');
%     hold on;
% end
% %Plotting points radially "outside" where electrodes are on scalp
% theta_1 = [7*pi/8:pi/8:17*pi/8];
% rad_1 = [0:1:8];
% for i = 1: length(rad_1);
%     x_mid_1 = rad_1(i)*cos(theta_1);
%     y_mid_1 = rad_1(i)*sin(theta_1);
%     plot(x_mid_1, y_mid_1, 'xk')
%     hold on;
% end
% %Plotting points radially "inside" where electrodes are on scalp
% theta_2 = [pi/4:pi/8:3*pi/4];
% rad_2 = [0:0.5:8];
% for i = 1: length(rad_2)
%     x_mid_2 = rad_2(i)*cos(theta_2);
%     y_mid_2 = rad_2(i)*sin(theta_2);
%     plot(x_mid_2, y_mid_2, 'xk')
```

```
%     %hold on;
% end

%% Radial lines drawn when plot used for each variable
theta = [-pi/2:pi/180:3*pi/2];
rad = [0:0.5:8];
for i = 1:length(rad)
   x_mid(i,:) = rad(i)*cos(theta);
   y_mid(i,:) = rad(i)*sin(theta);
   plot(x_mid(i,:), y_mid(i,:),'xk')
   hold on;
end
%Plotting points radially "outside" where electrodes are on scalp
% theta_1 = [0:pi/8:2*pi];
% rad_1 = [0:0.5:8];
% for i = 1: length(rad_1);
%     x_mid_1(i,:) = rad_1(i)*cos(theta_1);
%     y_mid_1(i,:) = rad_1(i)*sin(theta_1);
%     plot(x_mid_1(i,:), y_mid_1(i,:), 'xk')
%     hold on;
% end
%Plotting points radially "inside" where electrodes are on scalp
% theta_2 = [pi/4:pi/8:3*pi/4];
% rad_2 = [0:0.5:8];
% for i = 1: length(rad_2)
%     x_mid_2(i,:) = rad_2(i)*cos(theta_2);
%     y_mid_2(i,:) = rad_2(i)*sin(theta_2);
%     plot(x_mid_2(i,:), y_mid_2(i,:), 'xk')
%     hold on;
% end

%% Plots lines radially
%plot(x_mid, y_mid, x_mid_1, y_mid_1, x_mid_2, y_mid_2);

plot(x_mid, y_mid);
% Plotting values for electric potential at each point
%simplepointsbox;
%[v Ex Ey] = postinterp(fem, 'V', 'Ex_es', 'Ey_es', [x0; y0]);
%[v Ex Ey] = postinterp(fem, 'V', 'Ex_es', 'Ey_es', [rad; theta]);

% x_mid=linspace(rad*cos(0), rad*cos(2*pi), pi/48);
% y_mid=linspace(rad*sin(0), rad*sin(2*pi), pi/48);
% [x_mid,y_mid]=meshgrid(x_mid,y_mid);

 xy=[x_mid(:), y_mid(:)]';
%  xy1=[x_mid_1(:), y_mid_1(:)]';
```

```
 %xy2=[x_mid_2(:), y_mid_2(:)]';
 v_C3Cortvent=postinterp(fem, 'V', xy);
%  hold on;
 %v1=postinterp(fem, 'V', xy1);
 %hold on;
%  v2=postinterp(fem, 'V', xy2);
 %hold on;
xyv_rad_C3Cortvent = [x_mid(:), y_mid(:), v_C3Cortvent(:)]';
%xy1v = [x_mid_1(:), y_mid_1(:), v(:)]';
% xy2v = [x_mid_2(:), y_mid_2(:), v(:)]'
%v = postinterp(fem, 'V', [x_mid(:); y_mid(:)]);

%General form for postinterp
%y = postinterp(fem, 'V', xx); % for potential
%y = postinterp(fem, 'normE_es', xx);  % for electric field

% Example code from website in favorites list.
% x=linspace(-10,10,10);
% y=linspace(-10,10,10);
% [x,y]=meshgrid(x,y);
% xx=[x(:),y(:)]';
% result=postinterp(fem,'u',xx,'ext',1);

% for i = length(theta);
%     v = postinterp(fem, 'V', [x_mid; y_mid]);
%     hold on;
% end
```

3D Cases

Code for C3C4, C3CZ, CZOpp

```
global tes

TES_3D_geom_C3CZ;
TES_3D_C3CZ_init;

fem.geom = geomcoerce('solid', {a b c d e f});
%plotstuff = fem.geom;

fem.version.name = 'FEMLAB 3.1';
fem.var = {'epsilon0_es' '8.854187817e-12'};
fem.shape = {'shlag(2,"V")'};
fem.border = 1;
fem.appl.mode = 'Electrostatics';
```

```
fem.appl.assignsuffix = '_es';
fem.draw.s.objs = {}; fem.draw.s.name = {};
fem.draw.p.objs = {}; fem.draw.p.name = {};
fem.draw.c.objs = {}; fem.draw.c.name = {};

fem.appl.bnd.V0 = {[0] [0] tes.elec_pos_value tes.elec_neg_value};
fem.appl.bnd.type = {'cont' 'nD0' 'V' 'V'};

% Make vector with columns describing BC for each boundary segment
% By default, make all borders with 'cont' condition
fem.appl.bnd.ind = ones(1, geominfo(fem.geom, 'Od', [2], 'Out', 'no'));

% Compute which subdomains border each segment
bd_border = geominfo(fem.geom, 'Od', [2], 'Out', 'ud');

% Boundary segment i is an outside border if
% bd_border(1,i)*bd_border(2,i) = 0, so
bd_border = bd_border(1,:).*bd_border(2,:);

% Set outside borders to 'nD0' condition
fem.appl.bnd.ind(find(bd_border==0)) = 2;

% Set electrode voltage
fem.appl.bnd.ind(tes.elec_pos_loc) = 3;
fem.appl.bnd.ind(tes.elec_neg_loc) = 4;

% Set subdomain conductivites
% scalp, skull, csf, brain, electrode, electrode for C3CZ & CZopp
fem.appl.equ.epsilonr = {0.4 0.015 1.4 0.15 10000 10000};
% Subdomain conductivities for C3C4 geometry
% scalp, skull, electrode, csf, brain, electrode
%fem.appl.equ.epsilonr = {0.4 0.015 10000 1.4 0.15 10000};

% Create equ, bnd, pnt structures
fem = multiphysics(fem)

% Create mesh
fem.mesh = meshinit(fem);
fem.xmesh = meshextend(fem);


% Solve equation
fem.sol=femlin(fem, ...
'symmetric','on', ...
'solcomp',{'V'}, ...
'outcomp',{'V'}, ...
```

```
'linsolver','gmres', ...
'prefun','taucs_llt');



%fem.sol.u(find(fem.sol.u > 200)) = 200;
close all;

postplot(fem, 'tridata', 'V')
hold on;

%Radial Lines drawn for each angle
theta = [0:pi/180:2*pi]; %for opposite
%theta = [-pi/2:pi/180:3*pi/2];
rad = [0:0.5:8];
for i = 1:length(rad)
   for j = 1:length(theta)
   x_mid_3D(i,j) = rad(i)*cos(theta(j));
   y_mid_3D(i,j) = rad(i)*sin(theta(j));
   z_mid_3D(i,j) = 0;
   plot3(x_mid_3D(i,j), y_mid_3D(i,j), z_mid_3D(i,j),'xk')
   hold on;
   end
end



% Making matrices containing points of evaluation
xyz_3D=[x_mid_3D(:), y_mid_3D(:), z_mid_3D(:)]';
% Evaluating points in model
v_3D_C3CZ=postinterp(fem, 'V', xyz_3D);
% Matrix containg postion and value at that point
xyzv_rad_3D_C3CZ = [x_mid_3D(:), y_mid_3D(:), z_mid_3D(:), v_3D_C3CZ(:)]';

%Element number in matrix corresponding to radii in model, there are 81
%points on every radial line
%element = [rad*2 + 1]';
%rad = [(element - 1)/2];

% getting potentials for specific radii, radii plotted from r=0 to r=8, in
% 0.1 cm steps
 for i = 1:length(rad);
   for j = 1:length(theta);
   v_tang_3D(i,j) = v_3D_C3CZ(i + (j-1)*17);
   end
 end
```

```
%Plotting potential at one radius in the model = tangential potential
%values  rad = [(element - 1)/2];

  for i = 14;
    for j = 1:length(theta);
    v_tang_3D_14(j) = v_3D_C3CZ(i + (j-1)*17);
    end
  end

  %Writing data to excel file.
%xlswrite('C3CZ_3D', v_tang_3D');

% Plotting potential along one radial trajectory
%

% theta = [1];
% rad = [0:0.5:8];
% for i = 1:length(rad)
%     for j = 1:length(theta)
%     x_mid_3D(i,j) = rad(i)*cos(theta(j));
%     y_mid_3D(i,j) = rad(i)*sin(theta(j));
%     z_mid_3D(i,j) = 0;
%     xyz_3D_(1)=[x_mid_3D(:), y_mid_3D(:), z_mid_3D(:)]';
%     v_3D_rad_C3C4_(1)=postinterp(fem, 'V', xyz_3D_(1));
%     end
% end

% for i = 1:length(theta);%make constant)
%     for j = 1:length(rad)
%     v_rad_3D_theta(i) = v_3D_C3C4(i,j);
%     end
% end



 % for i = [1:1:17];
%     for j = [1:1:360];
%     v_tang(i, j) = v_3D_C3CZ(1 + i*2 + (j-1)*17);
%     end
% end

% for j = [1:1:10];
%     for i = [1:.5:8];
%         x_mid(i,j) = 1;
```

```
%         y_mid(i,j) = 2;
%         z_mid(i,j) = 3;
%     end
% end
```

Code for Epidural and Cortical Stimulation

```
global tes

TES_3D_geom_epidural;
TES_3D_epidural_init;

fem.geom = geomcoerce('solid', {e h});
%plotstuff = fem.geom;

fem.version.name = 'FEMLAB 3.1';
fem.var = {'epsilon0_es' '8.854187817e-12'};
fem.shape = {'shlag(2,"V")'};
fem.border = 1;
fem.appl.mode = 'Electrostatics';
fem.appl.assignsuffix = '_es';
fem.draw.s.objs = {}; fem.draw.s.name = {};
fem.draw.p.objs = {}; fem.draw.p.name = {};
fem.draw.c.objs = {}; fem.draw.c.name = {};

fem.appl.bnd.V0 = {[0] [0] tes.elec_pos_value tes.elec_neg_value};
fem.appl.bnd.type = {'cont' 'nD0' 'V' 'V'};

% Make vector with columns describing BC for each boundary segment
% By default, make all borders with 'cont' condition
fem.appl.bnd.ind = ones(1, geominfo(fem.geom, 'Od', [2], 'Out', 'no'));

% Compute which subdomains border each segment
bd_border = geominfo(fem.geom, 'Od', [2], 'Out', 'ud');

% Boundary segment i is an outside border if
% bd_border(1,i)*bd_border(2,i) = 0, so
bd_border = bd_border(1,:).*bd_border(2,:);

% Set outside borders to 'nD0' condition
fem.appl.bnd.ind(find(bd_border==0)) = 2;

% Set electrode voltage
fem.appl.bnd.ind(tes.elec_pos_loc) = 3;
fem.appl.bnd.ind(tes.elec_neg_loc) = 4;
```

```
% Set subdomain conductivites for epidural & cortical stimulation
% scalp, skull, csf, brain, electrode
fem.appl.equ.epsilonr = {0.4 0.015 1.4 0.15 10000};

% Create equ, bnd, pnt structures
fem = multiphysics(fem)

% Create mesh
fem.mesh = meshinit(fem);
fem.xmesh = meshextend(fem);

% Solve equation
fem.sol=femlin(fem, ...
'symmetric','on', ...
'solcomp',{'V'}, ...
'outcomp',{'V'}, ...
'linsolver','gmres', ...
'prefun','taucs_llt');

%fem.sol.u(find(fem.sol.u > 200)) = 200;
close all;

postplot(fem, 'tridata', 'V')
hold on;

%Radial Lines drawn for each angle
theta = [-pi/4:pi/180:7*pi/4];
rad = [0:0.5:8];
for i = 1:length(rad)
   for j = 1:length(theta)
   x_mid_3D(i,j) = rad(i)*cos(theta(j));
   y_mid_3D(i,j) = rad(i)*sin(theta(j));
   z_mid_3D(i,j) = 0;
   plot3(x_mid_3D(i,j), y_mid_3D(i,j), z_mid_3D(i,j),'xk')
   hold on;
   end
end

% Matrices with points, evaluating potential at those points, making a
% matrix with all the points and the potential in it for easy comparisons
xyz_3D=[x_mid_3D(:), y_mid_3D(:), z_mid_3D(:)]';
v_3D_C3Epi=postinterp(fem, 'V', xyz_3D);
xyzv_rad_3D_C3Epi = [x_mid_3D(:), y_mid_3D(:), z_mid_3D(:), v_3D_C3Epi(:)]';

%element = [rad*2 + 1]';
%rad = [(element - 1)/2];
```

```
% getting potentials for specific radii, radii plotted from r=0 to r=8, in
% half cm steps
 for i = 1:length(rad);
   for j = 1:length(theta);
   v_tang_3D(i,j) = v_3D_C3Epi(i + (j-1)*17);
   end
 end


%Plotting potential at one radius in the model = tangential potential
%values

  for i = 14;
   for j = 1:length(theta);
   v_tang_3D_14(j) = v_3D_C3Epi(i + (j-1)*17);
   end
  end

   %Writing data to file.
%xlswrite('C3Epi_3D', v_tang_3D');
%
% %Element number in matrix corresponding to radii in model
% element = [radius*2 + 1]';
% radius = [(element - 1)/2];
%
% % getting potentials for specific radii
%  for i = 1:length(radius);
%    for j = 1:length(theta);
%    v_tang(i,j) = v_3D_Cort(i + (j-1)*17);
%    end
%  end
%
% % Matrices with points, evaluating potential at those points, making a
% % matrix with all the points and the potential in it for easy comparisons
% xyz_3D=[x_mid_3D(:), y_mid_3D(:), z_mid_3D(:)]';
% v_3D_Cort=postinterp(fem, 'V', xyz_3D);
% xyzv_rad_3D_Cort = [x_mid_3D(:), y_mid_3D(:), z_mid_3D(:), v_3D_Cort(:)]';
% % for j = [1:1:10];
% %    for i = [1:.5:8];
% %        x_mid(i,j) = 1;
% %        y_mid(i,j) = 2;
% %        z_mid(i,j) = 3;
% %    end
% % end
```

Parameterizations

Half Scalp Paramterizations

```
% Electrodes at C3 and C4 locations

brain_size = 6.4; % measurements in cm
CSF_size = 0.4;
skull_size = 0.7;
scalp_size = 0.25;
%electrode_length = 1; electrode_height = 0.75;
kx1 = 0;
kx2 = 1;
ky1 = 0;
ky2 = 0.5;
theta = -pi/4 - 0.01;%rotation of electrodes, angle used to position right electrode
rad = brain_size+CSF_size+skull_size+scalp_size;
phi = pi/4 - 0.12;%angle used to position left electrode
x_r = (rad-0.1)*cos(theta - 0.05);
y_r = (rad-0.1)*sin(theta - 0.05);
x_l = (rad-0.1)*cos(phi + 0.05);
y_l = (rad-0.1)*sin(phi + 0.05);
csf_loop1x = 1.5; % x axis length of csf ellipse
csf_loop1y = .5; % y axis length of csf ellipse
csf_loop2x = .5;
csf_loop2y = 1.4;
s_x = 0; % x value for center of horizontal csf ellipse in brain
s_y = 2.5; % y value for center of horizontal csf ellipse in brain
t_x = 0; % x value for center of vertical csf ellipse in brain
t_y = 1.25; %y value for center of vertical csf ellipse in brain

a = circ2(0, 0, brain_size);
b = circ2(0, 0, brain_size+CSF_size);
c = circ2(0, 0, brain_size+CSF_size+skull_size);
d = circ2(0, 0, brain_size+CSF_size+skull_size+scalp_size);
```

```
e = rect2(kx1, kx2, ky1, ky2);%right electrode
e = rotate(e, theta);
e = move(e, x_r, -y_r);
e = e - e*d;
f = rect2(kx1, kx2, ky1, ky2);%left electrode
f = rotate(f, -theta +0.05);
f = move(f, -x_l, y_l);
f = f - f*d;
s = ellip2(s_x, s_y, csf_loop1x, csf_loop1y);
t = ellip2(t_x, t_y, csf_loop2x, csf_loop2y);
u = s -(t*s);

geom = geomcoerce('solid', {a b c d e f t u});
```

Half Skull Parameterizations

```
% Electrodes at C3 and C4 locations

brain_size = 6.4; % measurements in cm
CSF_size = 0.4;
skull_size = 0.35;
scalp_size = 0.5;
%electrode_length = 1; electrode_height = 0.75;
kx1 = 0;
kx2 = 1;
ky1 = 0;
ky2 = 0.5;
theta = -pi/4 - 0.01;%rotation of electrodes, angle used to position right electrode
rad = brain_size+CSF_size+skull_size+scalp_size;
phi = pi/4 - 0.12;%angle used to position left electrode
x_r = (rad-0.1)*cos(theta - 0.05);
y_r = (rad-0.1)*sin(theta - 0.05);
x_l = (rad-0.1)*cos(phi + 0.05);
y_l = (rad-0.1)*sin(phi + 0.05);
csf_loop1x = 1.5; % x axis length of csf ellipse
csf_loop1y = .5; % y axis length of csf ellipse
csf_loop2x = .5;
csf_loop2y = 1.4;
s_x = 0; % x value for center of horizontal csf ellipse in brain
s_y = 2.5; % y value for center of horizontal csf ellipse in brain
t_x = 0; % x value for center of vertical csf ellipse in brain
t_y = 1.25; %y value for center of vertical csf ellipse in brain

a = circ2(0, 0, brain_size);
b = circ2(0, 0, brain_size+CSF_size);
c = circ2(0, 0, brain_size+CSF_size+skull_size);
```

```
d = circ2(0, 0, brain_size+CSF_size+skull_size+scalp_size);
e = rect2(kx1, kx2, ky1, ky2);%right electrode
e = rotate(e, theta);
e = move(e, x_r, -y_r);
e = e - e*d;
f = rect2(kx1, kx2, ky1, ky2);%left electrode
f = rotate(f, -theta +0.05);
f = move(f, -x_l, y_l);
f = f - f*d;
s = ellip2(s_x, s_y, csf_loop1x, csf_loop1y);
t = ellip2(t_x, t_y, csf_loop2x, csf_loop2y);
u = s -(t*s);

geom = geomcoerce('solid', {a b c d e f t u});
```

Half CSF Parameterization

```
% Electrodes at C3 and C4 locations

brain_size = 6.4; % measurements in cm
CSF_size = 0.2;
skull_size = 0.7;
scalp_size = 0.5;
%electrode_length = 1; electrode_height = 0.75;
kx1 = 0;
kx2 = 1;
ky1 = 0;
ky2 = 0.5;
theta = -pi/4 - 0.01;%rotation of electrodes, angle used to position right electrode
rad = brain_size+CSF_size+skull_size+scalp_size;
phi = pi/4 - 0.12;%angle used to position left electrode
x_r = (rad-0.1)*cos(theta - 0.05);
y_r = (rad-0.1)*sin(theta - 0.05);
x_l = (rad-0.1)*cos(phi + 0.05);
y_l = (rad-0.1)*sin(phi + 0.05);
csf_loop1x = 1.5; % x axis length of csf ellipse
csf_loop1y = .5; % y axis length of csf ellipse
csf_loop2x = .5;
csf_loop2y = 1.4;
s_x = 0; % x value for center of horizontal csf ellipse in brain
s_y = 2.5; % y value for center of horizontal csf ellipse in brain
t_x = 0; % x value for center of vertical csf ellipse in brain
t_y = 1.25; %y value for center of vertical csf ellipse in brain

a = circ2(0, 0, brain_size);
b = circ2(0, 0, brain_size+CSF_size);
```

```
c = circ2(0, 0, brain_size+CSF_size+skull_size);
d = circ2(0, 0, brain_size+CSF_size+skull_size+scalp_size);
e = rect2(kx1, kx2, ky1, ky2);%right electrode
e = rotate(e, theta);
e = move(e, x_r, -y_r);
e = e - e*d;
f = rect2(kx1, kx2, ky1, ky2);%left electrode
f = rotate(f, -theta +0.05);
f = move(f, -x_l, y_l);
f = f - f*d;
s = ellip2(s_x, s_y, csf_loop1x, csf_loop1y);
t = ellip2(t_x, t_y, csf_loop2x, csf_loop2y);
u = s -(t*s);

geom = geomcoerce('solid', {a b c d e f t u});
```

APPENDIX B - ELECTRODE ORIENTATIONS

C3-C4 Orientation

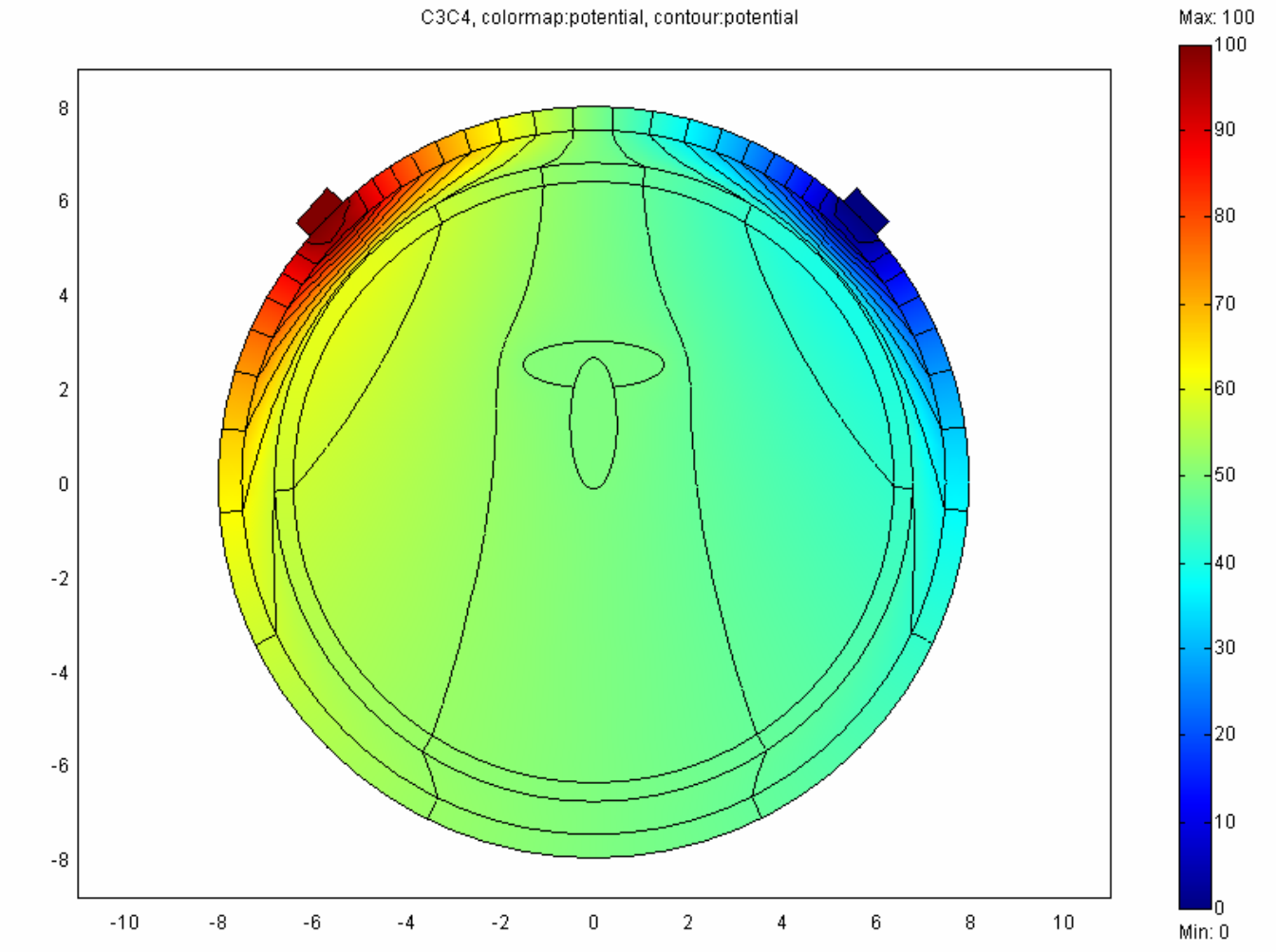

Figure 48: 2D potential model with C3C4 electrode placement with ventricles.

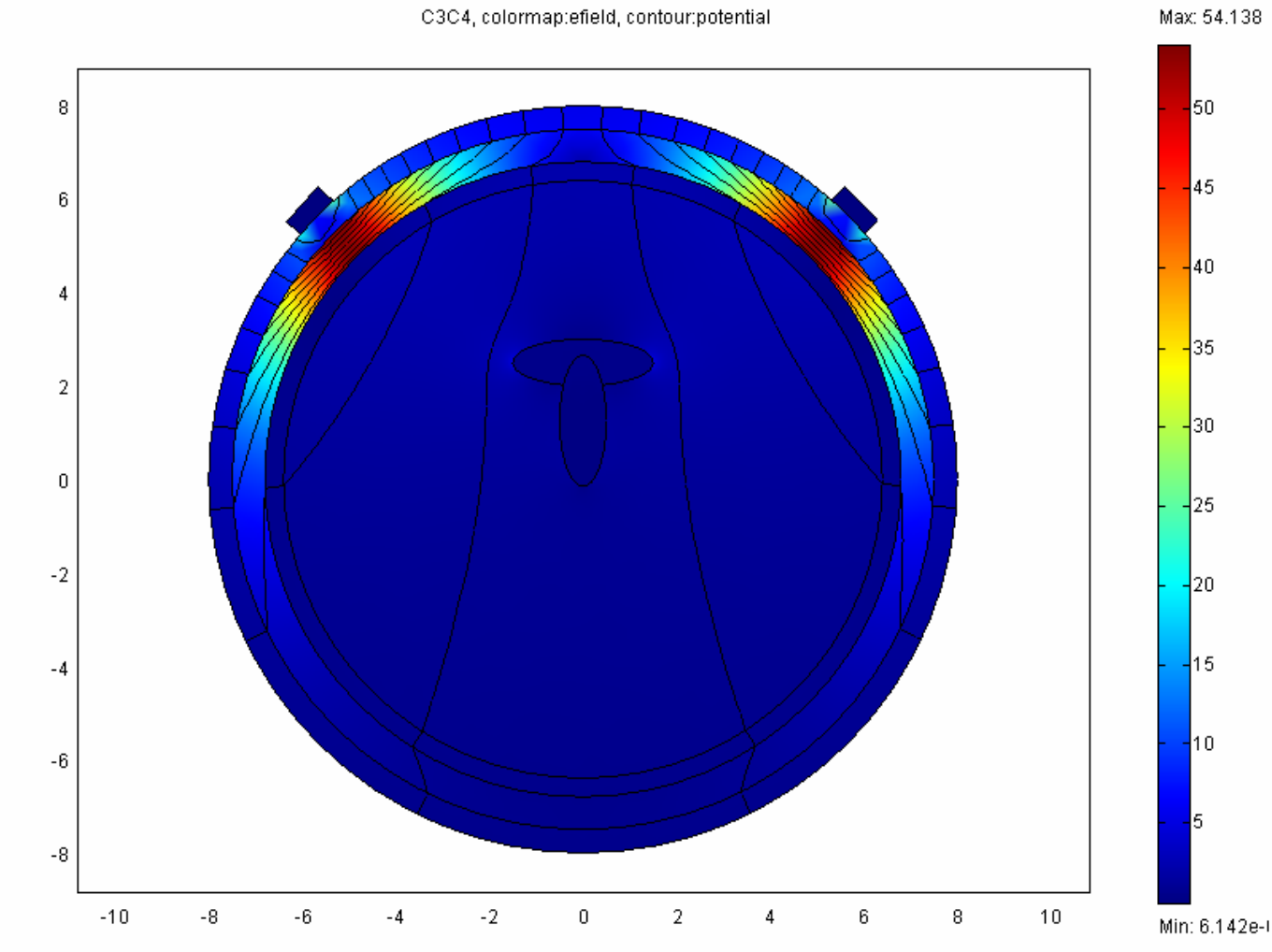

Figure 49: 2D electric field model with C3C4 electrode locations with ventricles.

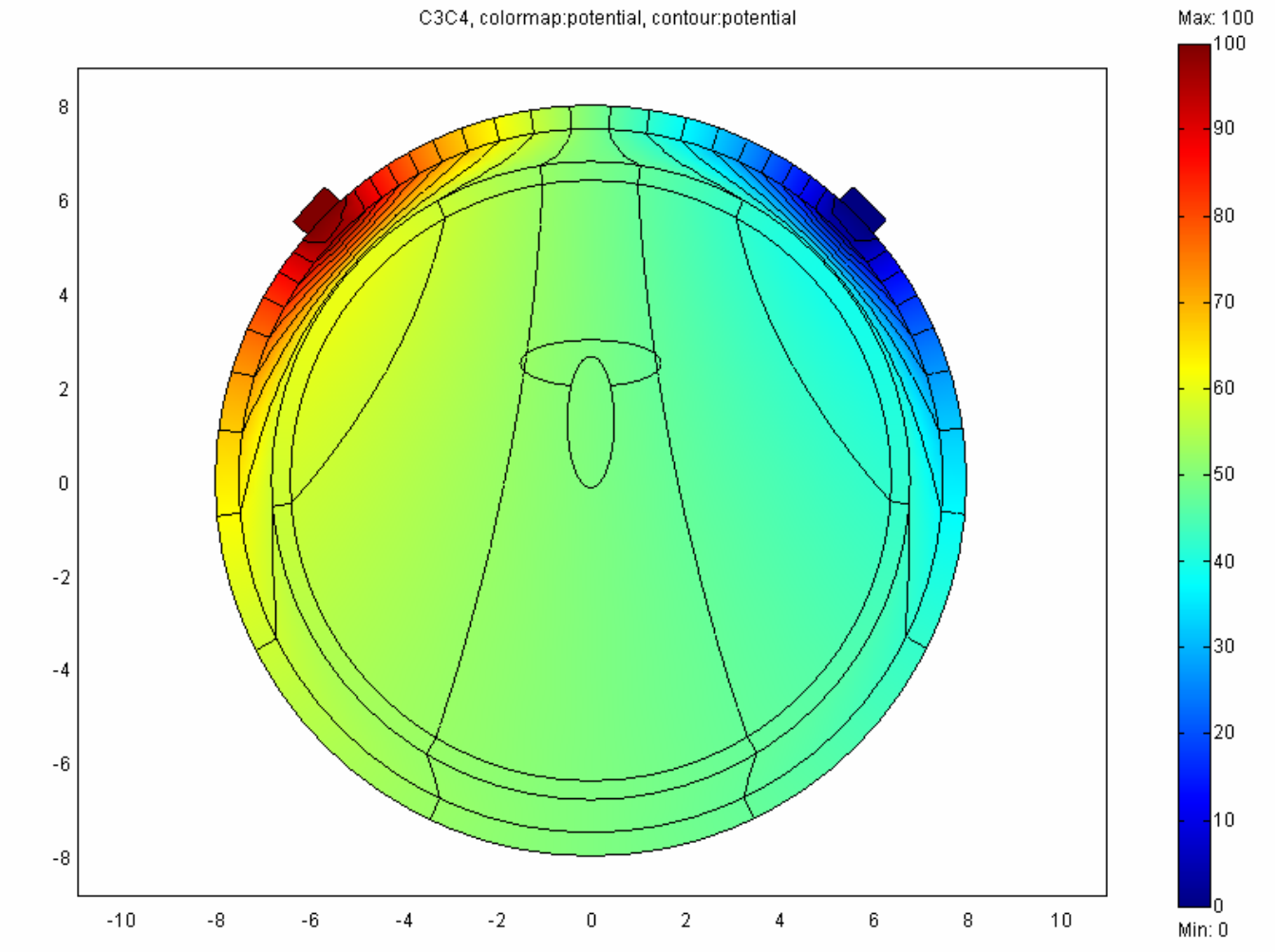

Figure 50: 2D potential model with C3C4 electrode placement and no ventricles.

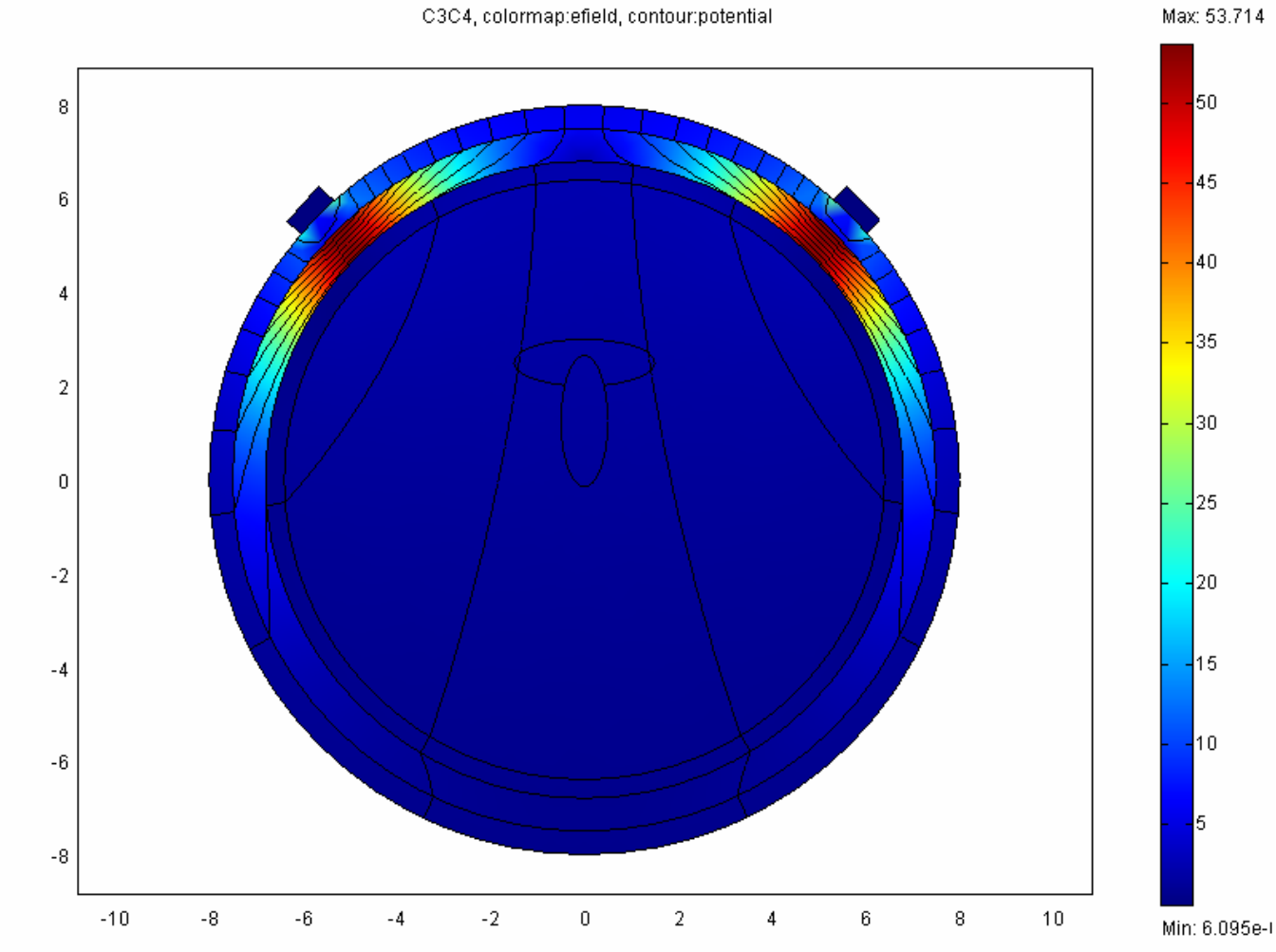

Figure 51: 2D electric field model with C3C4 electrode locations, no ventricles.

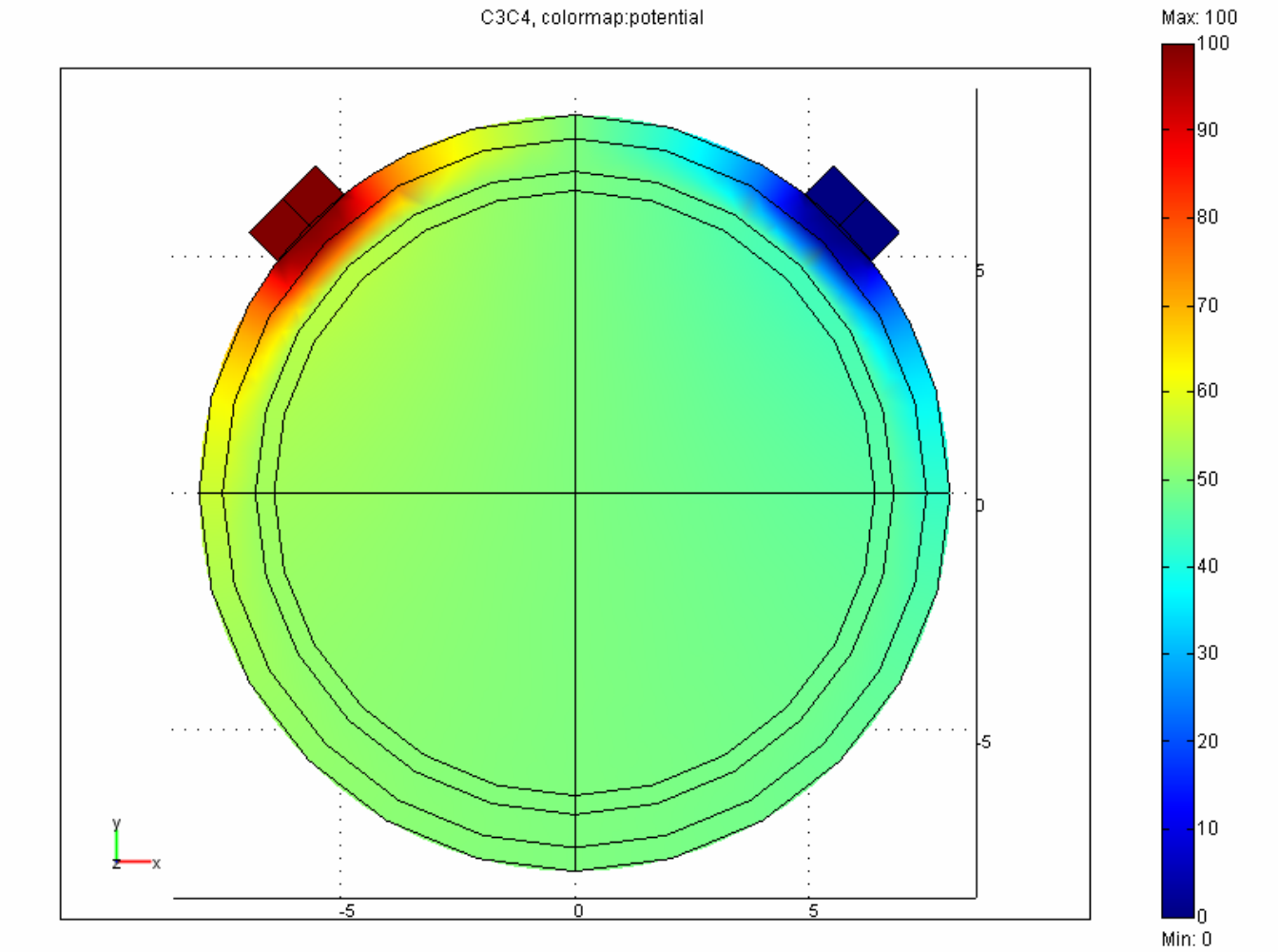

Figure 52: 3D potential model with C3C4 electrode placement and no ventricles, center slice shown.

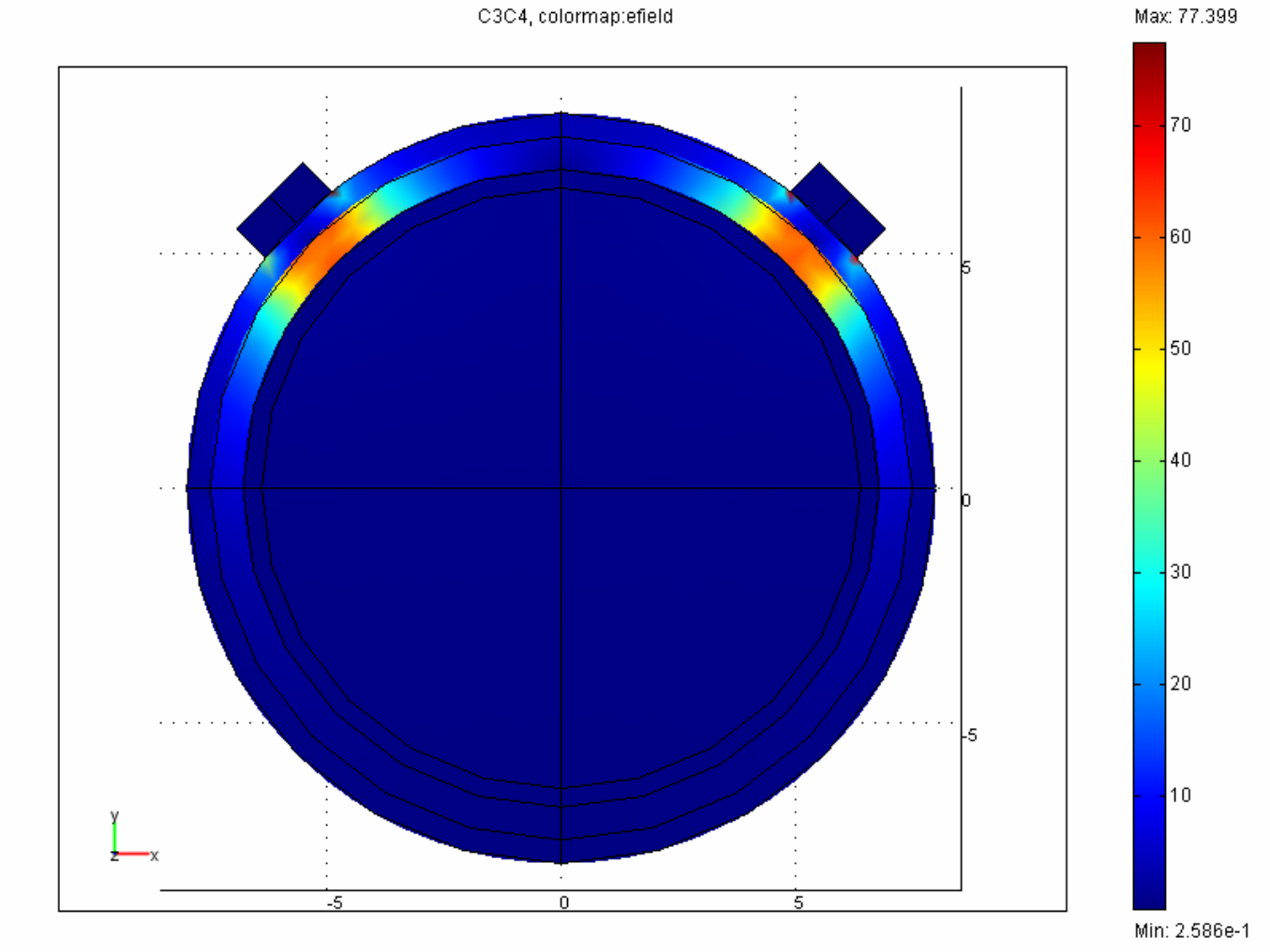

Figure 53: 3D electric field model with C3C4 electrode locations, no ventricles.

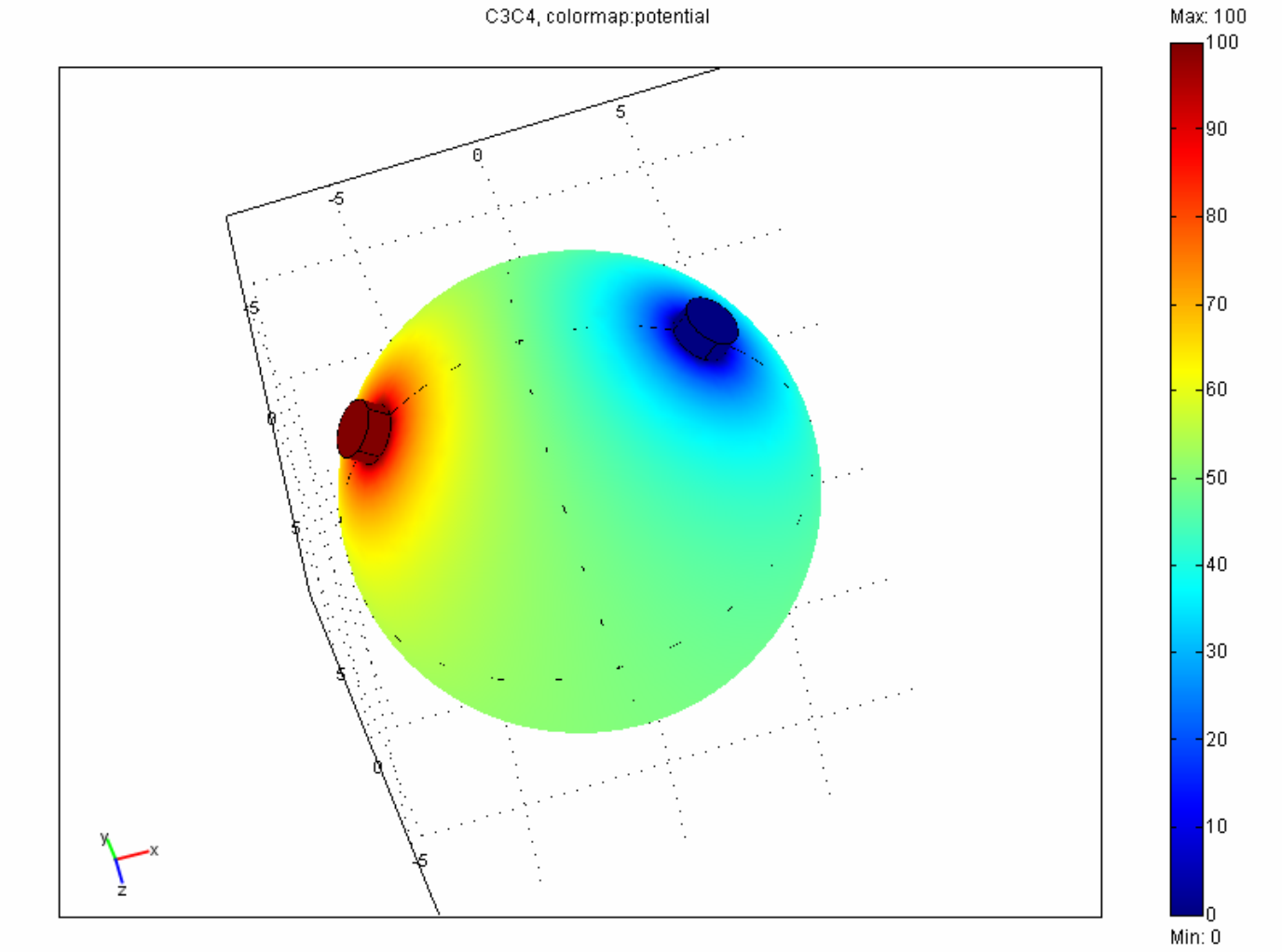

Figure 54: 3D surface potential for C3C4 model.

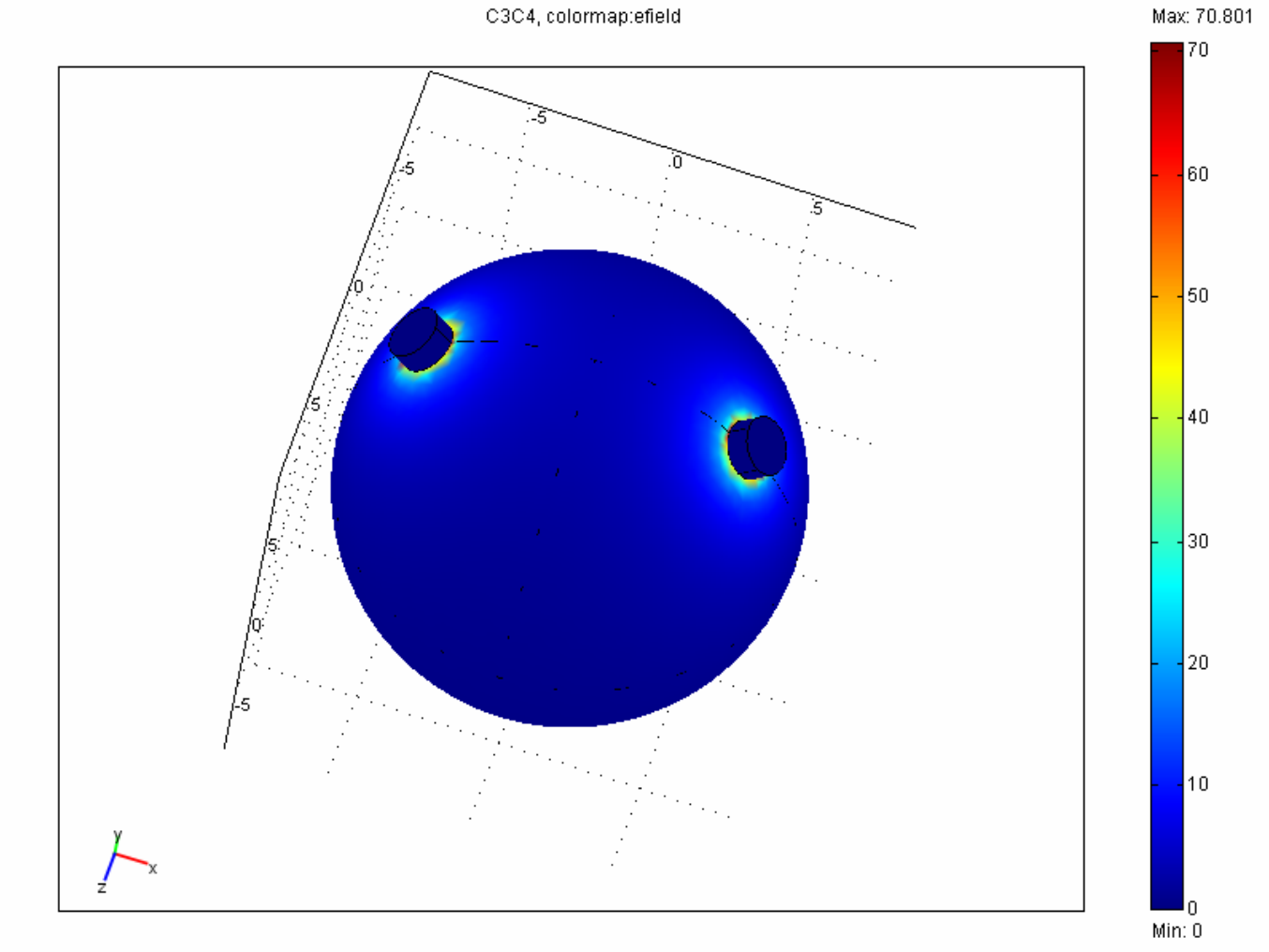

Figure 55: 3D surface plot of electric field for C3C4 electrode locations.

C3-CZ orientation

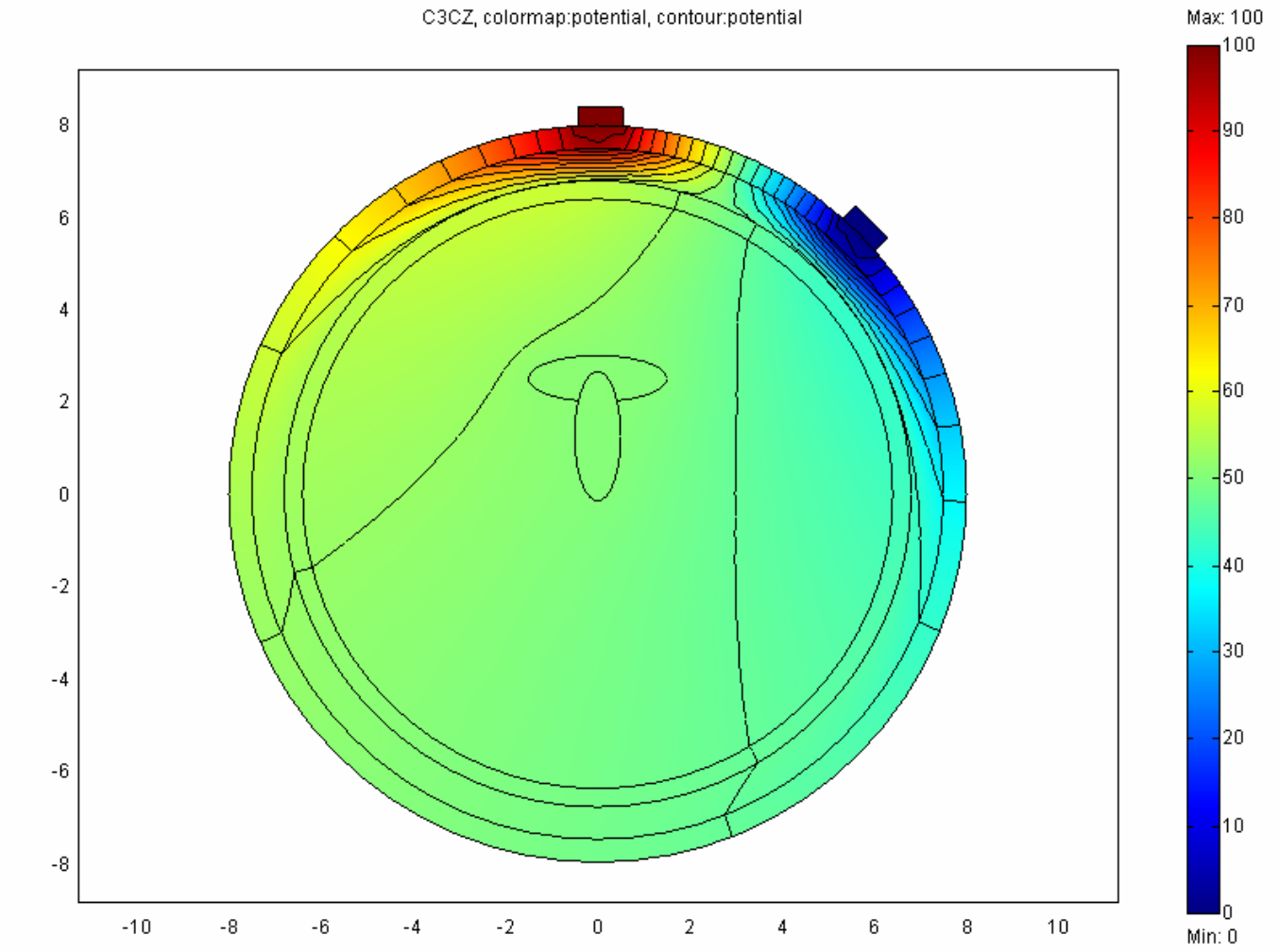

Figure 56: 2D electric potential for C3CZ electrode positions, ventricles included.

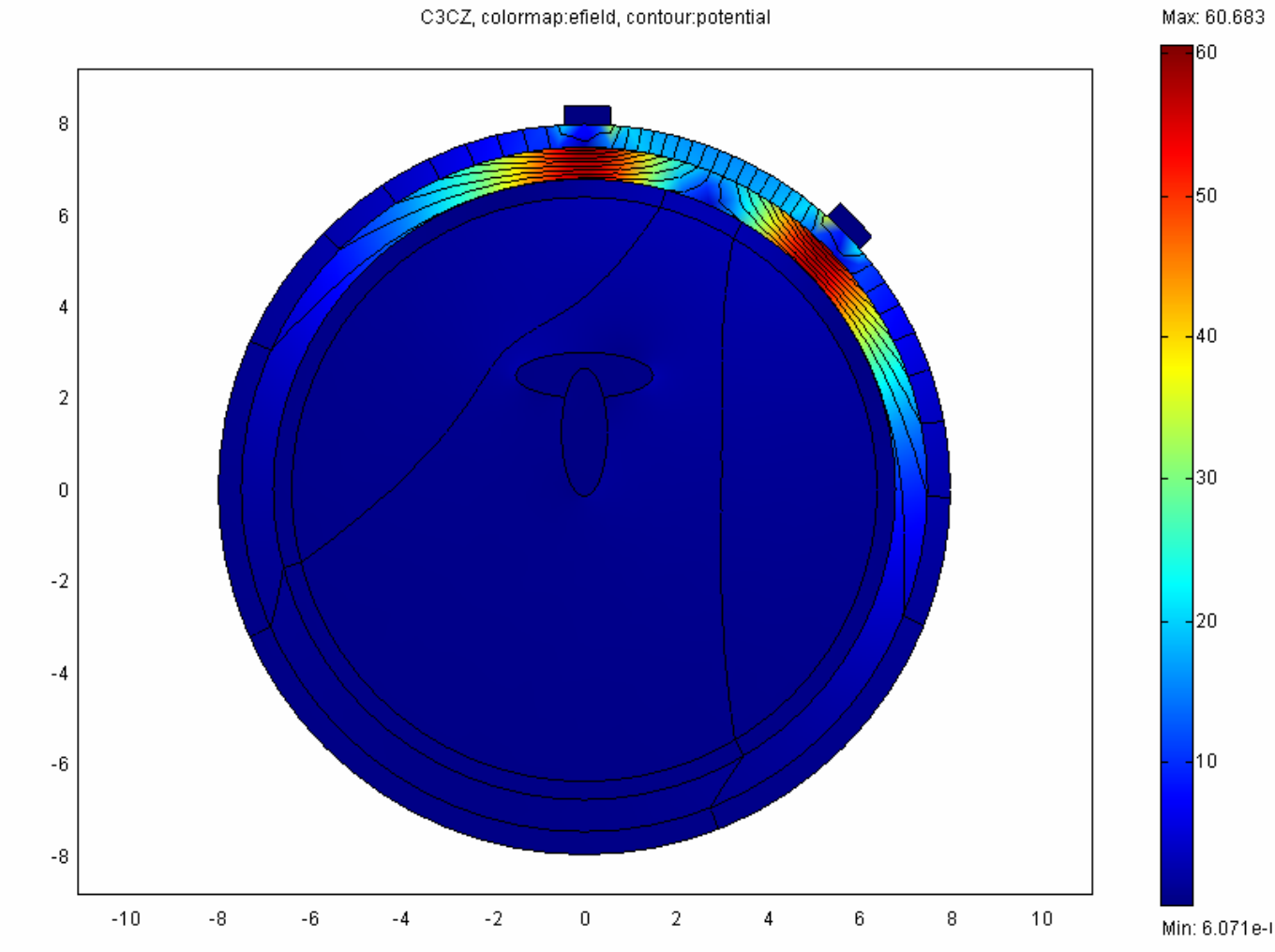

Figure 57: 2D electric field for C3CZ electrode positions, ventricles included.

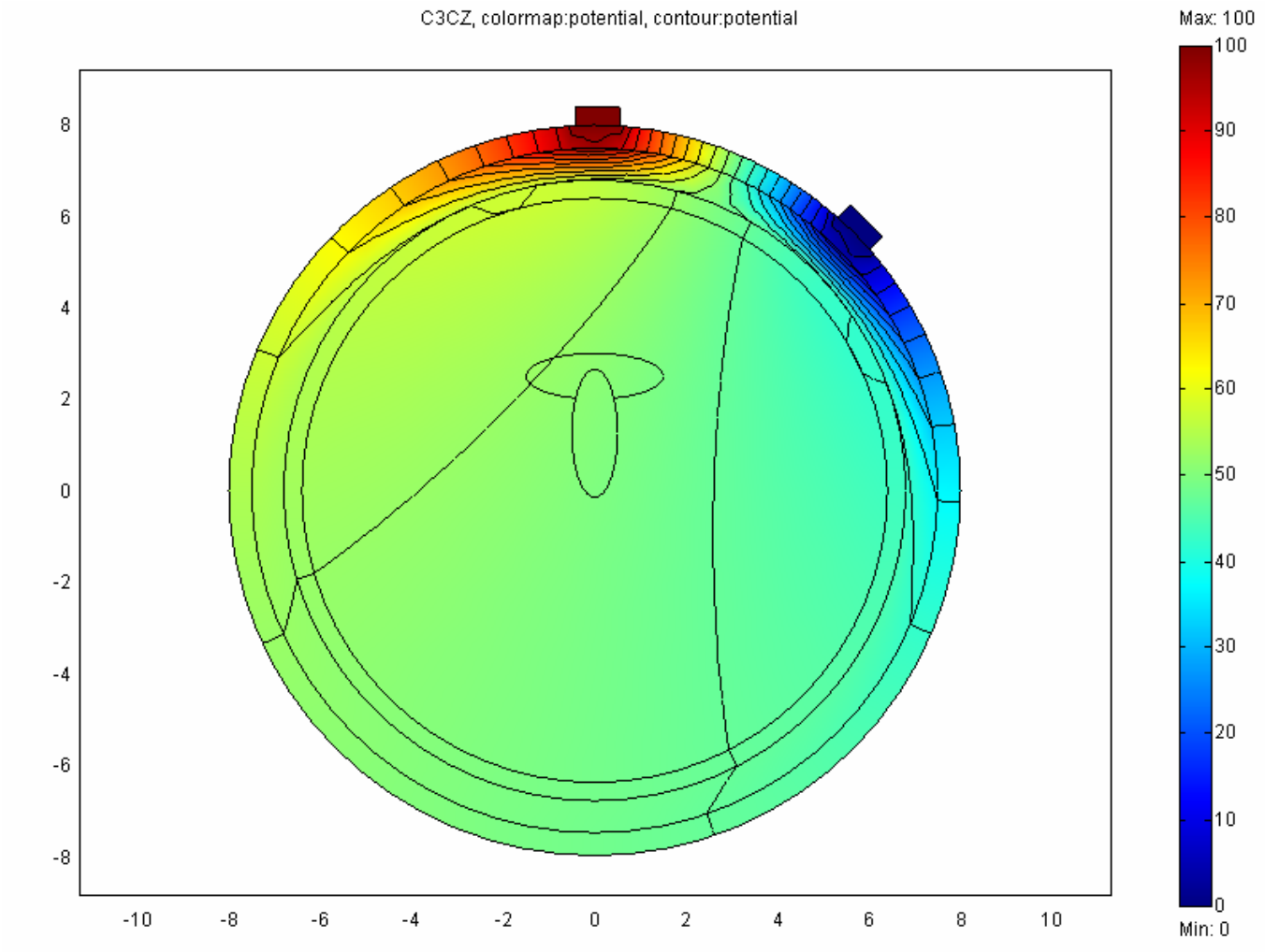

Figure 58: 2D electric potential for C3CZ orientation in model with no ventricles.

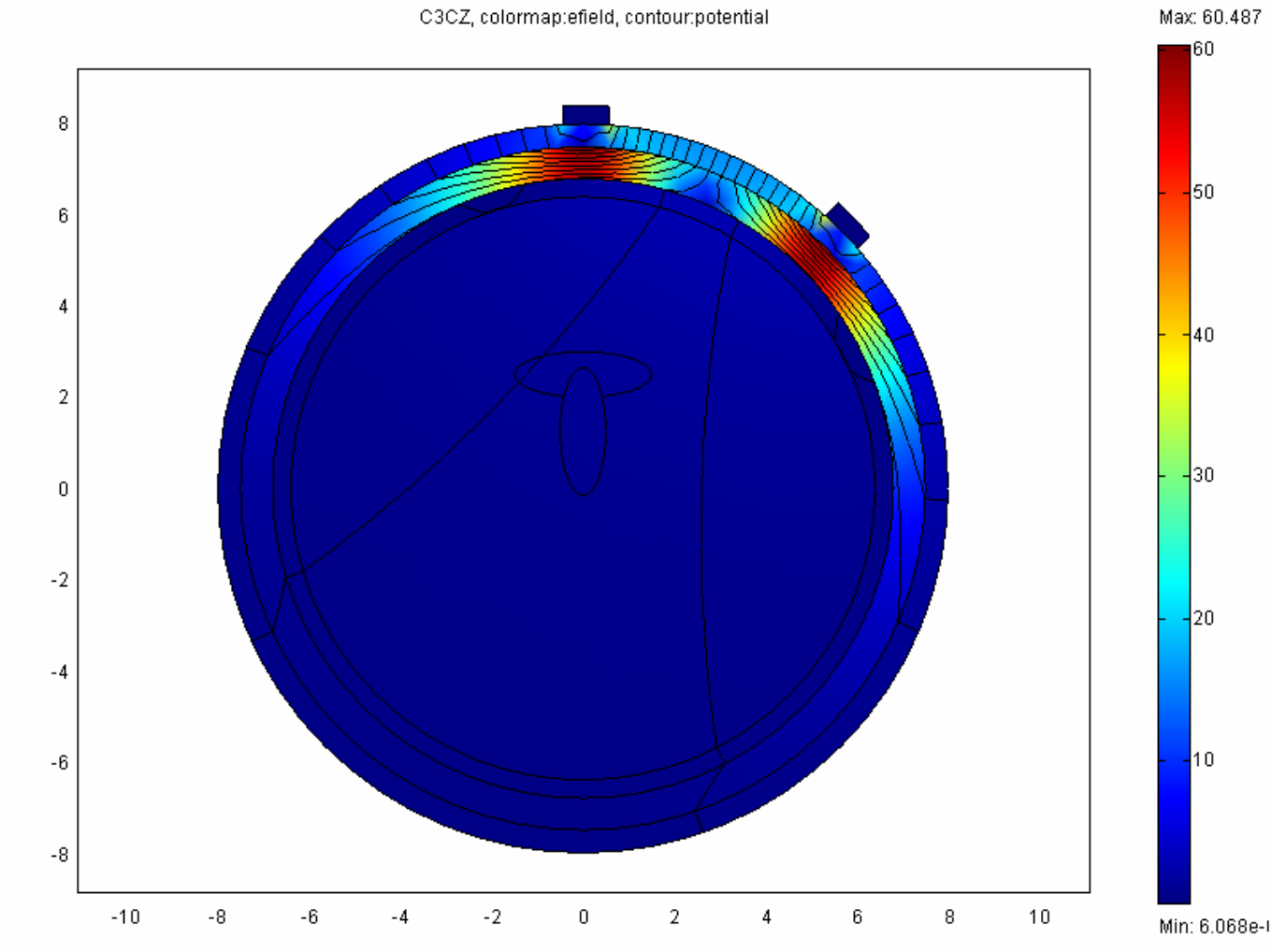

Figure 59: 2D electric field for C3CZ electrode positions, no ventricles included.

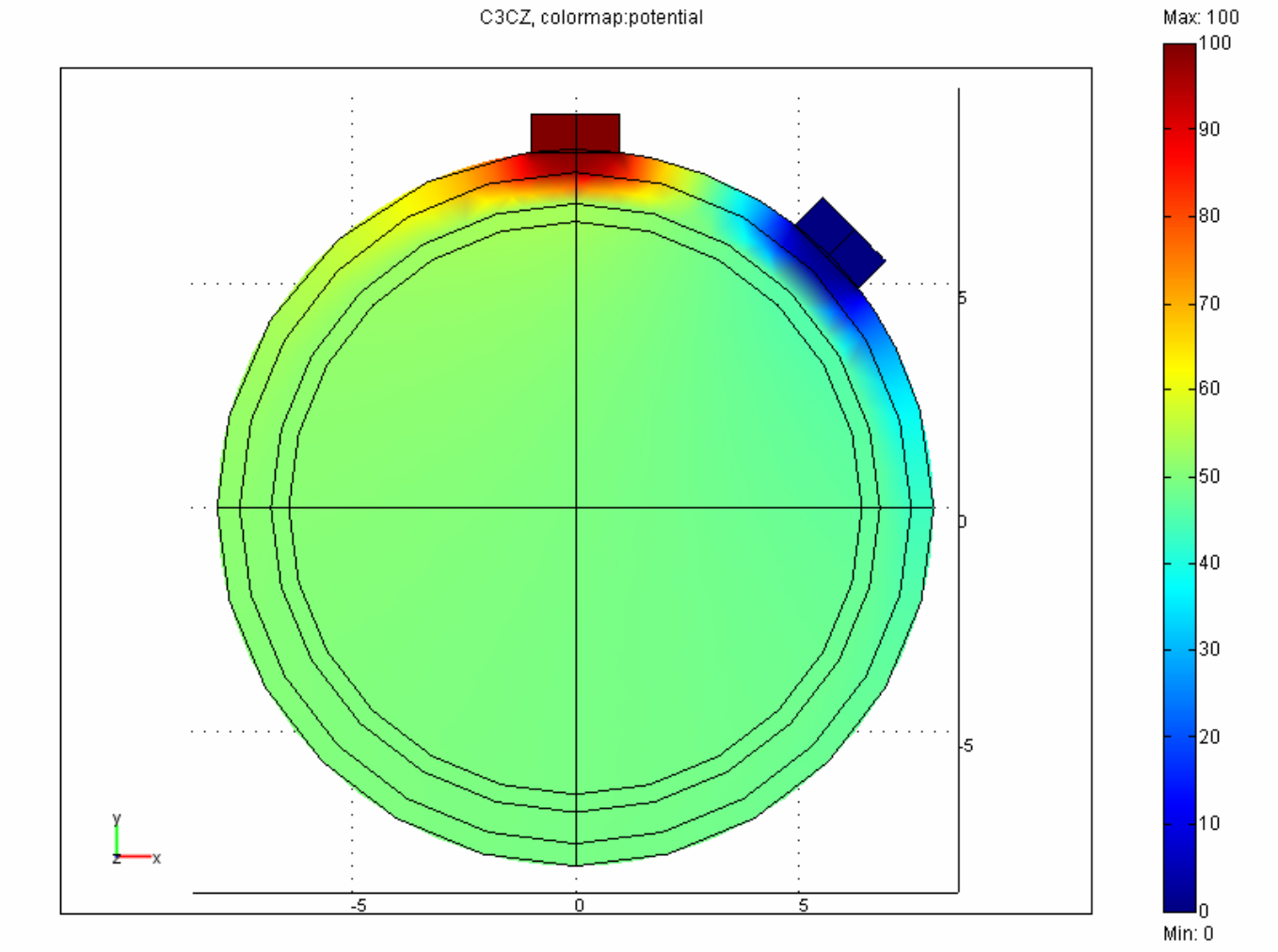

Figure 60: 3D slice plot for electric potential of C3CZ electrode orientation.

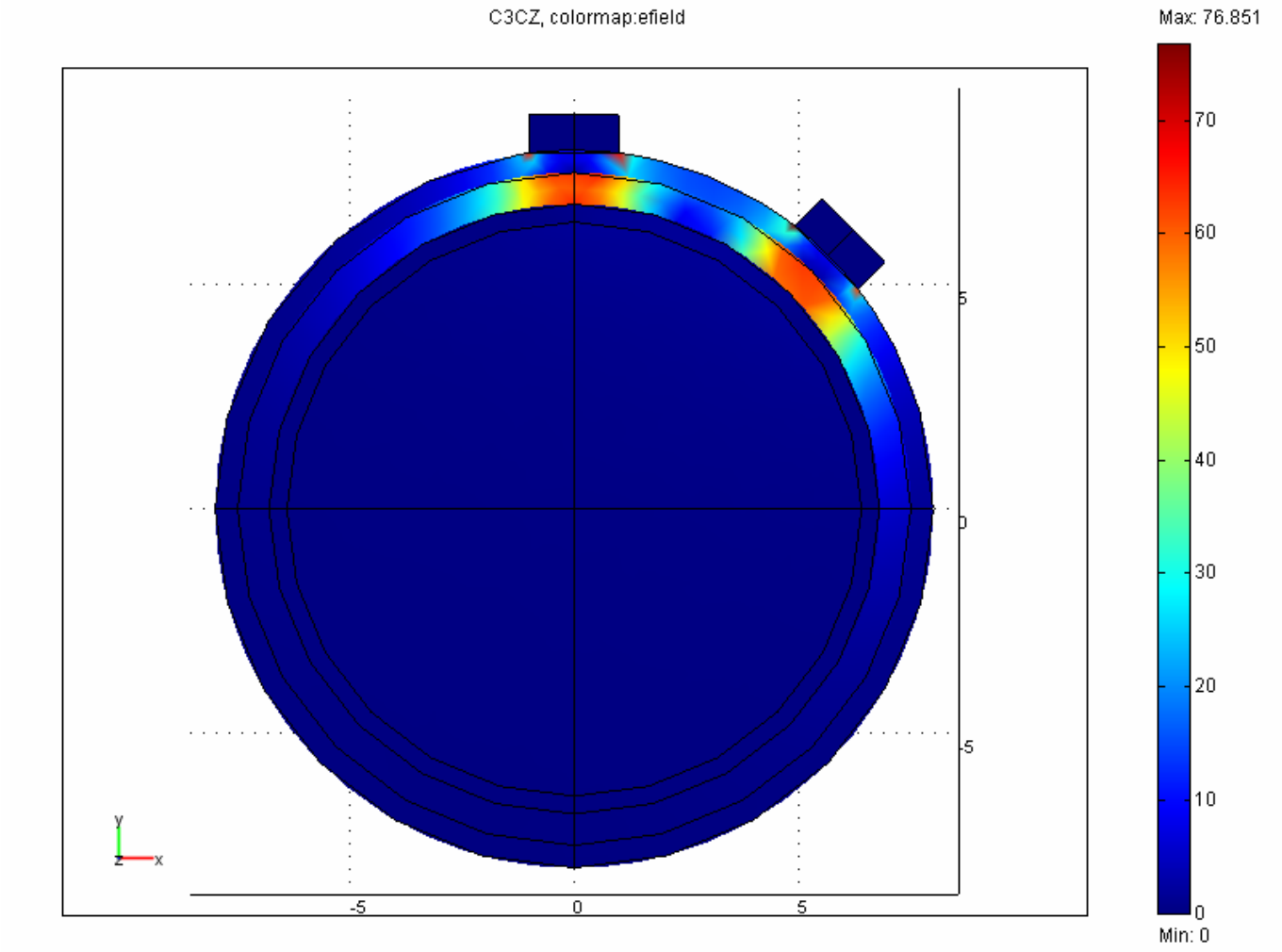

Figure 61: 3D slice plot of electric field for C3CZ orientation.

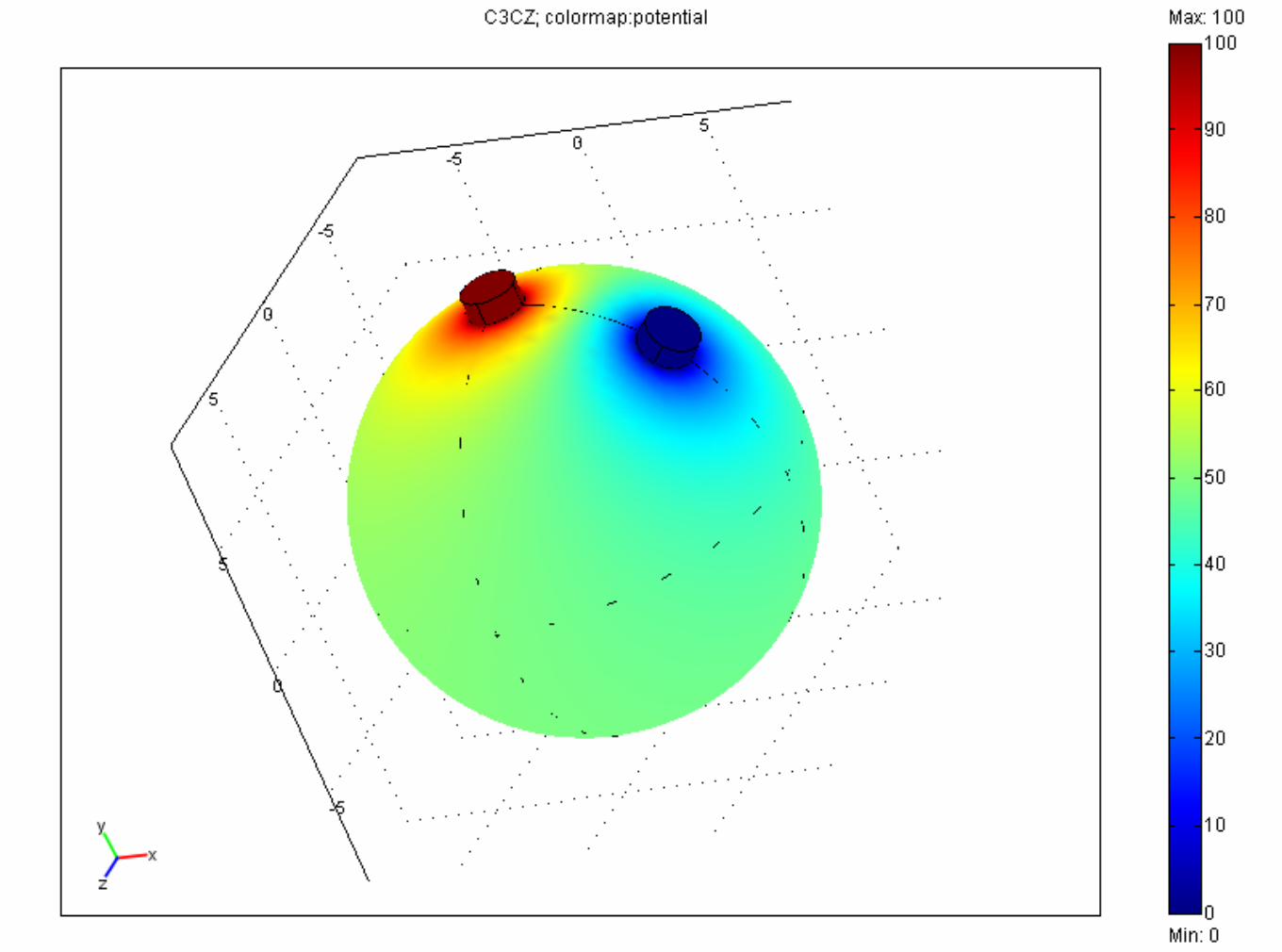

Figure 62: 3D surface plot for electric potential of C3CZ orientation.

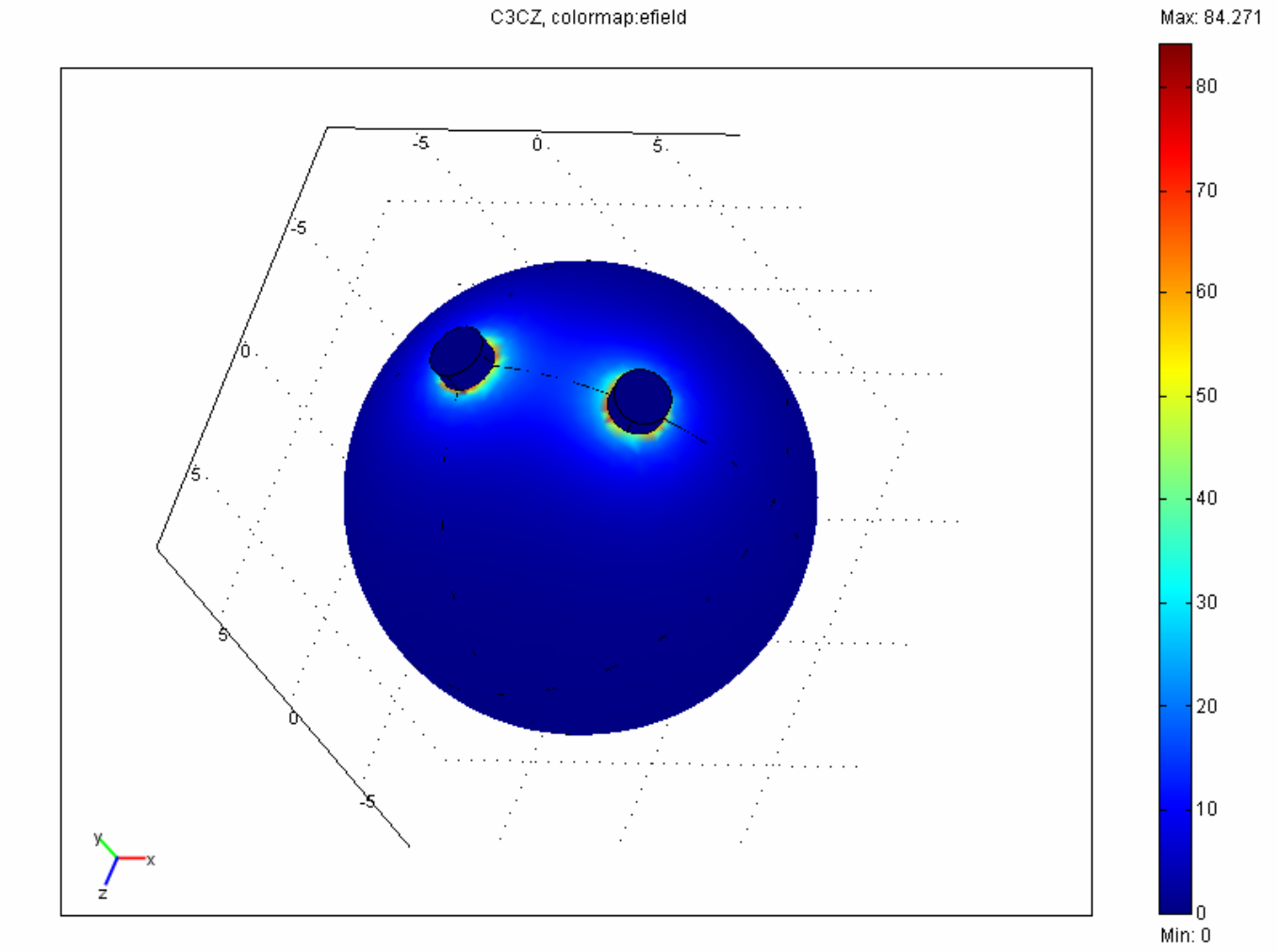

Figure 63: 3D surface plot of electric field for C3CZ orientation.

Diametric Orientation

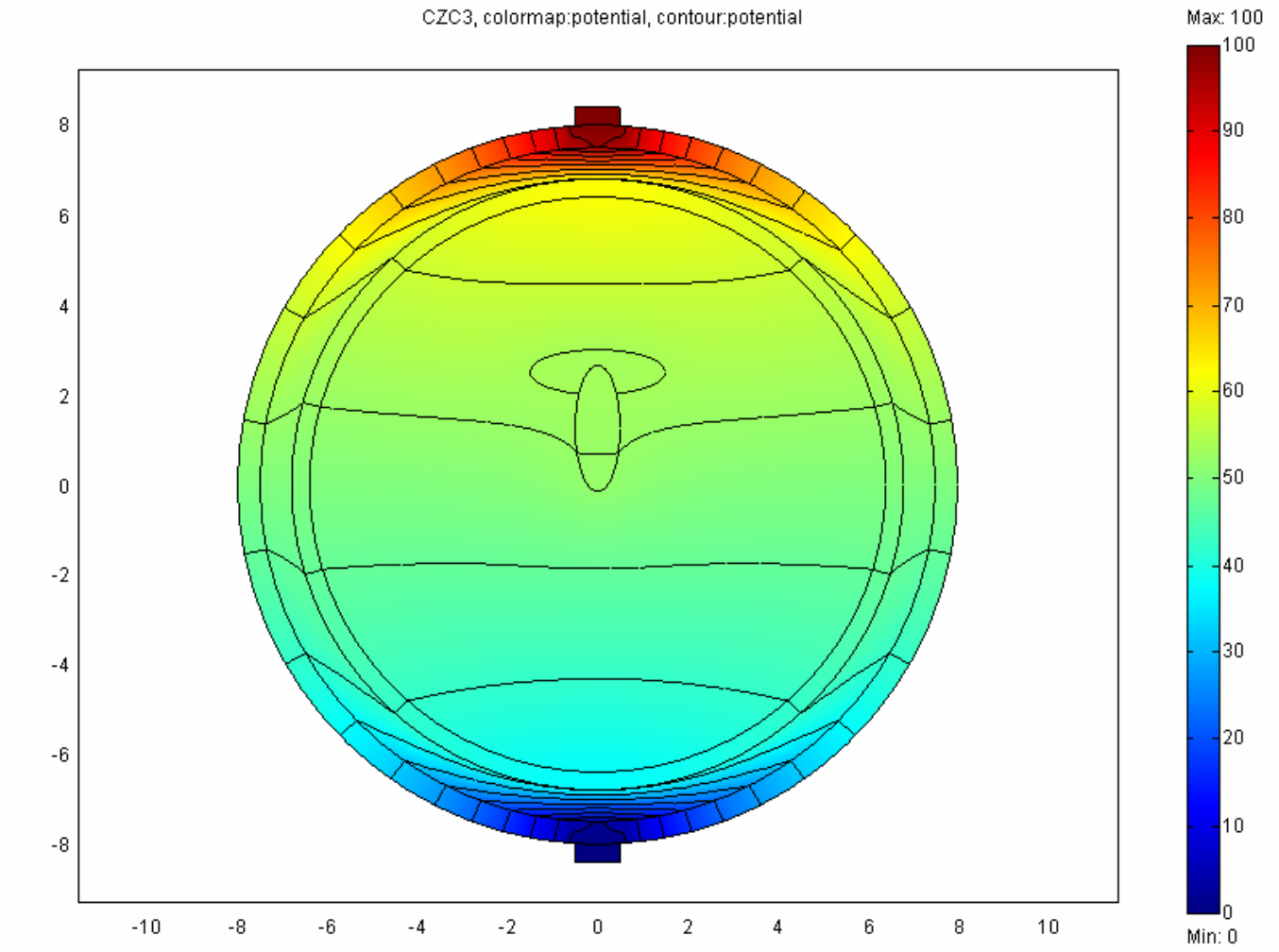

Figure 64: 2D electric potential for diametric orientation, ventricles included.

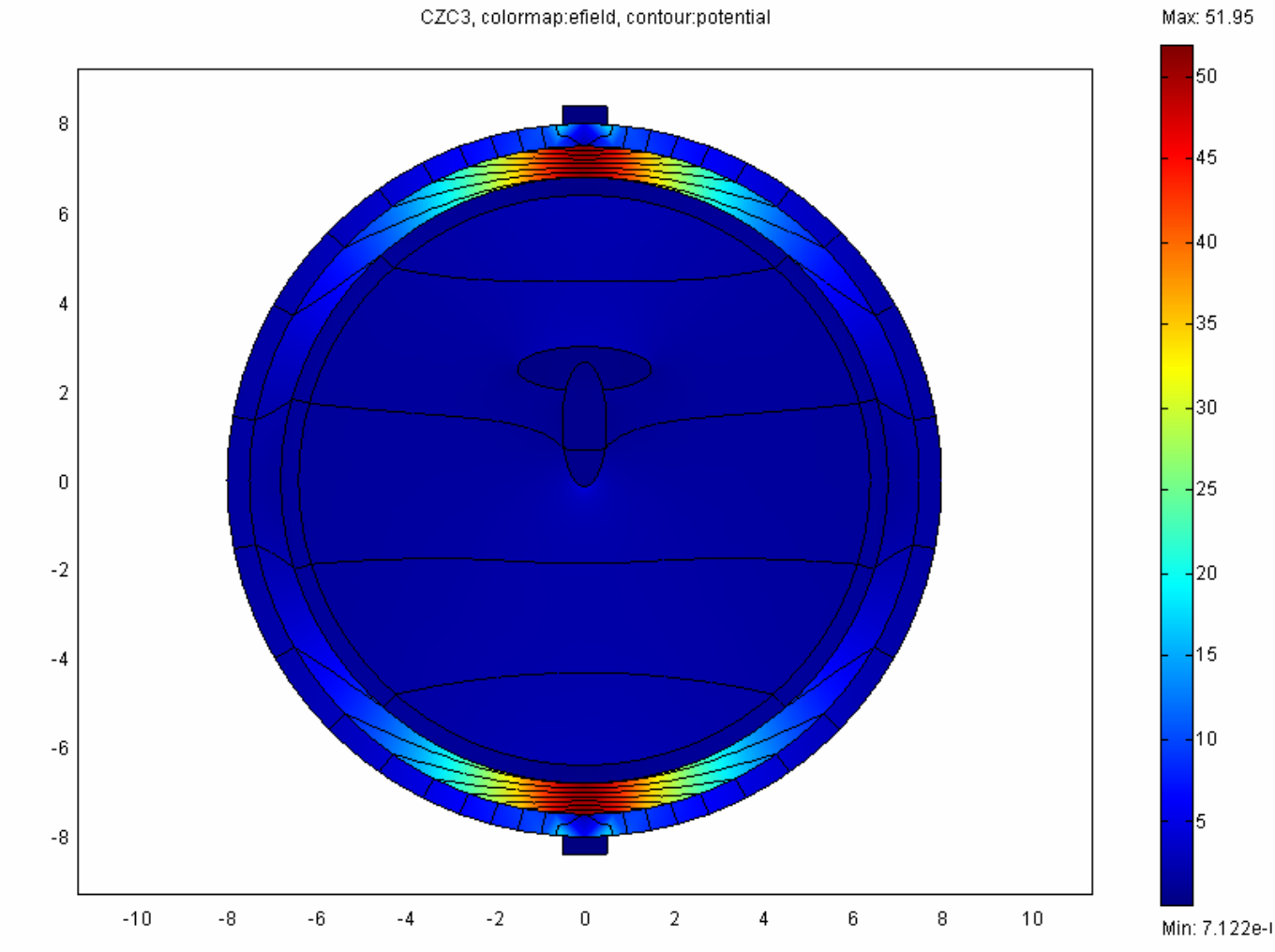

Figure 65: 2D electric field for diametric orientation, ventricles included.

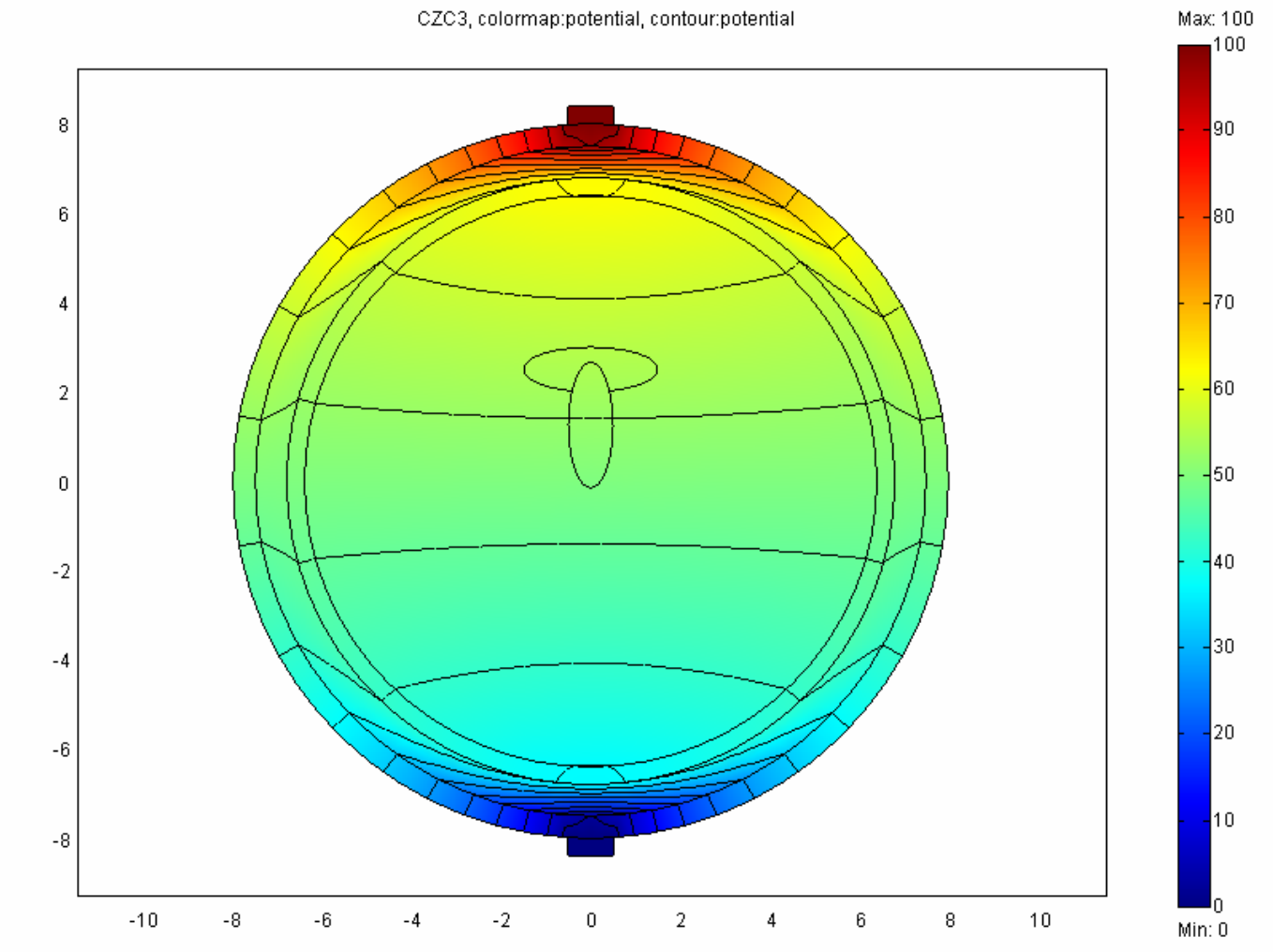

Figure 66: 2D electric potential for diametric orientation, no ventricles included.

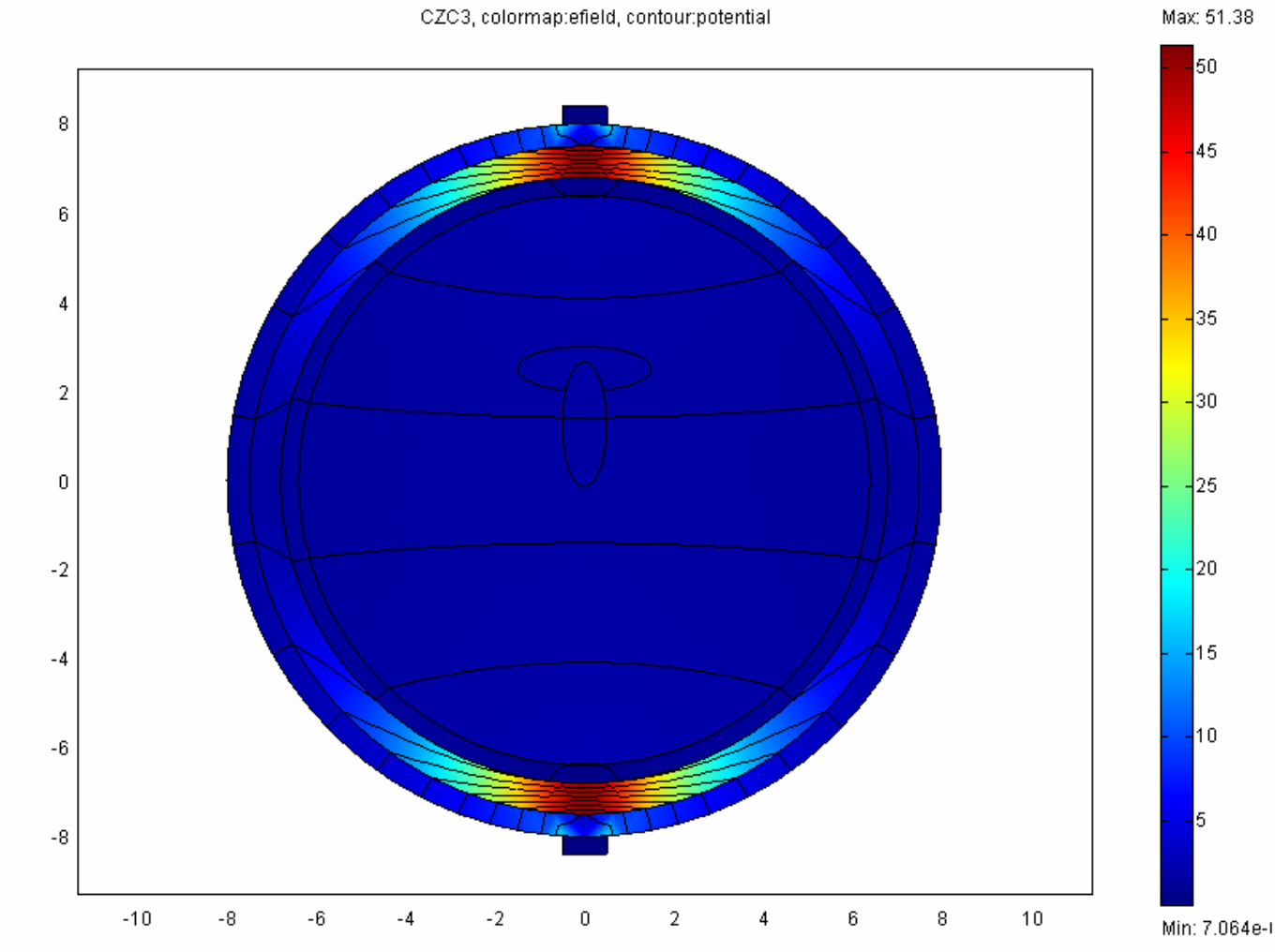

Figure 67: 2D electric field for diametric orientation, no ventricles included.

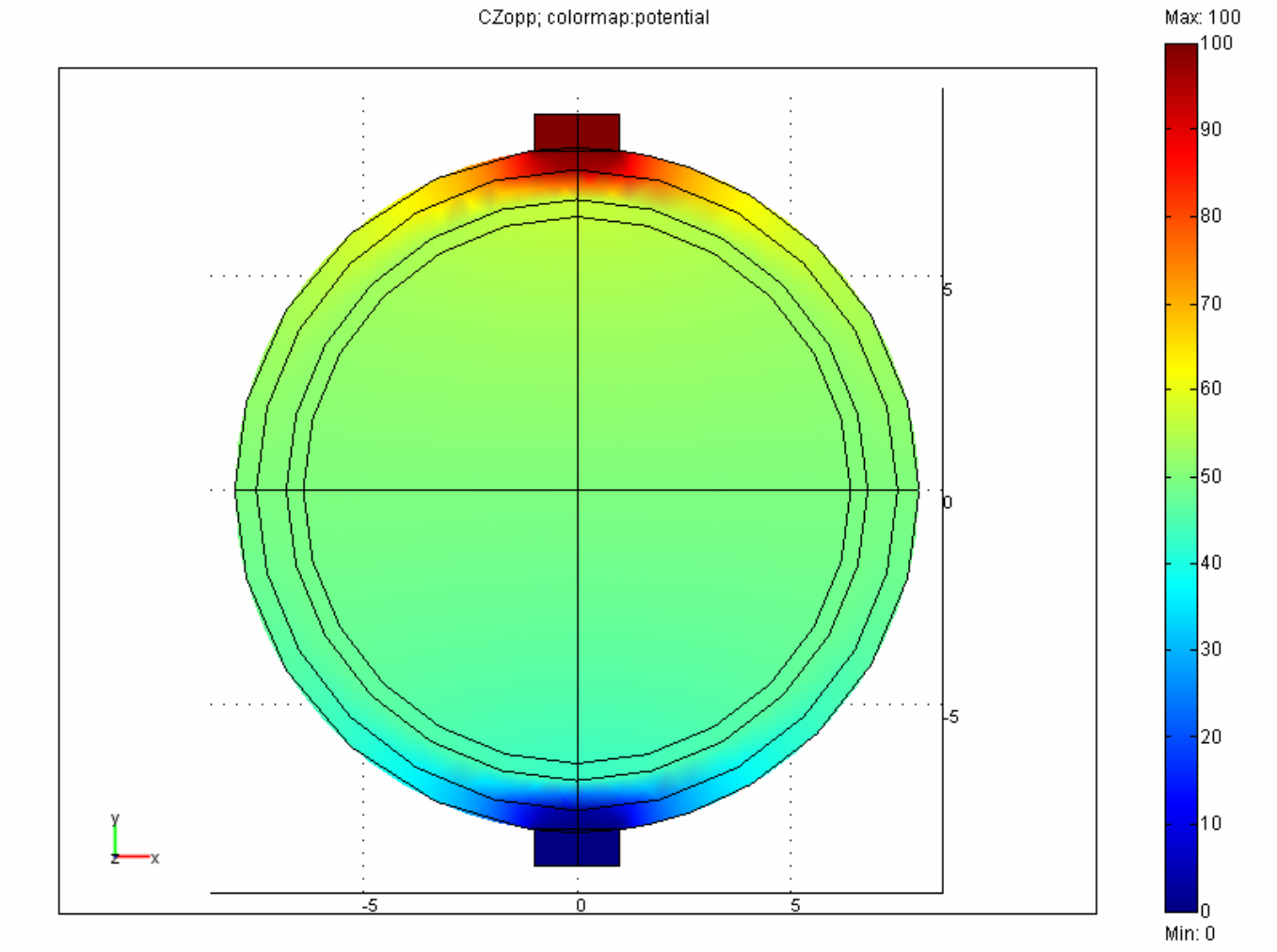

Figure 68: 3D slice plot electric potential for electric potential, no ventricles included.

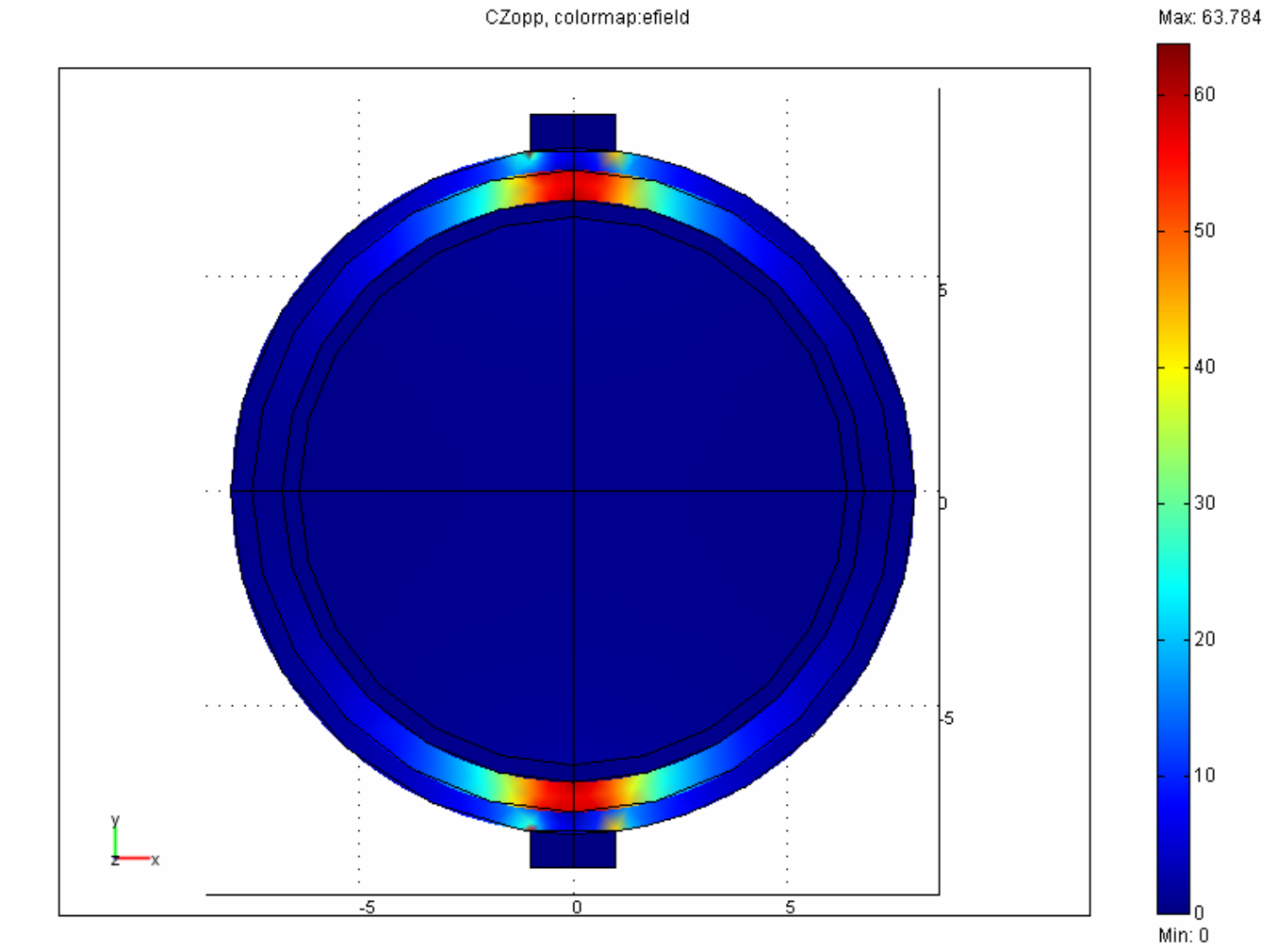

Figure 69: 3D slice plot of electric field for diametric orientation, no ventricles included.

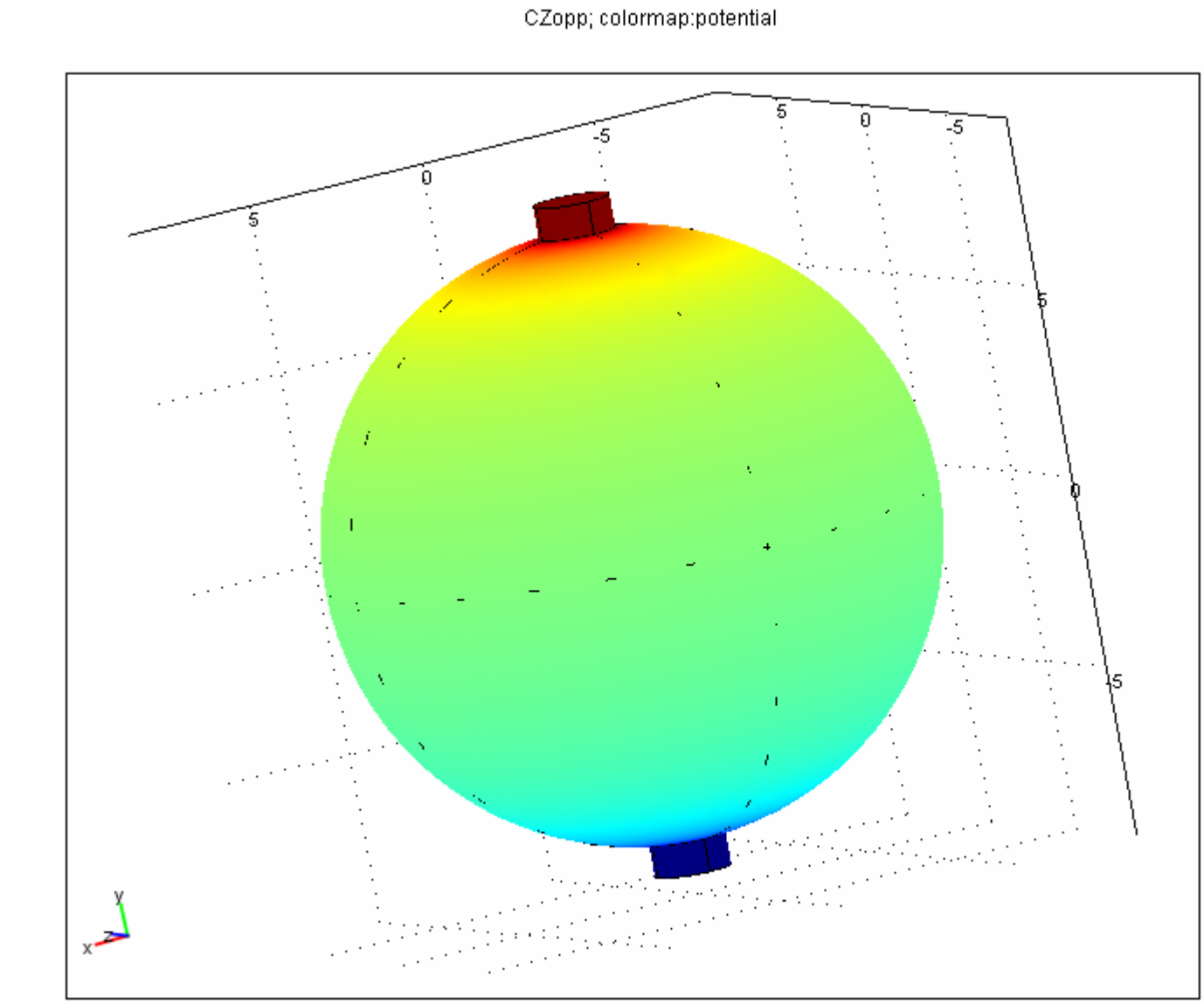

Figure 70: 3D surface plot of electric potential for diametric orientation.

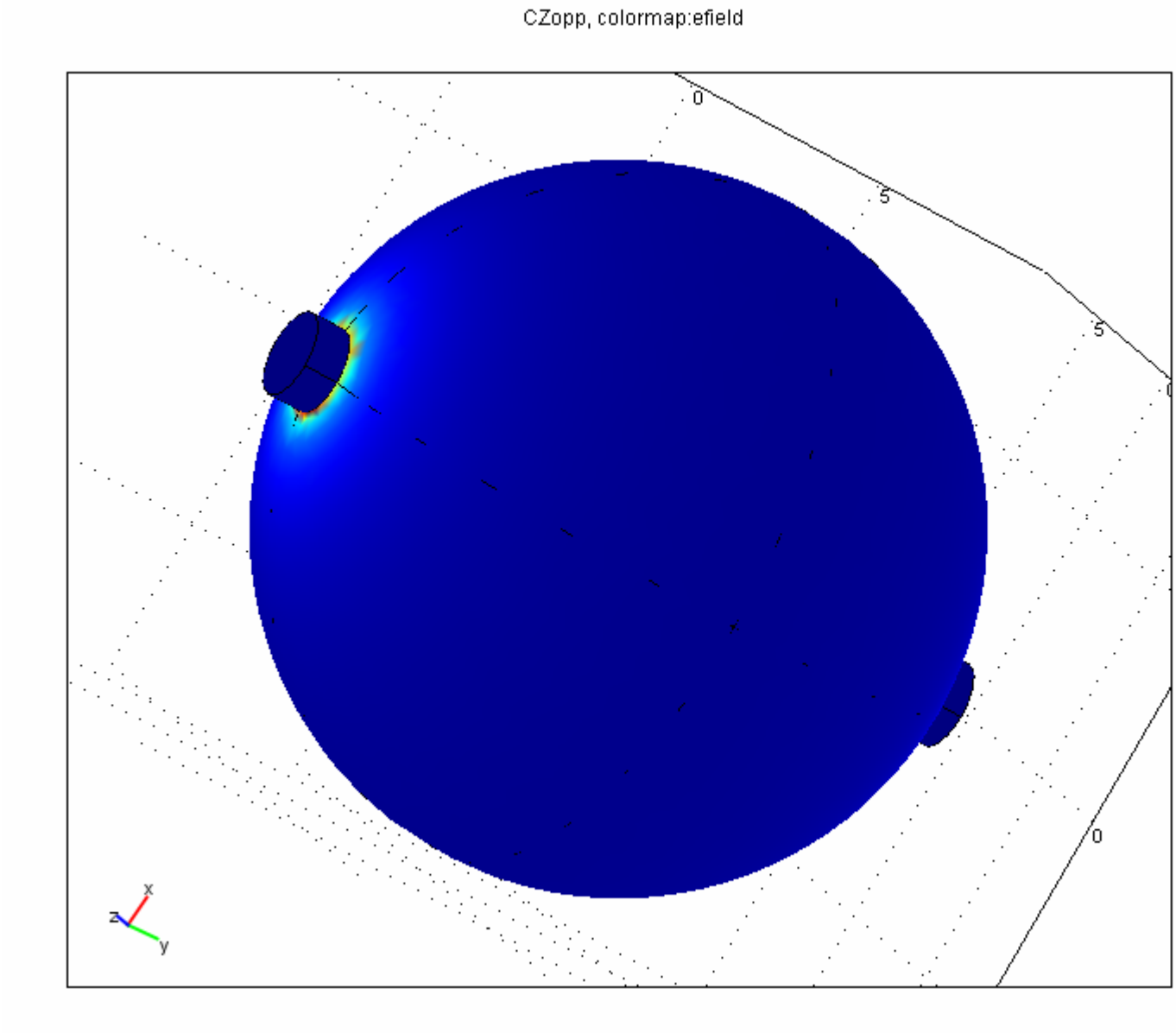

Figure 71: 3D surface plot for electric field of diametric orientation.

Epidural Stimulation Model

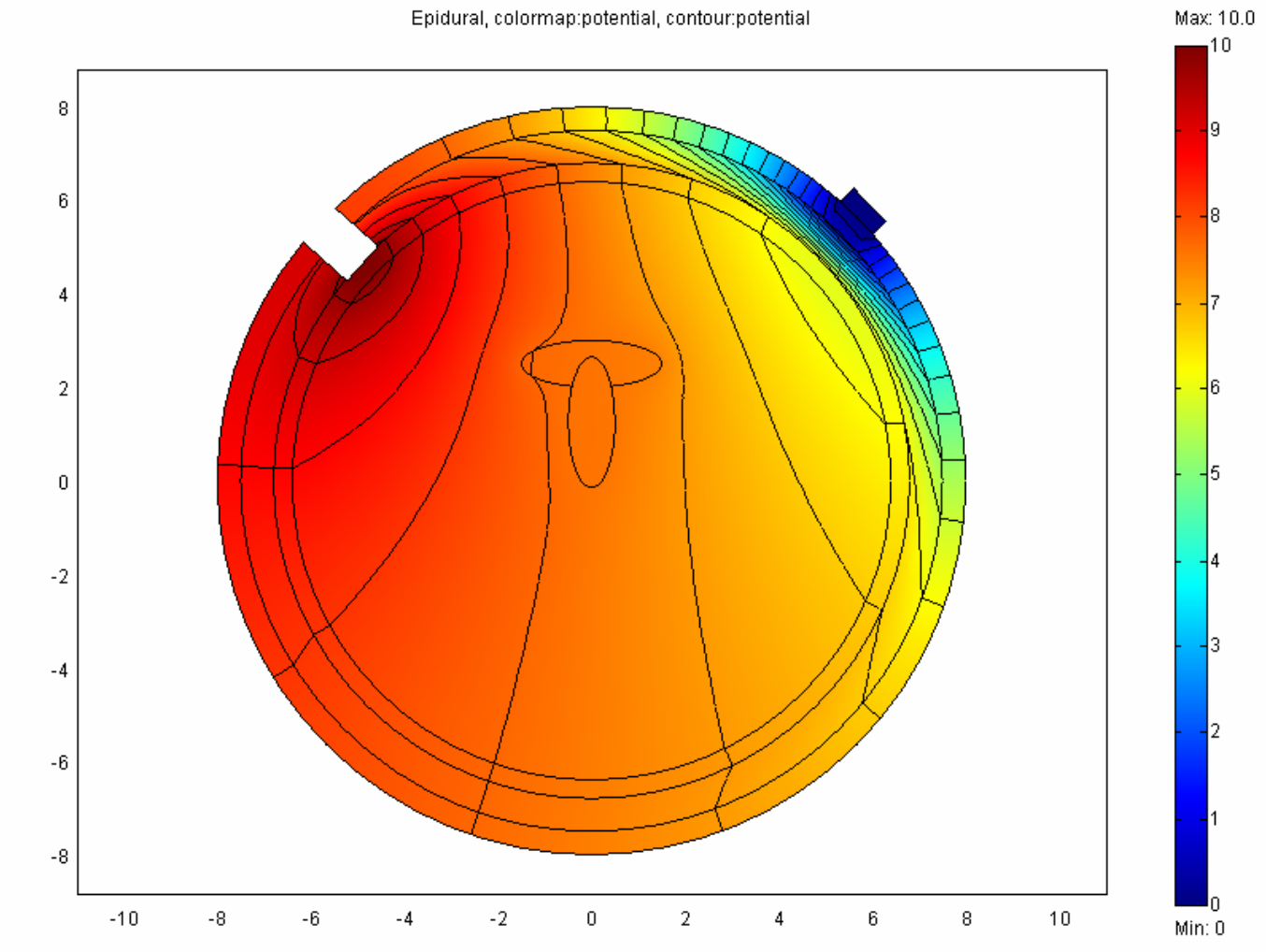

Figure 72: 2D electric potential for epidural stimulation model, ventricles included.

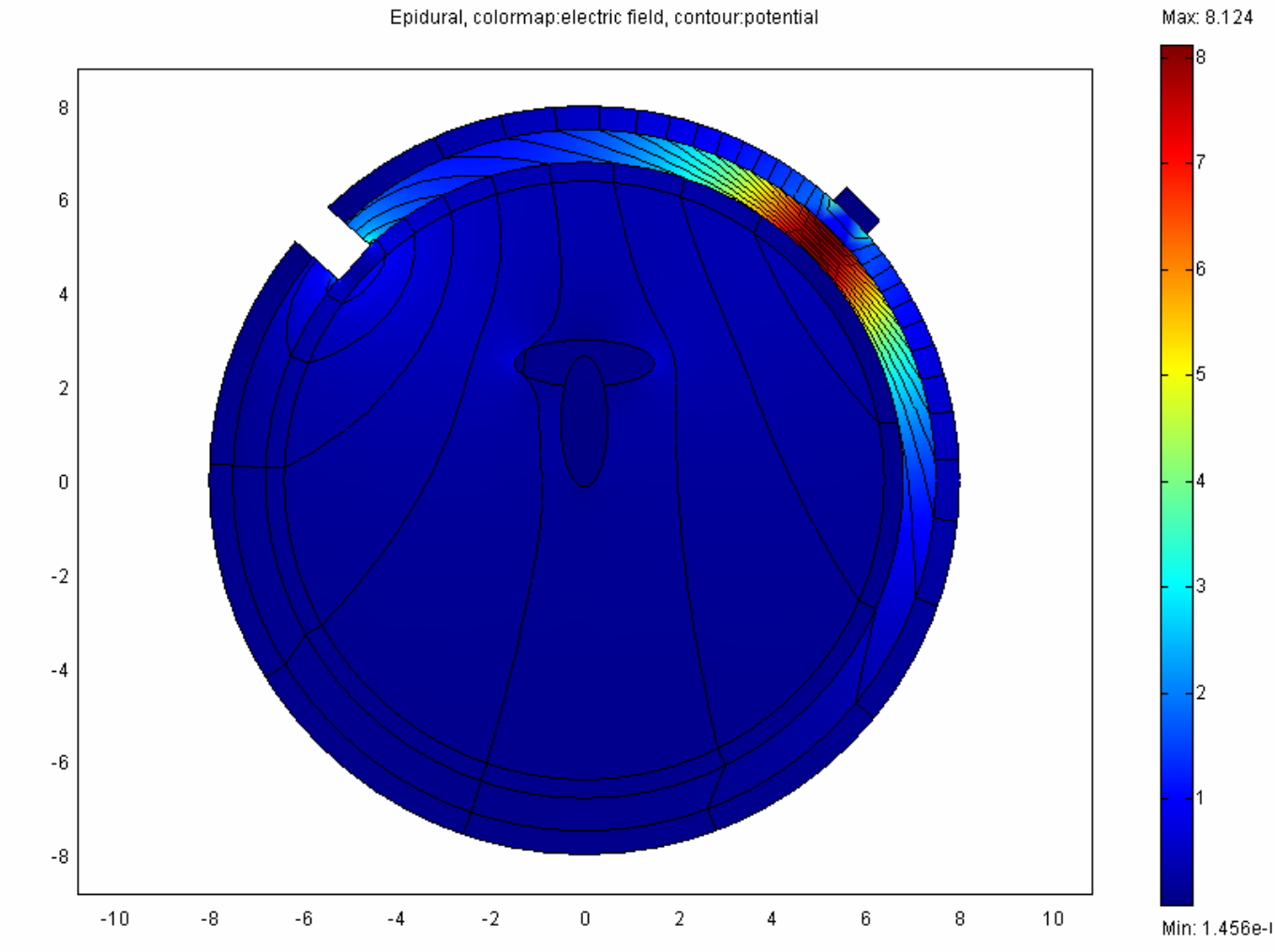

Figure 73: 2D electric field for epidural stimulation model, ventricles included.

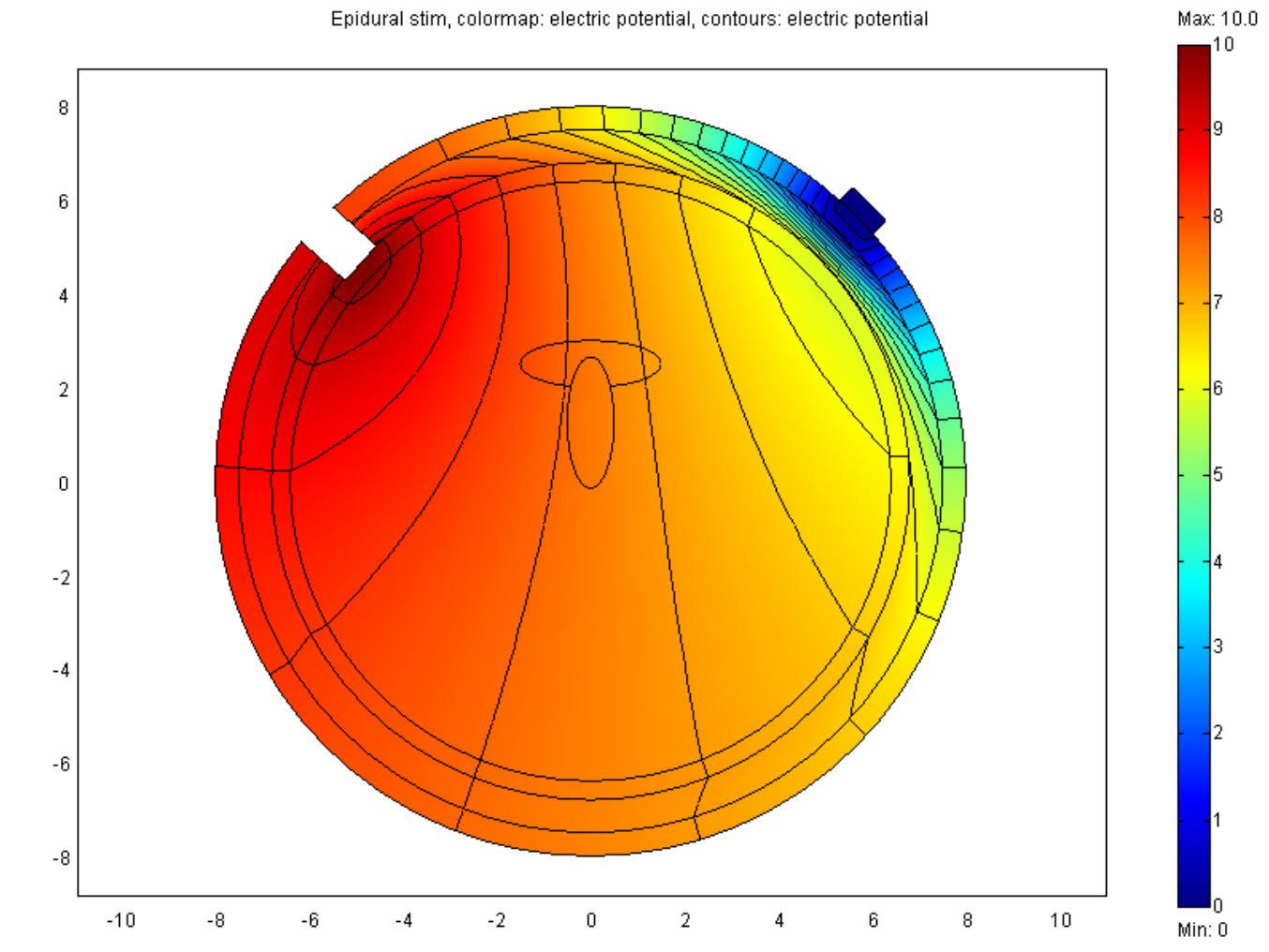

Figure 74: 2D electric potential for epidural stimulation model, no ventricles included.

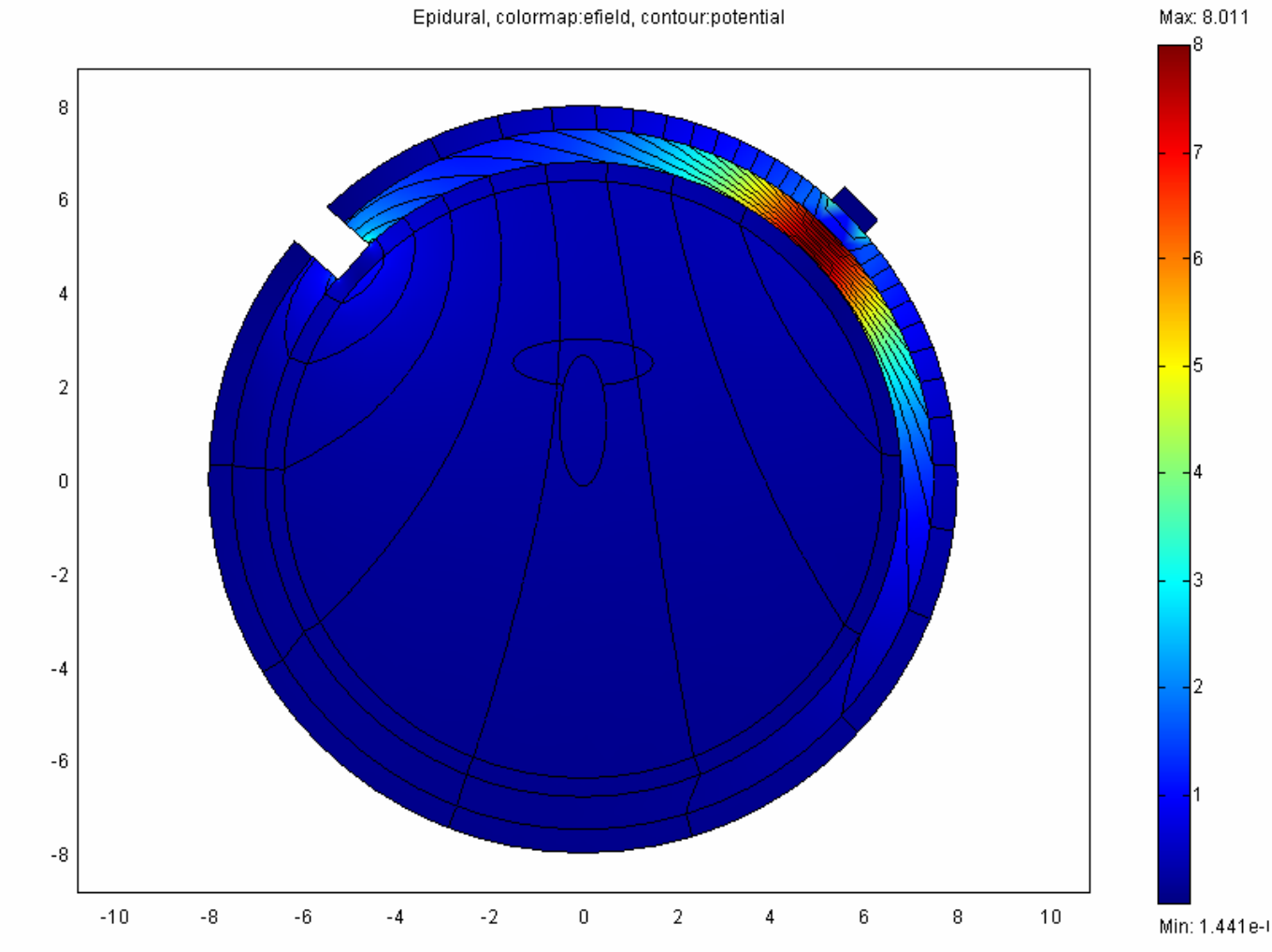

Figure 75: 2D electric field for epidural stimulation model, no ventricles included.

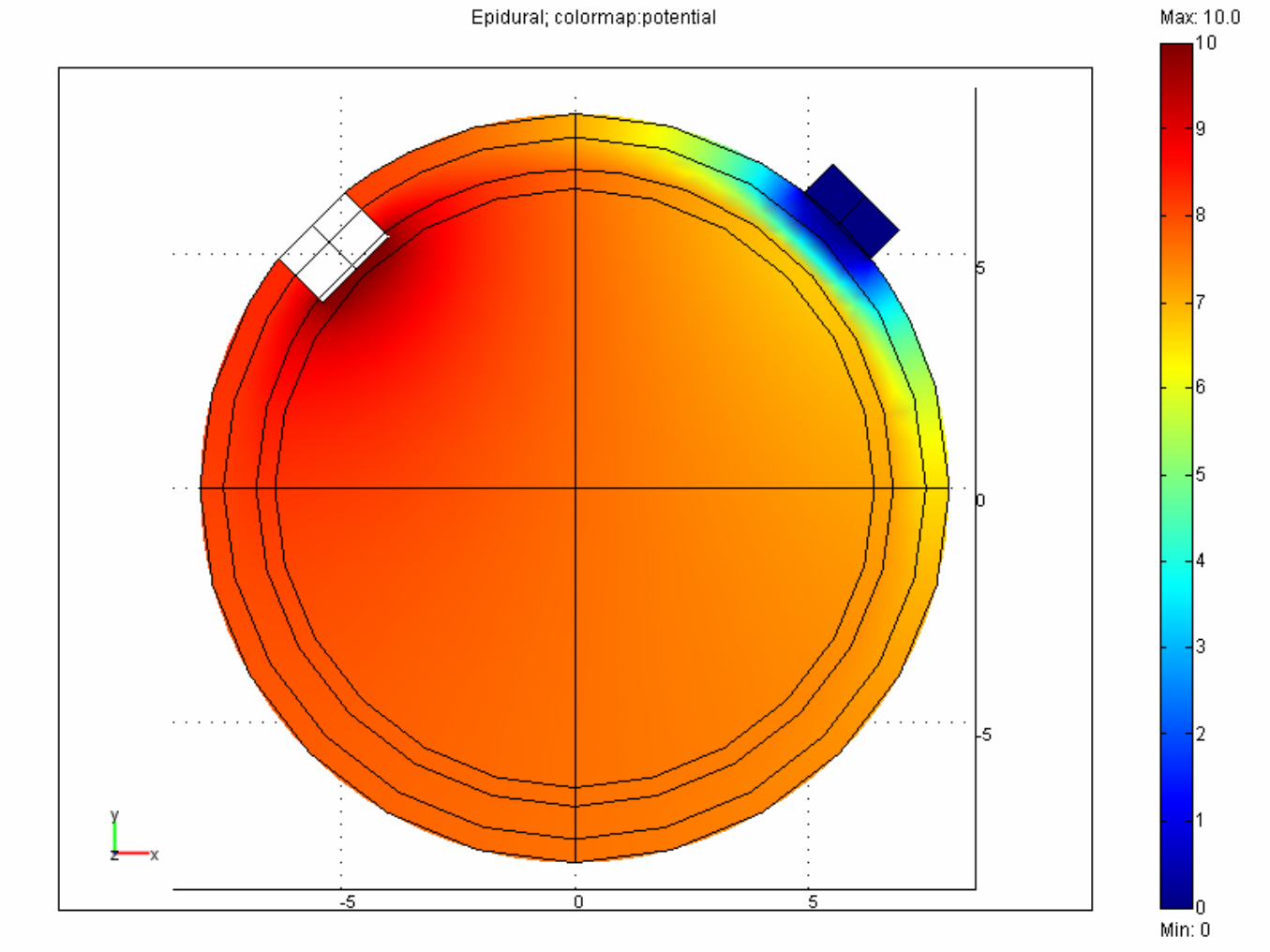

Figure 76: 3D slice plot for electric potential in epidural stimulation model, no ventricles included.

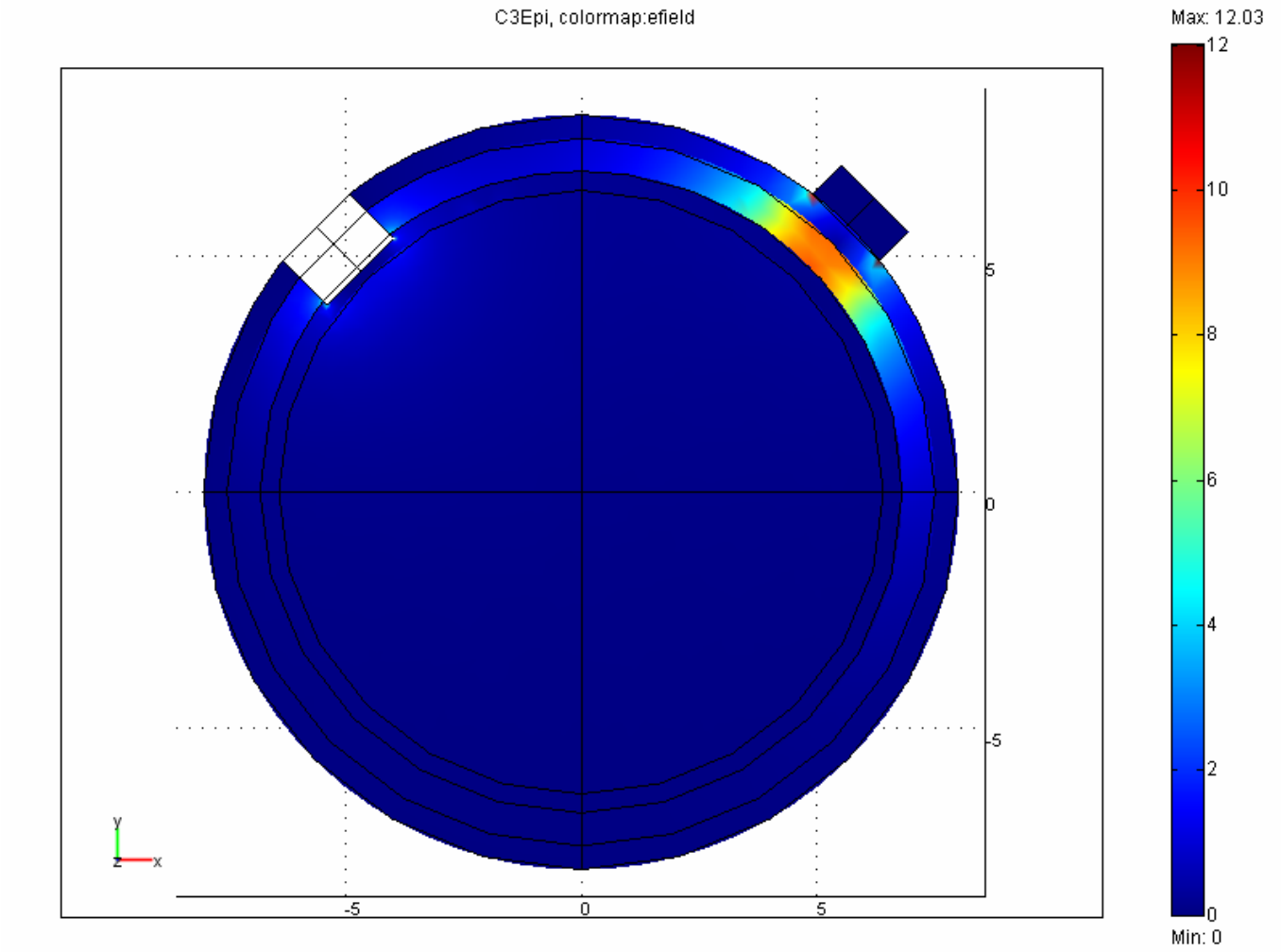

Figure 77: 3D slice plot of electric field in epidural stimulation model with no ventricles included.

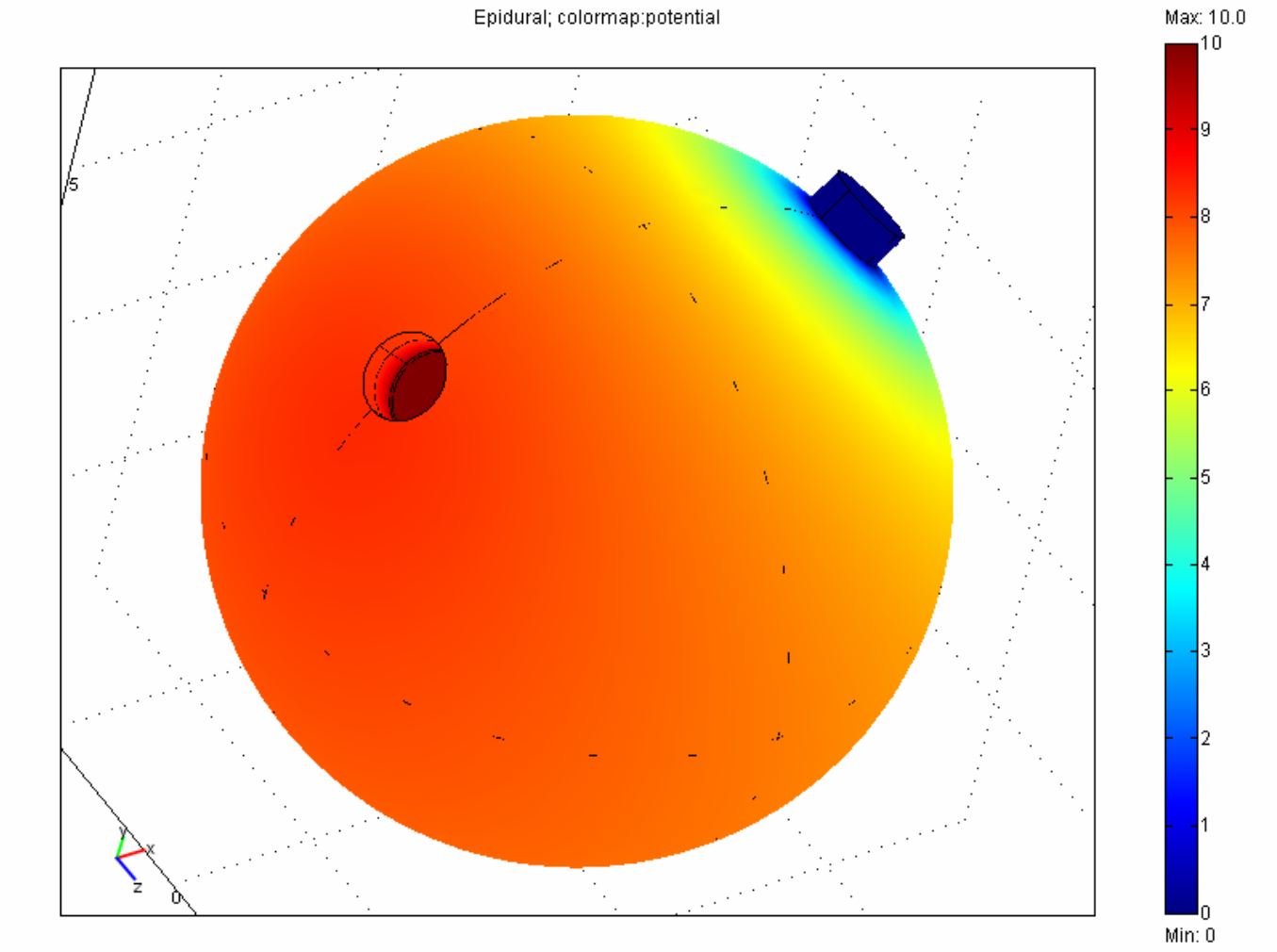

Figure 78: 3D surface plot of electric potential in epidural stimulation model.

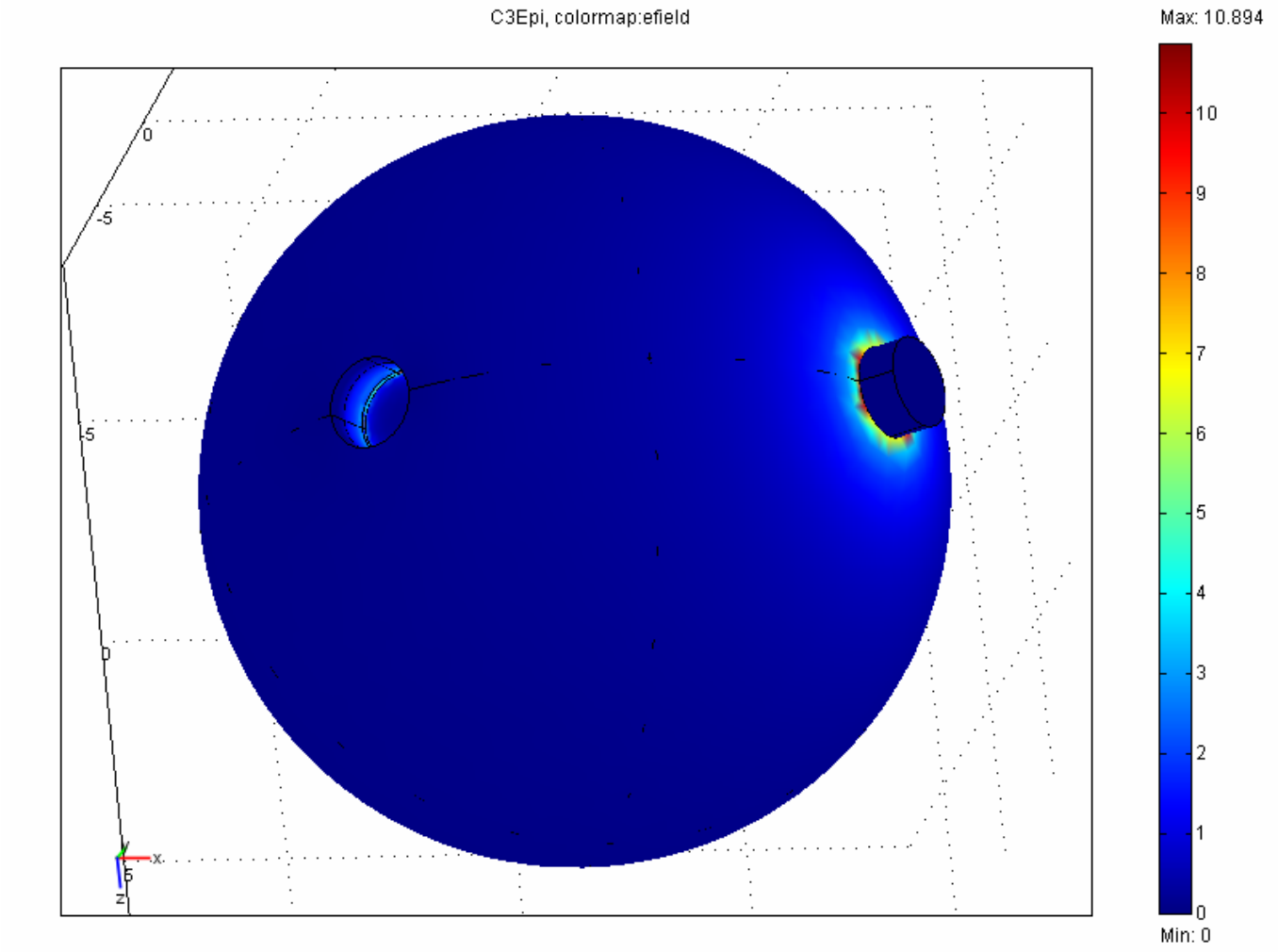

Figure 79: 3D surface plot of electric field for epidural stimulation model.

Cortical Stimulation Model

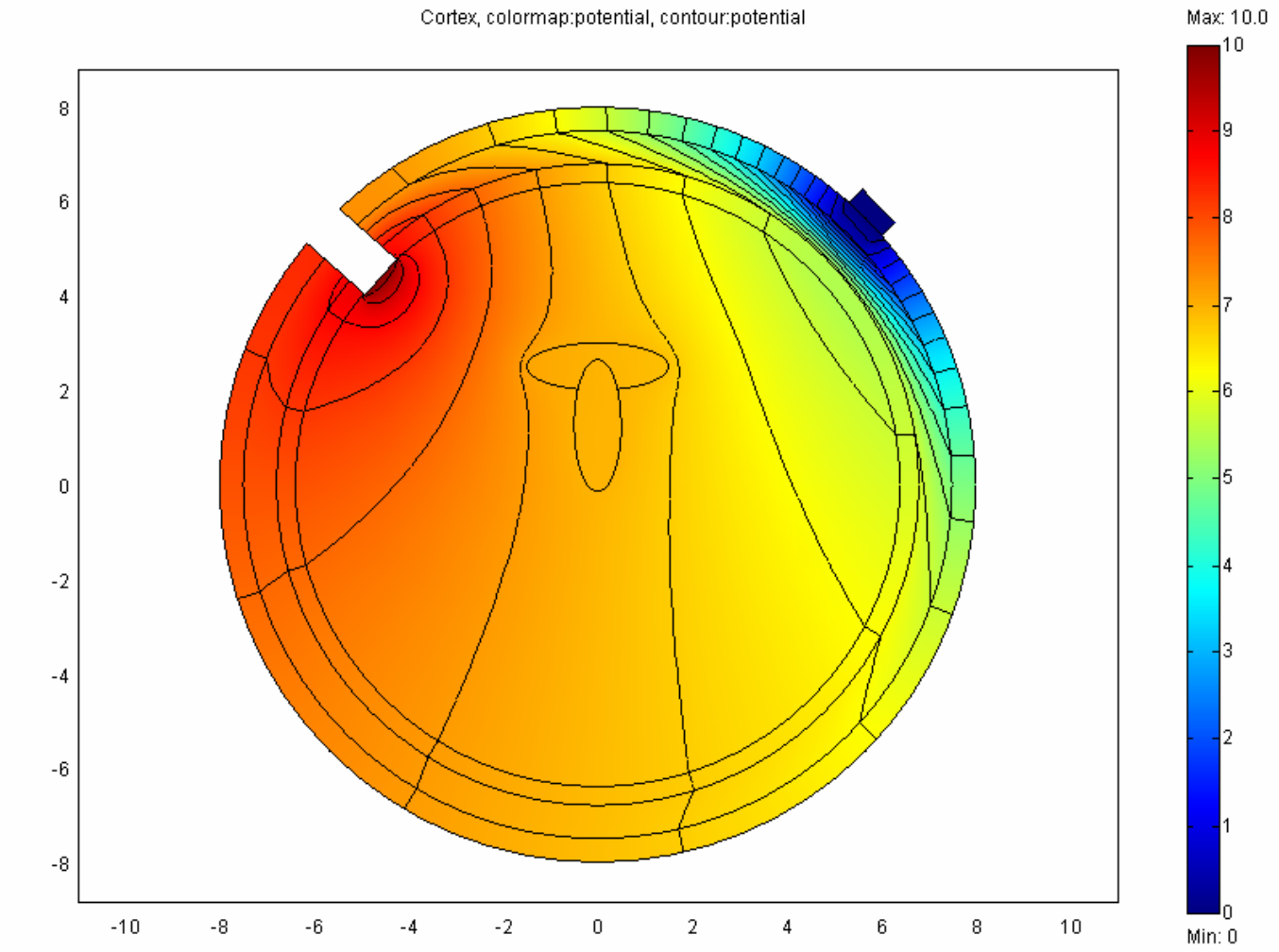

Figure 80: 2D electric potential in the cortical stimulation model, ventricles included.

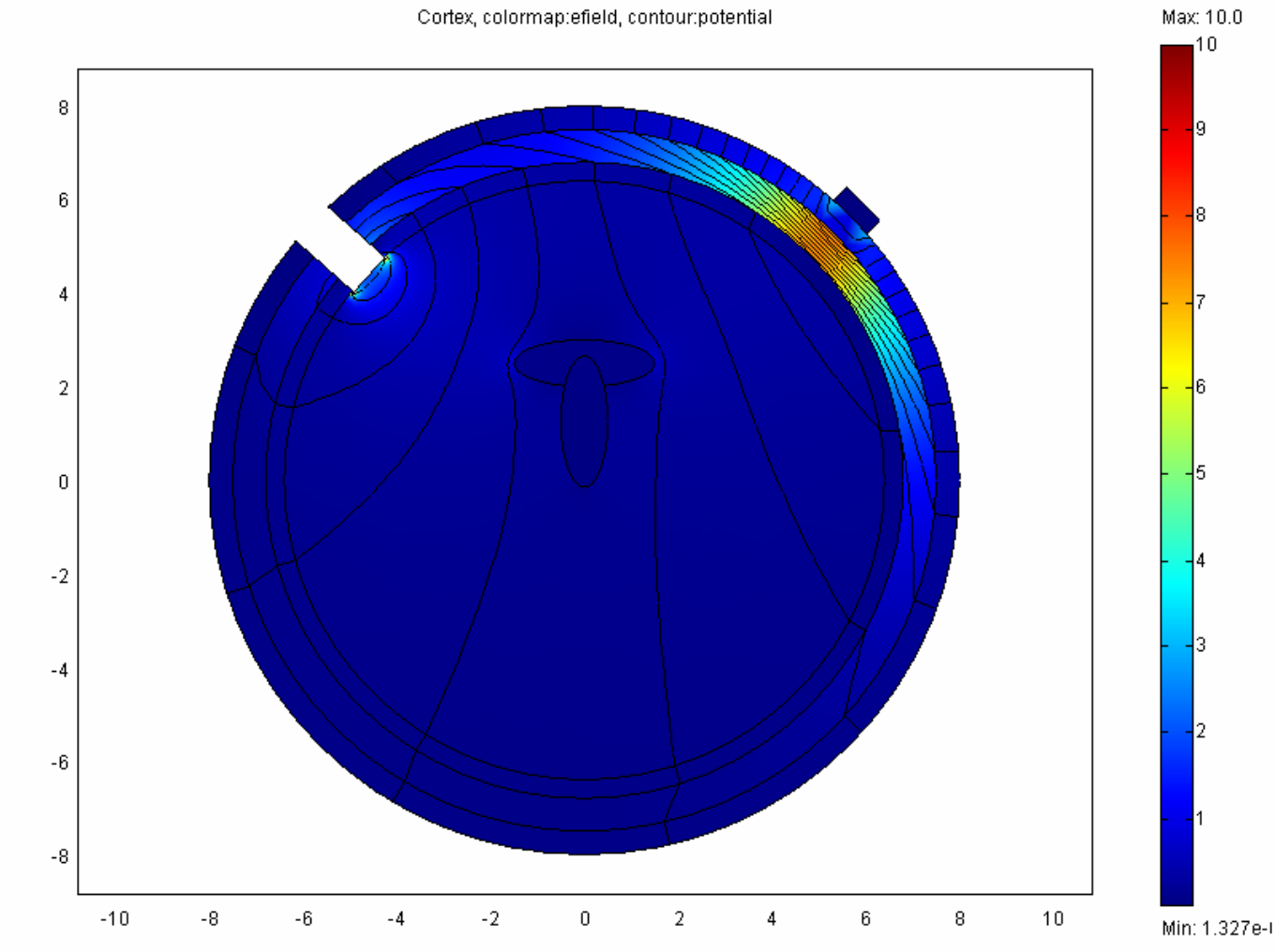

Figure 81: 2D electric field for cortical stimulation model, ventricles included.

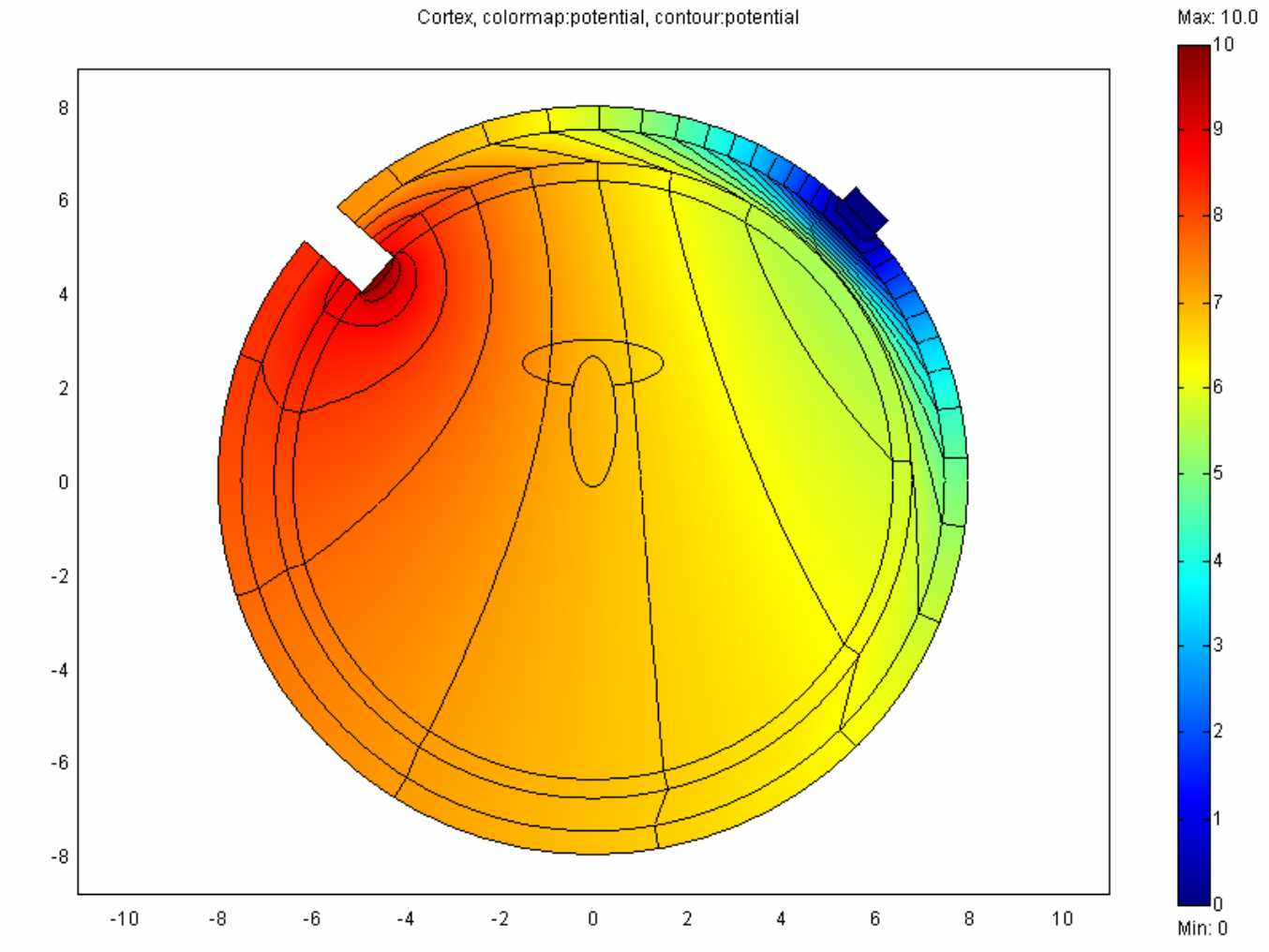

Figure 82: 2D electric potential for cortical stimulation model, no ventricles included.

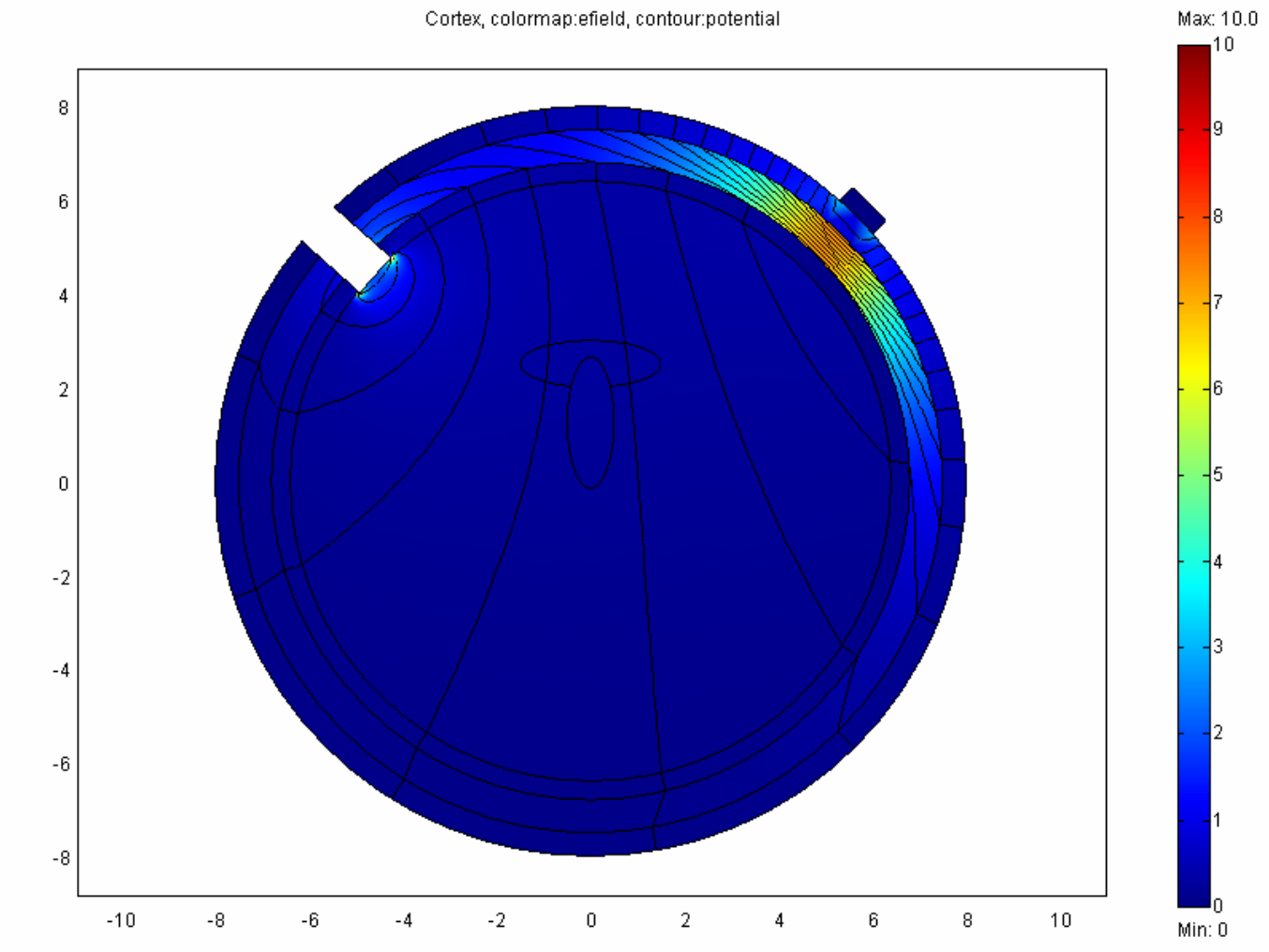

Figure 83: 2D electric field for cortical stimulation model, no ventricles included.

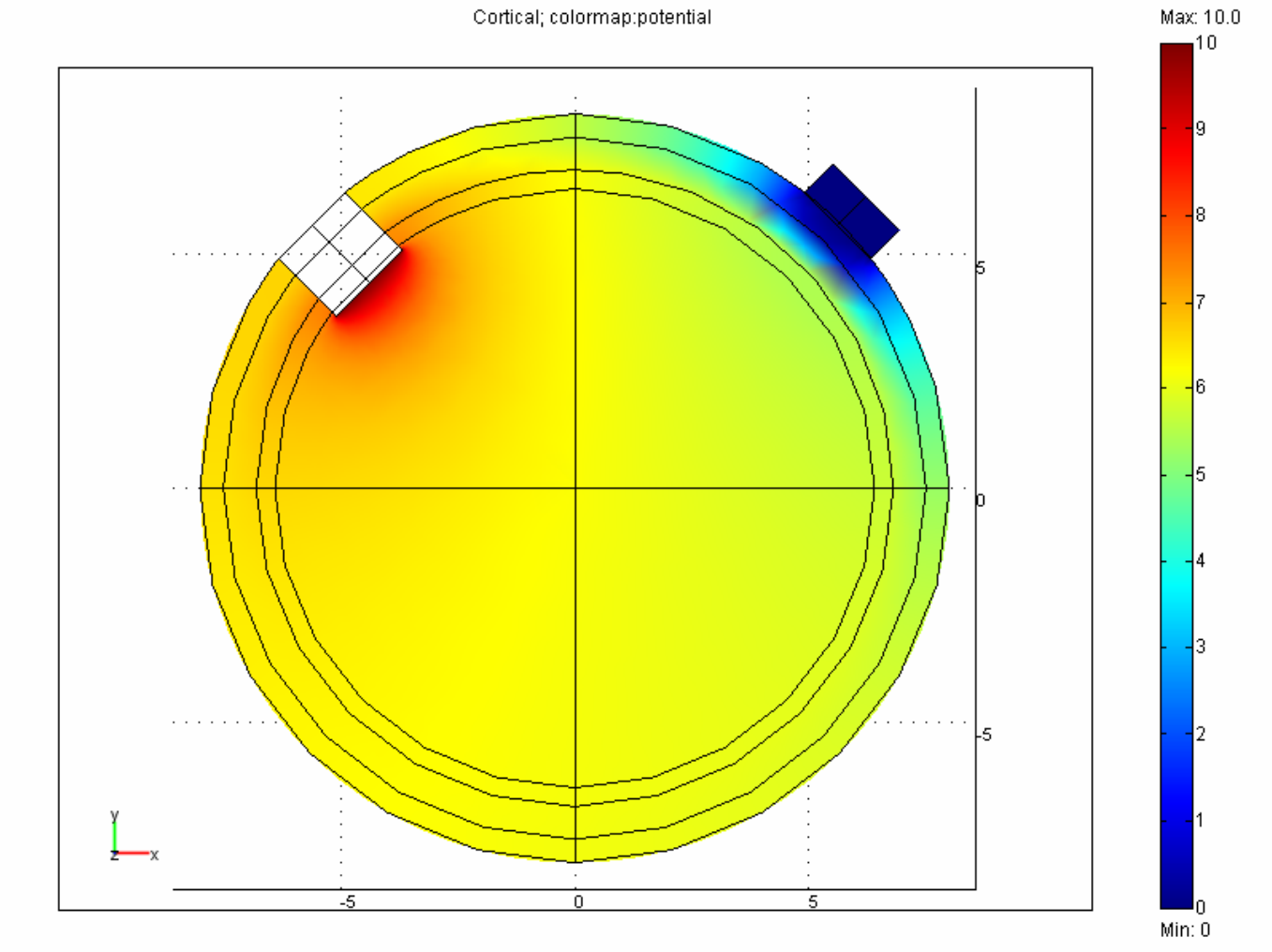

Figure 84: 3D slice plot of electric potential for cortical stimulation model, no ventricles included.

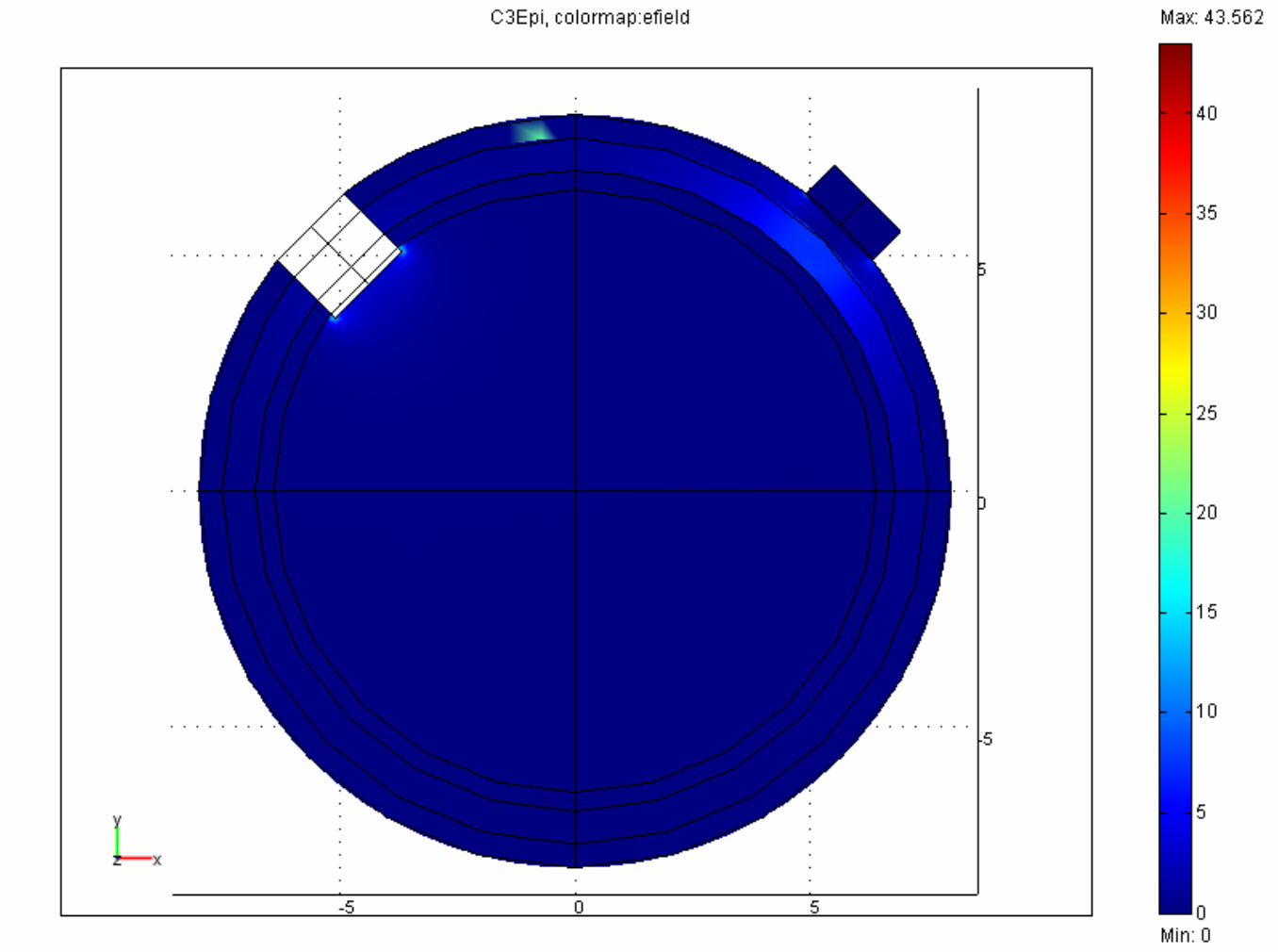

Figure 85: 3D slice plot of electric field for cortical stimulation model with no ventricles included.

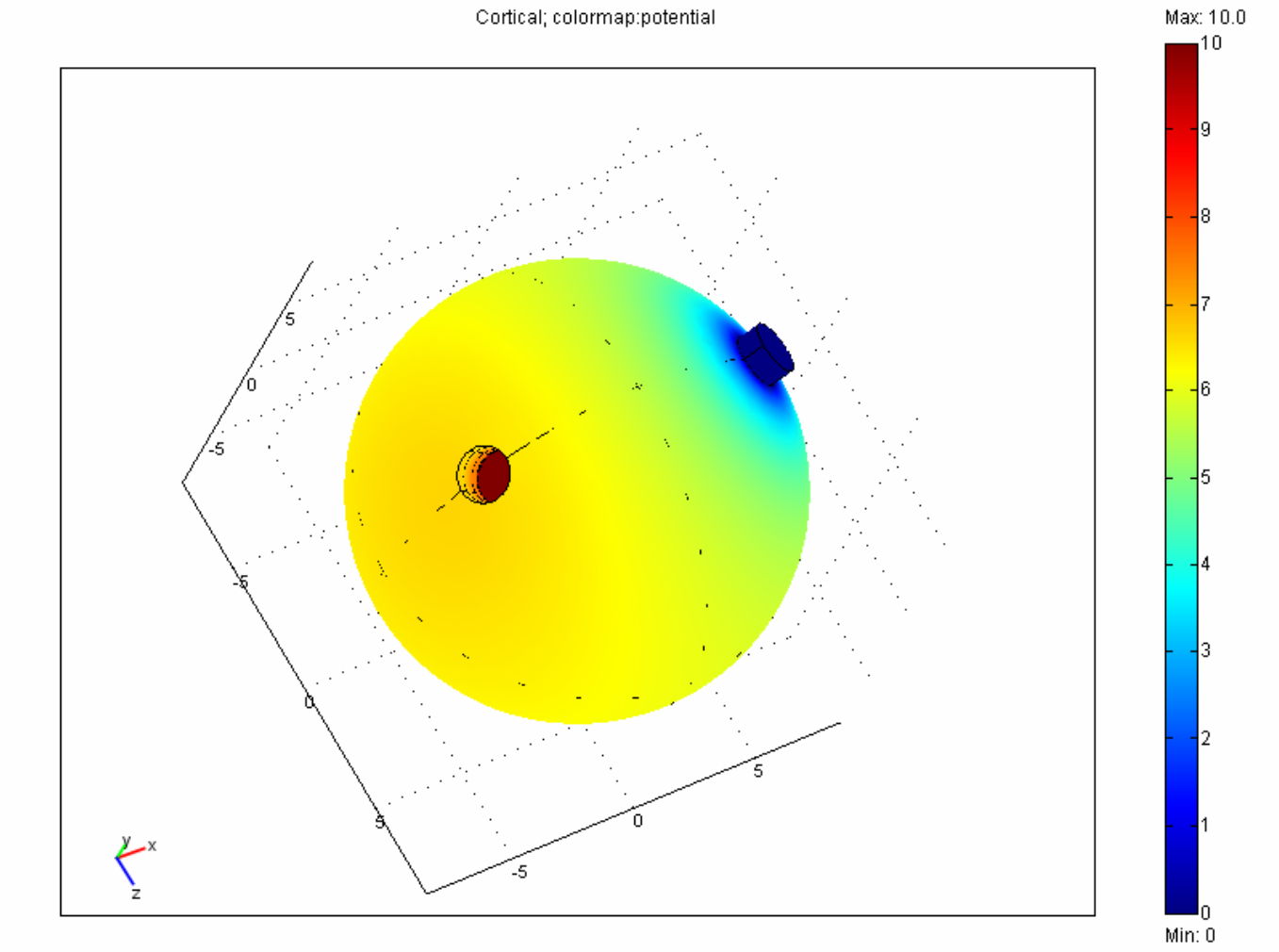

Figure 86: 3D surface plot of electric potential for cortical stimulation model.

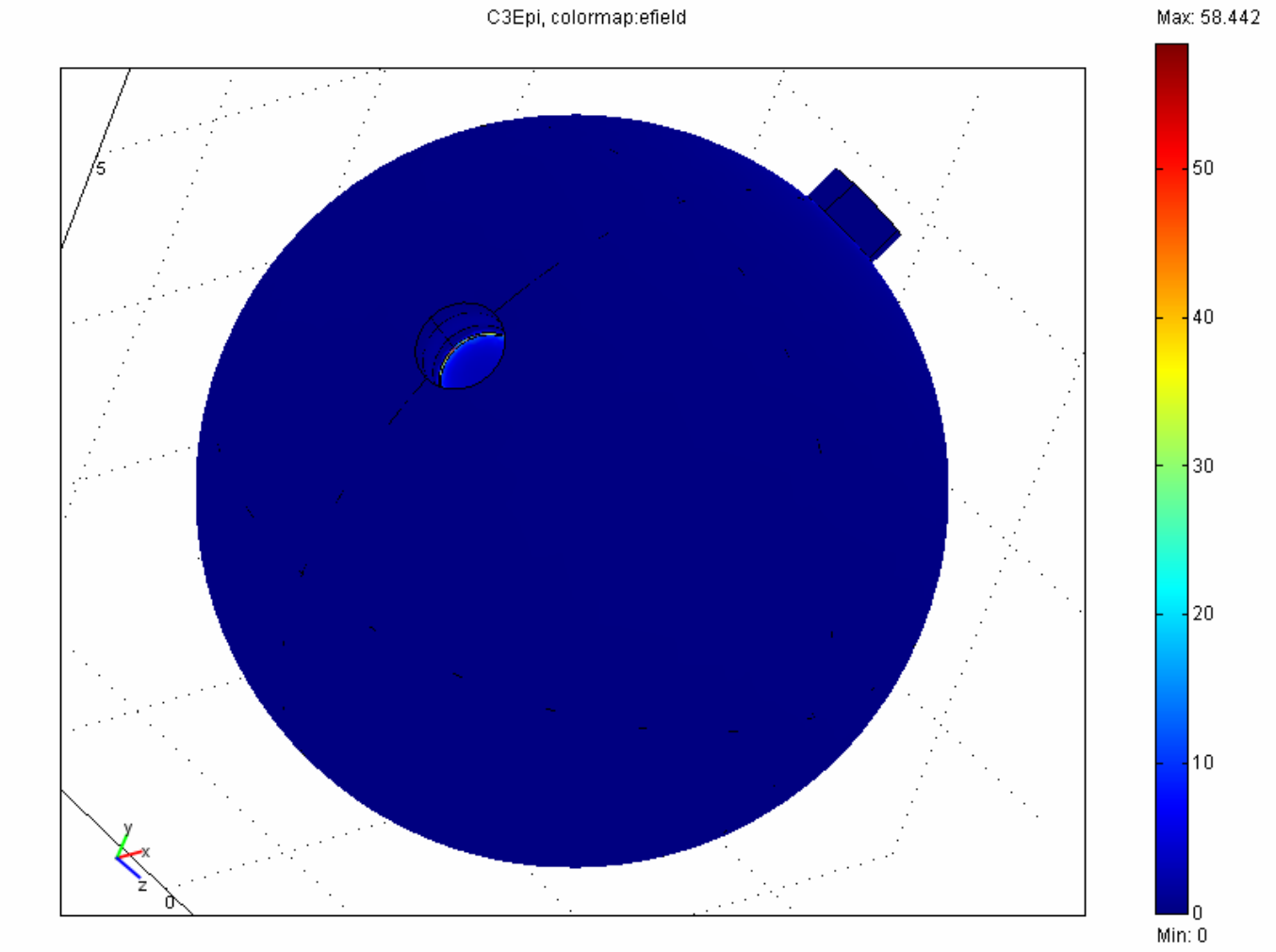

Figure 87: 3D surface plot of electric field for cortical stimulation model.

BIBLIOGRAPHY

[1] Rattay, F (1987) Ways to approximate current-distance relations for electrically stimulated fibers. J Theo. Bio. 125:339-349

[2] Devinsky O, Beric A, Dogali M, *Advances in Neurology: Electrical and Magnetic Stimulation of the Brain and Spinal Cord*, Vol. 63, Raven Press, New York, 1993. pp. 201-213

[3] Merton PA, Morton HB, "Stimulation of the cerebral cortex in the intact human subject", *Nature*, 1980;285:227

[4] Schramm J, Moller AR, *Intraoperative Neurophysiologic Monitoring in Neurosurgery*, Springer-Verlag, Berlin Heidelberg, Germany, 1991. pp.135-136

[5] Journee HL, Polak HE, de Kleuver M, Langeloo DD, Postma AA. "Improved neuromonitoring during spinal surgery using double-train transcranial electrical stimulation." Med Biol Eng Comput. 2004 Jan;42(1):110-113.

[6] Deletis V, Kothbauer K, "Intraoperative neurophysiology of the corticospinal tract", *Spinal Cord Monitoring*, 1998 Springer, Wien, New York

[7] Journee HL, Polak HE, de Kleuver M, "Influence of electrode impedance on threshold voltage for transcranial electrical stimulation in motor evoked potential monitoring." Med Biol Eng Comput. 2004 July;(42): 557-561.

[8] Suihko V (1998) Modeling direct activation of corticospinal axons using transcranial electrical stimulation. Electroencephalogr Clin Neurophysiol 109:238-244

[9] Rothwell J, Burke D, Hicks R, Stephen J, Woodforth I, Crawford M (1994) Transcranial electrical stimulation of the motor cortex in man: further evidence for the site of activation. J Physiol Lond 481:243-250

[10] Basser, P.J., *New Currents in Electrical Stimulation of Excitable Tissues*, Annual Review of Biomedical Engineering, 2000. 02:377-97

[11] http://www.painonline.org/NerveCells.htm

[12] Gulrajani, R.M., *Bioelectricity and Biomagnetism*, John Wiley and Sons, New York, NY, 1998, pp. 189-197

[13] Malmivuo J. and Plonsey R., *Bioelectromagnetism*, Oxford; New York: Oxford University Press, 1995, pp. 133-147

[14] Ragnar Granit Institute, Medical Engineering Laboratory, http://www.ee.tut.fi/rgi/kurssit/7102500/mallinnus/modelling02.pdf

[15] Mathworks : http://www.mathworks.com/access/helpdesk/help/toolbox/pde/ug/f8955.html

[16] Wessel, BL, "Analytical and Numerical Optimizatin of an Implantable Volume Conduction Antenna", University of Pittsburgh, 2002 http://etd.library.pitt.edu/ETD/available/etd-04152004-194608/unrestricted/Wessel2004.pdf

[17] http://www.engr.ucr.edu/~wasme/strongweak.htm

[18] http://www.pbs.org/wgbh/nova/mind/prob_map.html ,updated October 2001

[19] http://www.brainconnection.com/topics/?main=anat/motor-anat

[20] http://en.wikipedia.org/wiki/Neuron, for Figure 3.

[21] http://en.wikipedia.org/wiki/Axon

[22] http://en.wikipedia.org/wiki/Myelin

[23] Prodanov D, Marani E, Holsheimer J, "Functional Electric Stimulation for sensory and motor functions: progress and problems", Biomedical Reviews, 2003, 14:23-50

[24] Nadeem M, Thorlin T, Gandhi O, Fellow L, IEEE, Persson M, "Computation of Electric and Magnetic Stimulation in Human Head Using the 3-D Impedance Method", IEEE Transaction on Biomedical Engineering, Vol. 50, No. 7, July 2003

[25] Gabriel C, Gabriel S, Corthout E, "The dielectric properties of biological tissues: I. Literature Survey", Phys. Med. Biol. 41 (1996) pp. 2231-2249, Printed in the UK.

[26] Gabriel S, Lau R W, Gabriel C, "The dielectric properties of biological tissues: II. Measurements in the frequency range 10 Hz to 20 GHz" Phys. Med. Biol. 41 (1996) pp. 2251-2269, Printed in the UK.

[27] Gabriel S, Lau R W, Gabriel C, "The dielectric properties of biological tissues: III. Parametric models for the dielectric spectrum of tissues" Phys. Med. Biol. 41 (1996) pp. 2271-2293, Printed in the UK.

[28] Weisstein, Eric W., “Dirichlet Boundary Conditions.” From *Mathworld* – A Wolfram Web Resource, Wolfram Research Inc., 2004 http://mathworld.wolfram.com/DirichletBoundaryConditions.html

[29] Weisstein, Eric W., “Neumann Boundary Conditions.” From *Mathworld* – A Wolfram Web Resource, Wolfram Research Inc., 2004 http://www.mathworld.worlfram.com/NeurmannBoundaryConditions.html

[30] http://www.crossroadsinstitute.org/brainmap.html

[31] Pirotte B, et al, “Combination of functional magnetic resonance imaging-guided neuronavigation and intraoperative cortical brain mapping improves targeting of motor cortex stimulation in neuropathic pain.”, Neurosurgery, 2005 April, pp 56

[32] Stecker MM (2005) Transcranial electric stimulation of motor pathways: a theoretical analysis. Comput Biol Med 35:133-155

[33] Nowak, L. G. & Bullier, J. 1998a, "Axons, but not cell bodies, are activated by electrical stimulation in cortical gray matter. I. Evidence from chronaxie measurements", Exp.Brain Res., vol. 118, no. 4, pp. 477-488.

[34] Nowak, L. G. & Bullier, J. 1998b, "Axons, but not cell bodies, are activated by electrical stimulation in cortical gray matter. II. Evidence from selective inactivation of cell bodies and axon initial segments", Exp.Brain Res., vol. 118, no. 4, pp. 489-500.

[35] Manola, L., Roelofsen, B. H., Holsheimer, J., Marani, E., & Geelen, J. 2005, "Modelling motor cortex stimulation for chronic pain control: electrical potential field, activating functions and responses of simple nerve fibre models", Med.Biol.Eng Comput., vol. 43, no. 3, pp. 335-343